Enhancing Landslide Risk Management Through a Cost-Effective dGNSS Technology and a Method to Estimate Stability of Shore Landslides in Response to Climate Change

By

Ingrid Arantxa Berru Garcia

A thesis submitted in partial fulfillment of the requirements for the degree of

Master of Science

in

Geotechnical Engineering

Department of Civil and Environmental Engineering

University of Alberta

ABSTRACT

Climate change is having an impact on Canada, resulting in variations in temperature, precipitation, and evaporation, among other aspects. These changes could be significant in Alberta since agriculture is a major factor in the social-economic development of the province. For example, the region's farming districts are requiring additional water for irrigation, causing a major reliance on reservoirs that in result decreases more rapidly the water levels. This reduction, known as a drawdown, has the potential to exacerbate existing landslides or trigger new landslides in the region. The geology of the region contributes to this possibility since the bedrock frequently contains layers of bentonite and coal seams, both of which have lower shear strengths and can reduce the strength to a residual strength in any disturbance, such as an increase in groundwater levels or the loss of support at toe of a slope. This could worsen in the future as the effects of climate change seem to be intensifying. Thus, improving landslide risk management techniques is necessary to identify and monitor the possible landslides, assess their failure.

The thesis introduces a low-cost dGNSS technology and methodology as practical and cost-effective tools for improving landslide risk assessment and management in response to climate change effects, even under conditions of limited resources and multiple potential scenarios. Their reliability, efficiency and applicability to different landslide cases were evaluated in the Chin Coulee landslide in southern Alberta. This slow-moving landslide has disrupted a roadway since 1970 and has shown greater displacements when irrigation water demand increases.

The dGNSS technology described and adopted in this study is referred to as SparkFun units designed for surveying, capable of achieving millimeter accuracy necessary for landslide monitoring when additional components are assembled to the units. Additionally, these units offer high-frequency data collection (Every minute), independence from internet services for data management, and have an approximate capital cost of USD$2000 per unit. They were customized for landslide monitoring purposes, tested and deployed for 6 months to record horizontal and

vertical displacements. The monitoring data showed that the SparkFun system met its manufacturer accuracy specifications (14 mm horizontal and 10 mm vertical). The system error was within acceptable limits to monitor the landslides displacements, and the results were compared with another, commercially available, dGNSS landslide monitoring technology installed in the landslide area. The magnitude of displacement observed with the SparkFun system was lower than that of the other technology, primarily due to the monitoring period. However, both technologies exhibited similar displacement trends, aligning accurately in the vertical direction. This allows the conclusion that the SparkFun system appears to be a viable monitoring technique, enabling the management of a larger number of monitoring points in current and future landslide areas at a lower cost.

Furthermore, a practical methodology was introduced to assess landslide stability in the Canadian Plains under current and future drawdown scenarios, serving as a simple tool for various entities responsible for landslide management. The methodology identifies materials that govern the stability and the pore water pressure of the landslide. Moreover, it estimates and defines the reservoir water fluctuations, drawdown rates, hydraulic and restraint boundaries conditions. This methodology demonstrated good agreement between the estimated material shear strength and permeabilities with prior studies in the landslide area and literature review. The calculated slip surface was consistent with the one proposed in prior investigations. Scenarios of future stability were informed by current trends in drawdown trends and analyzed, resulting in a 5% drop in stability compared to current conditions under the 2050-year scenario, and the landslide stability was reduced by 11% when considering a critical scenario. These results demonstrated the practicability and effectiveness of this methodology to analysis the landslide stability.

PREFACE

The third and fourth chapters of this thesis have been submitted to two journals. The details are stated in the following lines:

Chapter 3 has been accepted in the Natural Hazards Journal with the citation described beneath. I was responsible for the work presented in this chapter, which includes a literature review, instrument assembly testing and deployment, analysis of data, and discussion of results, as well as the writing of the text. Dr. Macciotta contributed through his supervision, advice, comments, and editing.

Berru I, Macciotta R, Rodriguez J, Gräpel C, Skirrow R, Tappenden K (In Press). Introduction and Testing of a Cost-Effective GNSS System for Landslide Monitoring

Chapter 4 of this thesis has been submitted and is under review in the Landslide Journal. As with the Chapter 3 journal paper, I carried out the literature review, seepage and stability analyses, findings interpretation, discussion, and text writing. Dr. Macciotta helped with the study by giving supervision, direction, feedback, and editing. The citation of the journal is as follows:

Berru I, Macciotta R, Rodriguez J, Gräpel C, Skirrow R, Tappenden K (Submitted). Method for Estimating Landslide Stability under Future Drawdown Scenarios due to Climate Change - Chin Coulee Landslide

With love, I dedicate this thesis to my parents, Gerardo and Sara, whose support and sacrifices have allowed me to build a better future.

ACKNOWLEDGEMENTS

I would like to express my sincere gratitude to all those who have contributed and supported me in completing this thesis. First and foremost, my deepest appreciation goes to my supervisor, Dr. Renato Macciotta, who gave me the opportunity to be his student and to get to know the excellent person that he is. He has always encouraged me to step out of my comfort zone and made himself available for questions, even during the busiest times. His guidance, patience, expertise, and support have been invaluable throughout this research journey.

This research was conducted in collaboration with Alberta Transportation and Economic Corridors (TEC) and Klohn Crippen Berger (KCB). Special thanks go to Chris Gräpel from KCB for his constructive criticism and insightful suggestions that not only improved my writing skills but also contributed to my professional growth. I would also like to thank Roger Skirrow and Kristen Tappenden of TEC for taking the time to review my work and providing valuable comments.

I express my gratitude to everyone who contributed to my fieldwork and the data analysis. Special thanks to Jorge Rodriguez from KCB for his assistance in implementing the SparkFun system, sharing his knowledge of the research site, and providing me with excellent professional and life advice throughout the extensive trip to the site. I am also grateful to Aden Shipton and Katrina Cereno, also from KCB, who were instrumental in making the installation of the SparkFun system possible. I could not ask for a better team, their willingness to help, accompany me up and down the hill without complaint, and endure freezing temperatures during the process is priceless. Special appreciation goes to Essa Gierc, Taylor Wollenberg-Barron, and all those who supported me by either driving to the site or joining me to help configure the SparkFun system. Thanks also to Jennifer Stogowski for her help in coordinating the numerous field trips to the Chin Coulee site. My appreciation to Sohrab for taking the time to explain the methods to analyze the monitoring data and answer many of my questions.

I am grateful to all my colleagues and friends for welcoming me with open arms and sharing with me a part of their culture. Without knowing it, you have supported me emotionally in a country far from home. The laughs, lunches, trips, group project meetings, chats, and events we shared will always have a special place in my heart.

I also want to thank Hector, Pepe, Younger, and many others who have given me the opportunity to work in the geotechnical field, trusted my abilities, gave me excellent life advice, and encouraged me to pursue a post-graduate degree.

Most of all, I would like to extend special thanks to my parents for their unconditional love, care, belief, support, and endless encouragement. I am truly grateful for the foundation they have provided and the inspiration they continue to be in my life. I would also like to express my heartfelt appreciation to my husband for supporting me during both the good and challenging times since our undergraduate years. His encouragement, humor, patience, and valuable advice have been essential in navigating this unpredictable journey called life.

TABLE OF CONTENTS

LIST OF TABLES

LIST OF FIGURES

GLOSSARY OF TERMS

AEP	Alberta Environment and Parks
dGNSS	Differential Global Navigation Satellite System
ECCC	Environment and Climate Change Canada
FAT32	File Allocation Table 32
FEM	Finite Element Method
FoS	Factor of Safety
GLONASS	GLObalnaya NAvigatsionnaya Sputnikovaya
GND	Signals of Ground
GNSS	Global Navigation Satellite System
GPS	Global Positioning System
GWL	Groundwater Level
GWMA	Gaussian-Weighted Moving Average
HAE	Height Above Ellipsoid
IRNSS	Indian Regional Navigation Satellite System
KCB	Klohn Crippen Berger
LRT	Light Rail Transit
MSL	Mean Sea Level
MST	Mountain Standard Time
M-C	Mohr-Coulomb
QZSS	Quasi-Zenith Satellite System

RTK	Real-time Kinematic
RX	Signals of Receive
SAAs	ShapeAccelArrays
SD	Secure Digital
SI	Slope Inclinometers
SMA	Simple Moving Average
SRF	Strength Reduction Factor
SRM	Strength Reduction Method
SSR	Shear Strength Reduction
TEC	Alberta Transportation and Economic Corridors
TGR	Three Gorges Reservoir
TX	Signals of Transmit
UTC	Universal Time
UTM	Universal Transverse Mercator
VWPs	Vibrating Wire Piezometers
°C	Degree Celsius

1 INTRODUCTION

Landslides in the Canadian Interior Plains, which include portions of northeastern British Columbia, most of Alberta, central and southern Saskatchewan, and southwestern Manitoba (Biagini et al. 2022); are widespread and can cause estimated annual expenses ranging from $281 million to $450 million (Porter et al. 2019). For instance, there are about 122 occurrences related to rock and soil slopes along the highway system in Alberta alone (Tappenden and Skirrow 2020). This aligns with the national landslide susceptibility map, which indicates that some parts of Alberta are vulnerable to landslides, particularly those near rivers, lakes, or reservoirs (Bobrowsky and Dominguez 2012, Porter et al. 2019) (landslides where the toe of the slope is affected by fluctuations of water bodies, or shore landslides). This sensitivity forces organizations in charge of managing landslides to enhance and innovate methods for mitigating these landslide risks (Macciotta et al. 2020, Rodriguez 2021) and optimize resources to address and mitigate the potential magnitude of landslides. These methods encompass various stages, such as the identification, analysis, monitoring, and remediation of landslides. Among these stages, prioritizing the identification of triggering factors and analysing their impacts, along with emphasizing the reduction in the cost of monitoring instruments while maintaining precision, has become critical (Rodriguez 2021).

Failure mechanisms in the Alberta Plains are associated with its anisotropic geology, hydraulic properties, and soil and bedrock shear strength. Past glacial events sculpted the region's geology, leaving weak sedimentary bedrock interbedded with siltstones, sandstones, clay shales, coal, and bentonite (Biagini et al. 2022). According to Biagini et al. (2022), the latter two units often exhibit low shear strength and are prone to further reducing their strength in response to any disruption, possibly reaching their residual strength and initiating mass displacements. For example, the Chin Coulee landslide, situated at the northern bank of the Chin reservoir in Taber, Alberta (Rodriguez 2021), is identified as a retrogressive compound landslide sliding on a basal weak coal layer

(Biagini et al. 2022). Monitoring data revealed that throughout the summer months, when the demand for reservoir water to irrigate farmlands increases, the landslide displacements also intensify (Rodriguez et al. 2021). The decrease in water levels, commonly known as drawdown and identified as a triggering factor, is not exclusive to the Chin Coulee landslide and may potentially affect other slopes in the perimeter of reservoirs in the region. Agriculture is a major economic activity in the region, and as a result of climate change, there has been a significant rise in dependency on reservoir water for irrigating farmlands, driven by rising temperatures and a decrease in rainfall. For instance, the most recent report from Environment and Climate Change Canada (ECCC) predicts a temperature increase of 6.5°C for the Canadian Prairies, including Alberta (Bush et al. 2019; Muhammad et al. 2020; Berru et al. 2024). Furthermore, upon analyzing the Chin reservoir water levels, it was noted that the drawdown rates exhibit an increasing trend that might make this landslide instable (Berru et al. 2024). Given the imminent impact of climate change in the region, the increasing use of reservoir water, and the high susceptibility to landslides near reservoirs (Bobrowsky and Dominguez 2012); it is crucial to examine the effects of climate change, specifically the drawdown of reservoirs, on landslide stability. This urgency motivates the development of a practical methodology to estimate its effects under current and future conditions, allowing organizations to manage landslides more effectively.

Furthermore, monitoring is essential for understanding and mitigating the potential consequences of landslides. This risk may be exacerbated due to climate change, emphasising the importance of having an appropriate and cost-effective system for the region to guarantee adequate monitoring along corridors with many ongoing and future landslides (Rodriguez et al. 2021). Traditional in-situ landslide monitoring tools, like inclinometers (SIs) and piezometers, are often costly, restricting their use to specific sites or a limited number of monitoring points (Smethurst et al. 2017, Rodriguez et al. 2021, Berru et al. 2023). A cost-effective alternative for monitoring slope displacements is the Global Navigation Satellite System (GNSS) combined with the real-time

kinematic (RTK) technique, which form a network known as a differential GNSS (dGNSS). This technology has gained popularity due to its frequent data collection, relatively high accuracy, and the progressively decreasing cost in recent years (Berru et al. 2023). The dGNSS can enhance the accuracy of the network monitoring points to centimeter levels in the vertical and horizontal axes (Takasu and Yasuda 2009).

The Geocube system, a proven dGNSS for monitoring landslides, has been deployed on landslides in Western Canada. However, it encounters challenges due to the harsh Canadian winter and the remote locations where these landslides are situated. The Geocubes system requires uploading monitoring data to a cloud, which becomes problematic during periods when phone signals are lost. This emphasizes the ongoing need to explore more cost-effective monitoring options and evaluate their practicality, assembly costs, instrument precision, accuracy, and reliability in the Canadian environment. These efforts offer valuable opportunities to enhance landslide monitoring, especially anticipating an increase in landslide hazards due to imminent climate change in the region.

1.1 Problem Statement

The potential for landslides in the interior plains could be intensified by the effects of climate change, which is altering temperature, precipitation, and water usage patterns. This poses a major risk to diverse structures such as highways, railways, communities, reservoirs, and farmlands. To ensure maintenance resilience for these structures, assessing potential changes in landslide hazards and developing new monitoring tools are vital.

Drawdown is a climate change event that has the potential to produce large-scale soil mass displacement, generating or exacerbating the hazard posed by shore landslides. It incorporates multiple aspects, including shear strength, material behaviour, hydraulic parameters, reservoir water level, and estimates of present and future drawdown rates. All of these elements complicate

the procedure; hence, a consistent, systematic method is needed to investigate both present and future drawdowns induced by climate change's effects on landslide stability.

Exploring alternatives to traditional in-situ monitoring instruments is essential for addressing numerous current and future landslide cases, allowing for a better understanding of the failure mechanism, and reducing associated risks. An increase in landslide activity will require cost-effective monitoring strategies to allow adequate landslide risk management for the available resources. dGNSS networks are a promising option for monitoring landslide displacements due to their high collection frequency, relatively high accuracy, and decreased cost. However, it still faces challenges related to deployment in the remote and harsh conditions of western Canada. This highlights the need to continue exploring cost-effective dGNSS systems, and evaluating their implementation costs, instrument precision, accuracy, and reliability in the Canadian environment. This is essential for optimizing resources, addressing drawbacks, improving the system, and enhancing its robustness.

1.2 Research Objectives

The objective of this thesis is to develop practical and cost-effective tools for improving landslide risk management, especially in response to the increasing number of landslides in the Canadian plains due to climate change impacts. It aims to provide an affordable monitoring tool for managing different scenarios and a methodology for estimating current and future shoreline landslide instabilities.

The specific objectives of this research are:

i. Assembly (customize) and evaluate the viability of a cost-effective dGNSS technology as a surface landslide monitoring instrument in the Canadian plains, assessing aspects like accuracy, robustness, simplicity of configuration, and deployment expenses. Contrast the monitoring data with another proven dGNSS technology deployed at the same landslide

site. Identify and determine potential limitations to address these issues in future deployments.

ii. Provide a methodology for examining how the current and future drawdown scenarios, caused by climate change, impact the landslide stability in the Canadian Plains. Assess the methodology effectiveness by applying it on a landslide case study.

1.3 Overview of Methodology

The specific objectives are achieved by applying them to a real case in the Canadian plains, serving as a basis for extending these methods to similar landslides in the region. The selected landslide for this study is situated on the northern bank slope of a reservoir and has been impacting a highway since the mid-1970s; its description is presented in Chapters 3 and 4. A summary of the methodology used is as follows:

1.3.1 Introducing dGNSS Network

The methodology used to accomplish specific objective one is described below; a more detailed methodology is presented in Chapter 3.

1. Assembling and pre-testing dGNSS units before deployment to assess the appropriate components, manufacturer's capabilities, accuracies, including storage capacity, and the ability to form and maintain a dGNSS network.
2. Deploying the dGNSS units at a landslide site assess their capacity to maintain the dGNSS network, the robustness of the equipment to withstand harsh weather conditions in Canada, and to collect monitoring data.
3. Processing and analyzing monitoring data to interpret the results, such as measuring displacements, identifying variations in measurements, and tracking displacement trends.
4. Comparing the monitoring data with another proven dGNSS network installed at the site to confirm that dGNSS network exhibits similar displacement trends.

5. Evaluate the capital cost of the dGNSS network and identify challenges within the system to improve in subsequent deployments.

1.3.2 Methodology to analyze landslides as plausible Climate Change Scenarios

This section describes the approach taken to achieve the specific objective number two; a more detailed methodology is presented in Chapter 4,including methods of analysis, software used, and material parameters.

1. Reviewing background information of the landslide site, which includes site investigation reports, monitoring instrument reports, in-situ and laboratory testing reports, and reservoir water levels.
2. Defining the representative section and constitutive model that will reflect the landslide failure mechanism and materials behaviour.
3. Selecting the most representative properties for all stratigraphy units of the landslide based on background information and complementing them with the literature review.
4. Calculating drawdown rates that represent the most appropriate scenarios affecting the current stability of the landslide based on the reservoir water levels.
5. Conducting a permeability back analysis and a 2D stability back analysis to validate the landslide hydraulic and shear strength properties.
6. Estimating future drawdown rates and conducting a stability analysis of the landslide under these estimated drawdown rates to calculate the decrease in percentage of stability.

1.4 Thesis Structure

The thesis comprises five chapters. A brief overview of each chapter is as follows:

- Chapter one describes the introduction, outline the research objectives and methodology.

- Chapter two provides a literature review to establish the context for this study. It includes an explanation of how dGNSS networks work, prior implementations of this technology internationally and in Canada, discussions on the implications of climate change in Canada, and case studies on landslide instability resulting from drawdown. Additionally, the chapter explores available methods for evaluating drawdown scenarios. A more comprehensive literature review is provided in the first and second journal papers (Chapters 3 and 4, respectively).
- Chapter three (Manuscript #1) is presented in a form of a paper-based thesis. It introduces a dGNSS technology and assesses its suitability as a monitoring option for landslide displacements. It details its deployment, components, and testing results after a 6-month monitoring period at a landslide in southern Alberta.
- Chapter four (Manuscript #2) is also presented in a form of a paper-based thesis. It describes a methodology to analyze the stability of a landslide under current and potential future drawdown scenarios resulting from climate change. The approach is examined using a case study that compares its stability to the current state when larger drawdown rates are considered.
- Chapter five includes the conclusion and recommends a path for future research work.

2 LITERATURE REVIEW

This section provides a summary of relevant concepts for this research, including the differential Global Navigation Satellite System (GNSS) proposed as a low-cost tool to monitor landslide displacements, the impact of climate change on reservoir drawdowns, and the effects on landslide stability. A detailed account of the features, instruments, and methodologies applied in this research can be found in the respective chapters of the manuscripts, Chapters 3 and 4.

2.1 dGNSS Technology

GNSS units use data from at least four satellites (BeiDou, Galileo, GLONASS, GPS, IRNSS, and QZSS) to determine their geographic location (Berru et al. In Press). This is achieved by calculating the time it takes for signals from these satellites to reach the GNSS unit, estimating the distances, and then triangulating them to determine the GNSS unit's location (Harris 2023, Rodriguez et al. 2021, Berru et al. 2023). GNSS units can have single, dual, or multifrequency capabilities, where the frequency indicates the number of signals received from each satellite (Septentrio 2023). The use of dual or multi-frequencies reduces a significant portion of the signal delay caused by the ionosphere (Septentrio 2023). This is because having a larger number of frequencies allows for a more accurate measurement of atmospheric properties by comparing the time of arrival of different signals (Deane 2020). The accuracy of GNSS units is influenced by several aspects, including the performance of the GNSS receiver, the orbital position of satellites, and surrounding features such as buildings, tree cover, and weather conditions (Rodriguez et al.2021). Under ideal conditions, a GNSS unit can achieve an accuracy of approximately ±2 m (Ardusimple 2023, Deane 2020). However, most engineering applications require even more exact measurements (Deane 2020).

Real-time kinematic (RTK) technique is critical for improving accuracy and meeting engineering standards. This method requires a minimum of two GNSS units: one as the “Base unit”, which is installed in a fixed location and has pre-calculated coordinates, and the other as the “Rover unit”,

whose location must be determined (Berru et al. 2023). The base unit uses satellite signals to estimate its position and compares it with the pre-estimated coordinates to assess how much error is caused by environmental conditions and atmospheric interference (Rodriguez et al.2021, Berru et al. 2023, Berru et al. In Press) and estimate the corrections needed in the dGNSS network. Subsequently, the rover unit receives these corrections from the base, which allows it to have a greater accuracy (Figure 3.1). Using this technique, the rovers can achieve centimeter-level accuracy in both horizontal and vertical directions (Takasu and Yasuda 2009, Deane 2020, Berru et al. 2023). The base and rover units form the differential Global Navigation Satellite System (dGNSS). When more rover units are required, they can be added to the system as monitoring points (Berru et al. 2023). The GNSS manufacturer and the method used to transmit the errors determine the distance between the rover and the base units. The main requirement is that the rovers and base should be able to share the same atmospheric interferences. Additionally, a clear line of sight is required to minimize multipath errors resulting from nearby objects, rain, or snow, but these last two disruptions are of short duration (Deane 2020, Rodriguez et al. 2021).

The application of dGNSS technology for landslide monitoring has seen increased adoption (Berru et al. 2023). Malet et al. (2022) deployed a dGNSS network at the Super-Sauze earthflow in France, achieving millimeter accuracy. The GPS constellation was the only source of data for the dGNSS technology. The flow displacement measured by the dGNSS correlated with observations from other monitoring technologies at the site, facilitating continuous monitoring and providing 3D kinematics data that other technologies could not offer due to the area's instability and difficult accessibility (Malet et al. 2002). Tagliavini et al. (2007) used a GNSS network with dual-frequency capabilities and employed the GPS constellation to measure a landslide's velocity in Italy. The estimated velocities matched records from inclinometers installed near the GNSS units, validating a methodology for hazard mapping (Tagliavini et al. 2007).

Benoit et al. (2015a, b) tested a single-frequency GNSS system in the French Alps for monitoring surface landslide displacements. The system is referred as Geocube and was developed by Ophelia Sensors. These Geocube dGNSS units are equipped with an SL1206 antenna for differential positioning and LEA-6 T GPS chip. Employing the RTK technique, the Geocube dGNSS network used a base unit positioned in a stable area to correct the rovers' positions (monitoring points) and achieved millimeter accuracy (Benoit et al. 2015a; Rodriguez et al. 2021). The Geocube dGNSS network demonstrated favorable outcomes attributed to its ease of deployment, low power consumption (requiring only a 10 W solar panel), high data collection frequency (30 s data collection rate), cost-effectiveness enabling the installation of multiple GNSS units, and high accuracy in the millimeter range. Geocubes contributed to a more comprehensive understanding of the landslide's kinematics, including its periods of acceleration and dormancy (Benoit et al. 2015a, b; Rodriguez et al. 2021). Geocube units were deployed at the 10-Mile slide in British Columbia, Canada, and underwent an 8-month testing period. The recorded displacements by the Geocubes aligned with other monitoring technologies at the site, achieving millimeter accuracies (3 mm horizontal and 5 mm vertical), offering dense spatial coverage, and high collection frequency (60 s intervals). However, the system encountered challenges related to the power supply system due to extreme weather conditions and the necessary internet connectivity for uploading monitoring data to the Ophelia cloud server (Rodriguez et al. 2018), caused by the terrain landform. As a result, the data had to be collected manually.

In 2018, Geocube units were deployed at the Chin Coulee landslide, tested for approximately fourteen months to monitor displacements, and investigate additional flaws in the dGNSS network. Nine Geocube units were installed at the sliding area, with the base unit positioned at a stable area crossing the Chin reservoir. Helical piles, embedded 1 m into the ground, were used to mount the Geocubes, employing the same power supply system as the one used at the 10-Mile landslide. This power system included two 12 V, 100 Ah batteries and a 10 W solar panel

(Rodriguez et al. 2021). The GNSS achieved appropriate accuracy, with results consistent with the outcomes of Leica GPS measurements, suggesting that the dGNSS network is a viable technology for monitoring landslide displacements at a reasonable cost, enabling high spatial coverage and frequency (Rodriguez et al. 2021, Rodriguez 2021).

The SparkFun dGNSS units, developed by SparkFun Electronics, are designed for surveying purposes. They utilize the GPS, GLONASS, Galileo, and BeiDou constellations, and employ the RTK technique to enhance accuracy, achieving 14 mm in the horizontal and 10 mm in the vertical dimensions (Berru et al., 2024). While the SparkFun dGNSS units require additional components, such as dual-frequency antennas, power supply systems, and radios to transmit corrections from the base to the rovers as work as a dGNSS network, they possess dual-frequency capabilities, operate at a high data collection frequency (up to 20 Hz in a dGNSS), accommodate a 32 GB SD card, and have a power consumption of approximately 240 mA. These characteristics make the SparkFun dGNSS units a suitable alternative for investigating their effectiveness as a dGNSS system for monitoring landslide displacements in this research.

2.2 Climate Change

Climate change has the potential to modify precipitation, wind patterns, vegetation types, temperatures, and the frequency of floods (Bo et al. 2008). However, significant effects resulting from climate changes include extreme weather events related to temperature and precipitation (Tao et al. 2012, Labajo et al. 2014, Bagheri 2022). Natural soil slopes have a Factor of Safety (FoS) of one or slightly above, these changes may cause the resisting forces on those slopes to decrease and add new driving forces, creating an unstable slope (Bo et al. 2008).

It is anticipated that northern regions, such as Russia, Canada, or Greenland, will experience an increase in temperature every decade, ranging from 0.3°C/decade to 0.8°C/decade, with a maximum increase of 8°C (Bo et al. 2008). For example, an analysis of data from all Canadian stations from 1948 to 2016 as well as data from southern Canada, especially from 1900 to 2016,

revealed that Canada's climate is changing, with more hot days and nights occurring in the country's southern parts (Vincent et al. 2018, Bagheri 2022). The Canadian Prairies, comprising Alberta, Saskatchewan, and Manitoba, expected a temperature increase of 6.5°C. This warming may increase the rate of evapotranspiration, potentially amplifying the demand for water during the peak growing season (Muhammad et al. 2020).

The southern part of the Prairies is the driest due to its location beneath the shadow of the Rocky Mountains and its isolation from sources of moisture. In this region, precipitation has decreased by an estimated 10% since 1950 (Bhatti et al. 2021). These circumstances contribute to a significant increase in water resource usage. Water is distributed for various purposes, such as human consumption, industrial activities, and irrigation. In Alberta, irrigation water accounts for 60 to 65% of the province's average total water consumption (Alberta 2012). Alberta's irrigation sector constitutes 65% of the total irrigation area in Canada. For instance, to meet the demand for water resources, there are 32 off-stream reservoirs and 14 along-stream reservoirs in southern Alberta alone (Alberta 2023b).

Water used in agriculture typically does not return to the original ecosystem. Furthermore, some water is needed to maintain minimum water levels in canals and reservoirs, facilitating the transport of irrigation water within the system (Alberta 2012). This demand for water and the requirements of the irrigation system to work properly have led to major fluctuations in reservoir water levels, resulting in a higher probability of drawdown occurring in the southern region of Alberta if conditions get drier or dry periods are longer.

Drawdown can cause the reactivation of pre-existing landslides and the initiation of new landslides (Yin et al. 2016). This phenomenon reduces the external force applied by the reservoir water to the slope, acting as a support. It may also lead to higher excess pore water pressures, depending on the permeability of the soils constituting the landslide and the drawdown rate (Bo et al. 2008, Alonso and Pinyol 2009). For instance, at the Grand Coulee Dam in Washington, United States

of America, about 150 landslides were triggered during two drawdown periods, with reductions in water levels ranging from 10 m to 20 m (Schuster 1979). A deep-seated rockslide system above the Gepatsch Dam reservoir in Austria experienced acceleration during drawdown, reaching maximum velocities when the reservoir levels were at their lowest (Zangerl et al. 2010). In Spain, a landslide (40×10^6 m³) on the left bank of the Canelles reservoir was reactivated following a significant decrease in the reservoir level. The drawdown rate ranged from 0.5 m/day to 1.2 m/day (Pinyol et al. 2011). In the Three Gorges region in China, significant deformation of the Liangshuijing landslide occurred during the drawdown of the Three Gorges reservoir. This event resulted in the blockage of the Yangtze River for several days, and concurrently, the Gongjiafang landslide was also reactivated (Yin et al. 2016).

2.3 Drawdown Analysis

The stability of slopes, whether partially or entirely submerged, can be significantly influenced by a drawdown event (Alonso and Pinyol 2016). This scenario combines the effects of external loads, such as the removal of supporting forces, and seepage forces within the slope, both of which come from the drop in water levels (Alonso and Pinyol 2016). The slope permeability and drawdown rate determine how much excess pore water pressure is dissipated on a slope during the drawdown. This dissipation of excess pore pressure might happen instantaneously or take several months, causing a decrease in stability and the probable failure of the slope (Berilgen 2007, Alonso and Pinyol 2016). These analyses can be conducted using the Limit Equilibrium Method or numerical methods (Berilgen 2007). However, numerical methods like the Finite Element Method (FEM) allow for the assessment of the stability by incorporating the effects of stress, seepage, nonlinear material behavior, intricate boundary and loading conditions, and the inclusion of transient drawdown, where the drawdown rate is considered (Berilgen 2007). This approach is typically known as a FEM coupled analysis.

In FEM analysis, the strength reduction method (SRM) is commonly employed for stability analysis. This involves applying different trial strength reduction factors (SRF) to the material shear strength parameters until the slope reaches the failure point, preventing numerical convergence issues. The process aids in identifying the critical SRF, equivalent to the Factor of Safety (FoS) in limit equilibrium analysis (Renani and Martin, 2019). The SRM applied to a material using the Mohr-Coulomb method, can be obtained through the following equations (Rocsience 2004):

Equation 2.1 $$\frac{\tau}{SRF} = \frac{C\prime}{SRF} + \frac{\tan \varphi\prime}{SRF}$$

Equation 2.2 $$\frac{\tau}{SRF} = C^* + \tan \varphi^*$$

Equation 2.3 $$C^* = \frac{C\prime}{SRF}$$

Equation 2.4 $$\phi^* = \tan^{-1}\left(\frac{\tan \varphi^*}{SRF}\right)$$

where τ is the shear stress, c is the cohesion, φ' is the friction angle, C^* and is ϕ^* are the reduced Mohr-Coulomb parameters (Rocsience 2004).

Echuan et al. (2009) created a three-dimensional (3D) numerical model to analyze the Tangjiao village landslide deformation after a drawdown event. The model results were compared to on-site observations, demonstrating good agreement. Tensile cracks, and multi-stage small landslides were observed on the frontal and mid-ground surfaces. These deformations are directly linked to the reservoir water level fluctuation, dropping from 156 m on March 15 to 149 m on April 11, 2007. (Echuan et al. 2009). The Canelles landslide in Spain was analyzed under a drawdown scenario to investigate if this phenomenon led to the reactivation of a dormant translational slide. Reservoir water levels significantly decreased after a dry period, reaching a level of 426 m, with the maximum recorded water level being 505 m (Alonso and Pinyol 2016). Residual strength values were considered for the analysis as the landslide reactivated. The stress–strain behavior

of the materials was characterized using a linear elastic law determined by Young's modulus and Poisson's ratio. Piezometer records were used to validate the numerical model, and reservoir elevation records were simulated for the four years preceding the drawdown (Pinyol et al. 2011). Further sensitivity analysis, simulating drawdown at different rates, revealed the challenging nature of implementing practical control over the drawdown (Pinyol et al. 2011). The Qiaotou Landslide, located adjacent to the Three Gorges Reservoir (TGR) in China, exhibited significant displacements during the drawdown. To understand its deformation mechanism, a numerical simulation employing the saturated and unsaturated fluids theory was performed. The findings revealed that the region of maximum displacement in the landslide mass transitions from the upper section, marked by a steeper bedrock surface and thinner deposit, to the middle section, characterized by a less steep bedrock surface and a thicker deposit, as the drawdown progresses (Jian et. al. 2009).

3 INTRODUCTION AND TESTING OF A COST-EFFECTIVE GNSS SYSTEM FOR LANDSLIDE MONITORING

A version of this chapter has been accepted for publication in the journal *Natural Hazards* with the title “Introduction and Testing of a Cost-Effective GNSS System for Landslide Monitoring”.

Abstract

The use of Global Navigation Satellite System (GNSS) in combination with real-time kinematic (RTK) technique, known as differential GNSS (dGNSS), has increased in recent years for monitoring landslide displacements and detecting early signs of potential failure, enabling earlier response for risk mitigation than traditional monitoring techniques. GNSS offers several advantages, including high accuracy and high-frequency data collection. Although more cost-effective, their affordability may still present challenges for public organizations managing multiple landslides in their territory. The SparkFun is a suite of components for GNSS assembly designed for topographic surveying, that integrates u-blox ZED-F9P or ZED-F9R modules. The system offers the benefits of dGNSS technology while being more affordable than other market options. It also avoids relying on phone signals for data storage on a cloud server. This paper presents the SparkFun system, its components, and how it can be assembled to create a dGNSS system for landslide monitoring. The deployment and testing at the Chin Coulee landslide in Alberta are discussed. Over the 6-month testing period, the system achieved milimeter accuracy (up to 14 mm), aligning with the manufacturer's specifications. Estimated system errors were found to be comparable to a commercially available dGNSS system (Ophelia Geocube). Additionally, the system exhibits displacement trends similar to the 2018 Geocube monitoring campaign; however, for future deployments, the robustness of the power supply system and the insulation of the equipment need to be enhanced. Overall, the SparkFun system appears to be a promising and cost-effective alternative to monitor landslide displacements.

Keywords

dGNSS system, Cost-effective, Landslide, Monitoring

3.1 Introduction

Slope monitoring is a fundamental approach for managing the risks posed by landslides. Monitoring aims to detect early signs of slope failure to provide timely warnings and is an important step in risk mitigation plans (Chae et al. 2017). Landslide monitoring often involves drilling boreholes and installing in-situ instruments such as ShapeAccelArrays (SAAs), slope inclinometers (SI), and piezometers (Smethurst et al. 2017; Rodriguez et al. 2021). Borehole drilling for down-hole instrumentation carries high installation costs that may result in a limited number of instrumentation installations due to budget constraints. Additionally, gaining access to drill pad sites might involve building access roads and clearing trees, obtaining permission for accessing privately owned land, and strategies to minimize the potential impact on the stability of these slopes due to earthworks (Rodriguez et al. 2021; Berru et al. 2023). The location of overhead and underground utilities may also affect the ideal placement of boreholes. These limitations highlight the need for exploring the use of cost-effective monitoring devices that offer more extensive and accurate coverage of landslides while minimizing their impact on the environment (Rodriguez et al. 2021) as a complement or alternative to down-hole instrumentation (depending on the characteristics of the site).

The use of Global Navigation Satellite Systems (GNSS) units to monitor landslide displacements has increased due to their ability to collect data at high frequencies, high level of accuracy, and a gradual decrease in their cost over the last decades (Shen et al. 2019). GNSS units estimate their position by calculating the time it takes for signals from at least four satellites across different constellations (BeiDou, Galileo, GLONASS, GPS, IRNSS, and JQZSS) to reach them. These time measurements are used to calculate the distances from the satellites to the units. Subsequently, these distances are triangulated to determine the GNSS unit's position (Harris 2023). Also, GNSS units can calculate the position using single-frequency or multi-frequencies from the constellations

they track. Multi-frequency GNSS units provide a more robust calculation of the position, reaching millimetre accuracy; however, these commercial devices can be very costly. Alternatively, single-frequency GNSS units have a horizontal accuracy of approximately 1.89 m (Deane 2020), because they are unable to correct errors caused by atmospheric layers, multipath errors resulting from signal reflections off nearby objects, internal noise within the device, and satellite orbits (Doberstein 2012; Miller et al. 2015). The real-time kinematic (RTK) technique can correct these signal errors and significantly improve the relative accuracy of the GNSS unit. Typically, an RTK setup comprises at least two GNSS units: a GNSS unit, known as the “base”, which is installed at a location known to be stable and fixed, with known coordinates, and a GNSS unit, known as the "rover", whose coordinates are unknown. The satellite signals received by the base and rover have errors. However, the base can correct the errors of the rover by transmitting differential correction data calculated by the GNSS module based on its fixed position. The transmitted corrections increase the position accuracy of the rover to within centimeters or millimetres, depending on the system (Figure 3.1 for a layout example). Some GNSS units allow more than one rover to be linked to a base, which establishes a monitoring network of survey monuments.

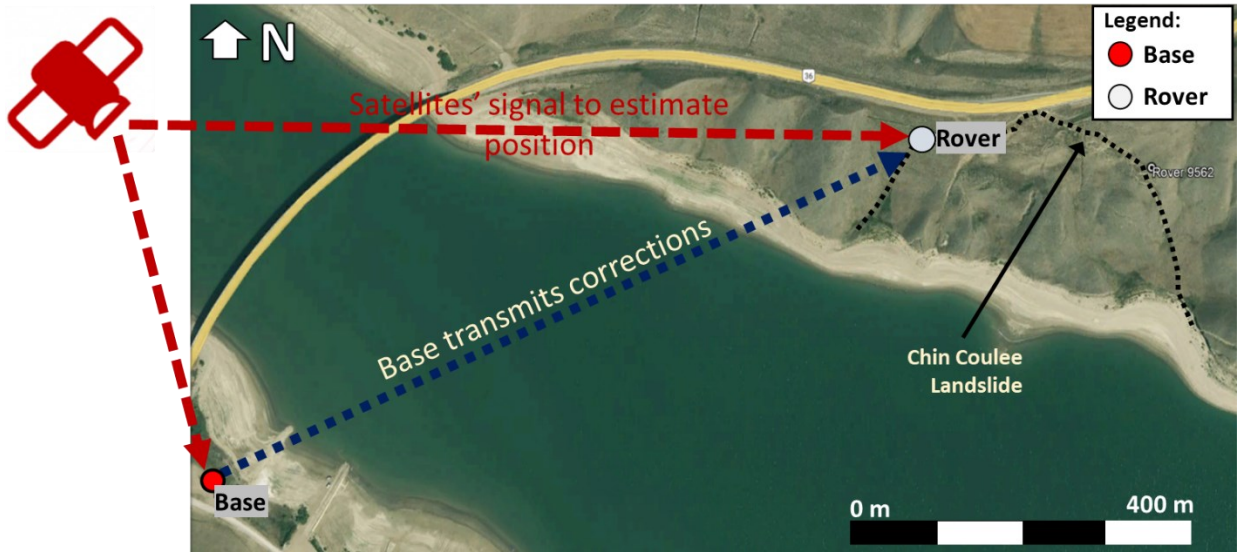

Figure 3.1 Real-Time Kinematic technique schematic (Photo right: S. Alberta MDs and Counties, Google Earth Image)

GNSS measurements using the RTK technique are commonly known as differential systems (dGNSS), which offer similar advantages to a single GNSS unit but with increased accuracy. Modern dGNSS can achieve horizontal and vertical accuracies of 1 cm and 2 cm, respectively (Takasu and Yasuda 2009). Various studies have assessed the performance of dGNSS for landslide monitoring. Gili et al. (2000) demonstrated that using only the GPS constellation, dGNSS could achieve centimeter-level accuracy, even in diverse weather conditions. Malet et al. (2002) reported millimeter-level accuracy in hourly monitoring sessions at the Super-Sauze earthflow in France, using solely the GPS constellation. In Italy, a dual-frequency dGNSS system was employed to verify a landslide hazard assessment, with base-to-rover distances ranging from 100 m to 3000 m. The deformation rates obtained from the dGNSS were compared with inclinometer data in the area, which showed rates of 4.75 cm/month and 3.8 cm/month for the inclinometer and the GNSS unit in its proximity, respectively (Tagliavini et al. 2007). Takasu and Yasuda (2009) developed a low-cost, single-frequency RTK-GNSS unit and an open-source package library containing position algorithms. The system achieved 1 cm accuracy using only the GPS constellation, with an estimated component cost of $400 USD (Currently approximately $570 USD). However, it presented some limitations: the single frequency requires more time to estimate the position compared to a multi-frequency. The unit needs to be connected to a PC to estimate its position, limiting its deployment to sites with a constant power source. Users must also be knowledgeable about configuring the unit's serial port and IP address. Despite these limitations, this system highlights the potential for cost-effective monitoring alternatives.

Differential GNSS (dGNSS), using various satellite constellations, has enhanced accuracy and reliability (Rodriguez et al. 2021). Technological advancements have enabled the development of low-cost, compact, and energy efficient GNSS units capable of accurate displacement monitoring (Cina and Piras 2015). As a result, this technology has been used in a variety of applications. For instance, Manzini et al. (2022) tested a dGNSS network to study its suitability for structural health

monitoring (SHM) applications. The system demonstrated the capability to track displacements of 4 mm, highlighting its promising performance in accurately detecting displacement. Similarly, Xue et al. (2022) tested low-cost dGNSS networks to evaluate their performance in monitoring dynamic motion. The testing showed that the accuracy of the low-cost GNSS receivers could be increased between 2 mm and 4 mm. Caldera et al. (2022) demonstrated that a dGNSS network, comprising three GNSS units, achieved up to 2 mm accuracy when was tested in bridge structure for 4 years.

Regarding the use of dGNSS to monitor landslides, Cina and Piras (2015) evaluated the capability of single-frequency mass-market GNSS units to detect minimal deformations. Their results demonstrated promising outcomes, with the GNSS units achieving millimeter accuracy. Although they emphasized the necessity for additional testing in real-case scenarios to further assess their capabilities. The French Institut Géographique National developed the Geocube system, a single-frequency GNSS system that combines a GNSS wireless network and a multi-sensor unit (Benoit et al. 2015a). Deployed in the French Alps at the Super-Sauze landslide and the Glacier d'Argentière (Benoit et al. 2015a, b; Rodriguez et al. 2021), the Geocubes have demonstrated ease of deployment, high frequency of measurements, low power consumption (0.27 watts), millimeter precision (2 mm) even in challenging field conditions and a relatively low capital cost of approximately $4500 CAD per unit (Currently approximately $3925 USD) (Rodriguez 2021; Berru et al. 2023). These characteristics make them a suitable option for monitoring locations where power restrictions or budget constraints previously limited monitoring possibilities (Benoit et al. 2015a, b; Rodriguez et al. 2021). Hamza et al. (2023) developed and tested a cost-effective GNSS monitoring system on a Slovenian landslide site. The system's results were compared to those of high-end geodetic instruments, revealing differences of up to 7 mm between the two technologies, concluding that the developed system presents a viable option for accurately monitoring slow movements.

In Canada, Geocubes were initially deployed at the 10-mile and Ripley landslides in British Columbia (Rodriguez et al. 2018). This was soon followed by their implementation at the Chin Coulee landslide in Alberta, Canada (Rodriguez et al. 2021). Ten Geocubes were deployed at the Chin Coulee site: four were installed on the moving soil mass, five on the landslide's perimeter near the scarps to monitor for potential landslide retrogression, and one on a fixed and known position across the reservoir (Rodriguez et al. 2021) (Figure 3.2).

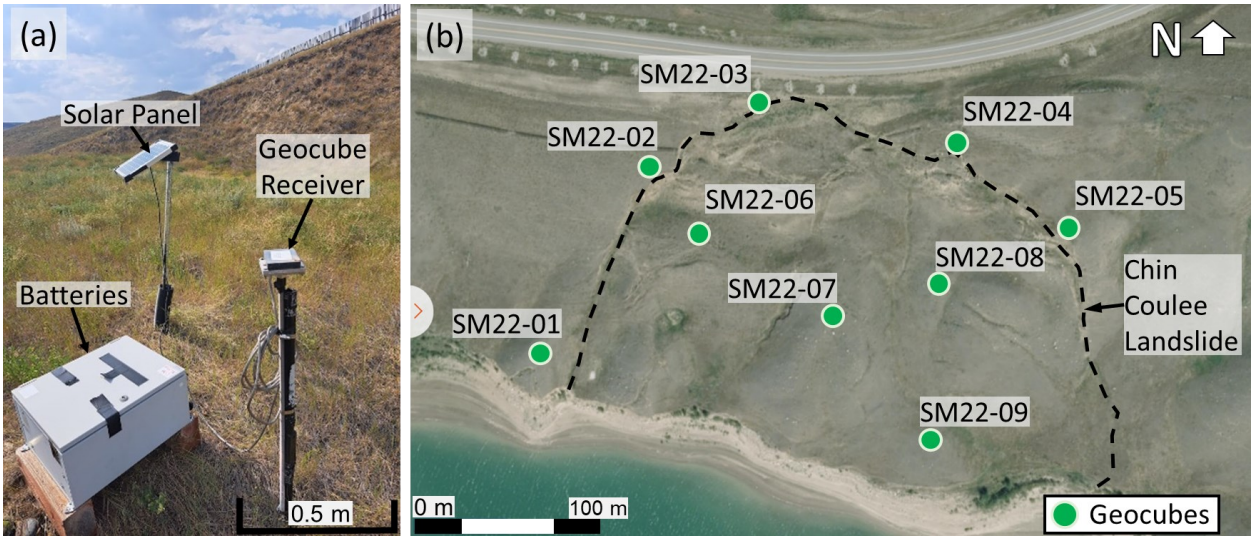

Figure 3.2 (a) Geocube unit schematic and (b) Location of Geocubes units at Chin Coulee Landslide (Figure B's right: Ophelia Sensors)

The performance of the Geocubes was tested considering the Chin Coulee is a slow-moving landslide (up to 50 mm/year) according to the classification by Cruden and Varnes (2013). The findings indicated that the Geocubes provide reasonably accurate data at a relatively low cost, reaffirming their suitability as an alternative for landslide monitoring and early warning systems. However, the Geocubes system requires a phone signal at the monitoring area because it needs to upload the monitoring raw data to Ophelia's cloud server, where the manufacturer post-processes the data and provides near-real-time positioning on a fee for service basis. While this service is convenient for users with healthy budgets, the costs are not inconsequential for long term monitoring campaigns. Relying on the manufacturer for data post-processing can be problematic in remote locations with limited internet access or for organizations that require

secure, non-shared monitoring information to comply with their corporate cybersecurity policy. This limitation raises the question of whether there are alternative options with similar technical advantages to Geocubes but without the need to depend on the manufacturer for post-processing the data or incurring additional data maintenance costs.

In this quest, the SparkFun RTK emerged equipped with dual-frequency capabilities, for high-frequency measurements and the capacity to achieve millimeter-level accuracy when combined with real-time kinematic (RTK). The recorded data from SparkFun units is stored on a microSD card, eliminating the need for cloud storage services or third-party post-processing. The capital cost of each SparkFun in a RTK setup in 2022 is approximately $1930 USD, making it a cost-effective solution for those with budget constraints or those requiring multiple monitoring points on a moving mass. These attributes position SparkFun GNSS units as a practical alternative for landslide monitoring (Table 3.5).

This paper provides an overview of the GNSS SparkFun system and assembly for landslide monitoring, including pre-deployment tests conducted to determine the optimal configuration for displacement monitoring. It describes the deployment of the GNSS system at the Chin Coulee landslide and compares its monitoring data with the results obtained from the Geocubes system. The goal of the work in this paper was to evaluate the viability of the GNSS SparkFun system as a reliable monitoring solution and report the results to-date to the geotechnical community for its adoption and further development by others.

3.2 Chin Coulee Landslide

The Chin Coulee landslide is located in southern Alberta, approximately 20 km south of Taber, adjacent to Highway 36, specifically on the north slope of Chin Reservoir (Deane et al. 2020; Deane 2020; Rodriguez 2021; Rodriguez et al. 2021) (Figure 3.3a,b). The landslide is approximately 50 m height and 350 m wide, has an approximate volume of 2 Mm^3 and a slope inclination that varies from 9^o to 13^o (Deane et al. 2020).

Several site investigations have been conducted to characterize the landslide stratigraphy, which comprises three main units. The uppermost unit is a medium plasticity clay fill layer, placed as part of the highway construction. Beneath the clay fill is a layer of stiff to very stiff glacial till, with low to medium plasticity and containing sand and silty lenses. The thickness of the glacial till ranges from 5 m at the toe to 40 m near the head scarp. The lowest layer is sedimentary bedrock which consists of interbedded layers of grey to brown siltstone, sandstone and medium to high plasticity silty clay shale. Coal seams were encountered within the clay shale (Deane et al. 2020; Deane 2020; Rodriguez 2021; Rodriguez et al. 2021) (Figure 3.3b, c).

Field instruments were installed during multiple campaigns. Standpipe and vibrating wire piezometers, as well as measurements of the reservoir water level, indicate that the groundwater table depth varies from 12 m near the head scarp to 3.5 m at the landslide toe (Rodriguez 2021). slope inclinometers (SI) were installed at the head scarp to monitor the retrogression of the landslide, which could potentially affect the nearby highway. The SI measurements, in correlation with a low shear strength zone associated with coal seams encountered within the clay shale, suggest that the Chin Coulee landslide is a translational deep-seated landslide that is sliding over a sub-horizontal coal seam encountered at a depth of approximately 62 m below the head scarp (Deane et al. 2020; Deane 2020; Rodriguez 2021; Rodriguez et al. 2021).

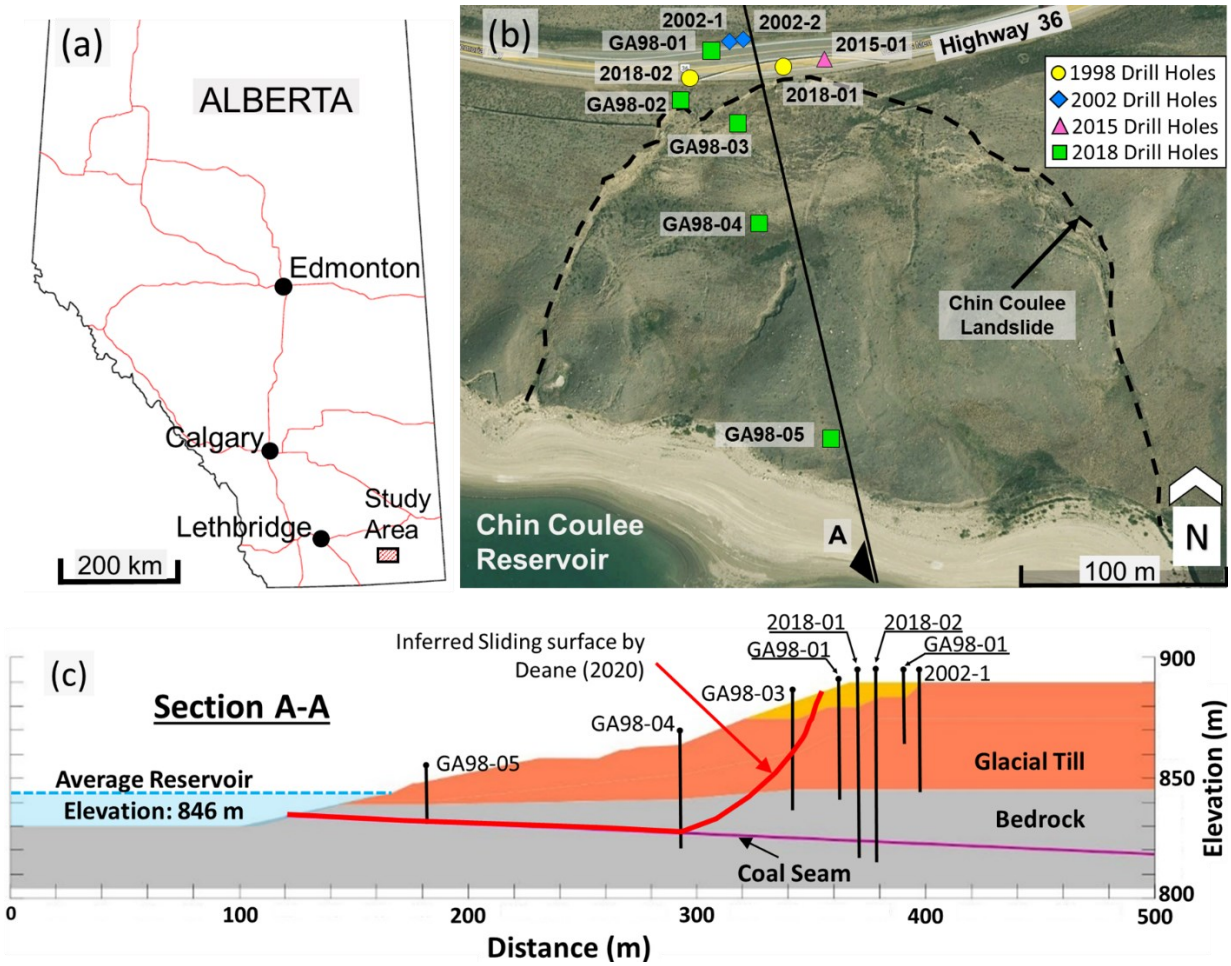

Figure 3.3 (a) Chin Coulee landslide location in Alberta (b) Plan view and site investigation's locations (C) Typical section (Figure B's right: Alberta MDs and Counties, Google Earth Image)

3.3 GNSS SparkFun System

SparkFun Electronics specializes in producing and offering a diverse range of electronic components (SparkFun 2023a), such as circuit boards, sensors, and antennas. They have also developed topographic survey GNSS units, known as SparkFun RTK. These units integrate a high-precision positioning GNSS module built by u-blox (SparkFun 2023b, c). The SparkFun unit model discussed in this paper includes either a ZED-F9P or ZED-F9R module (Ublox 2023a, b). Both modules can receive and track four global navigation satellite system constellations (GPS, GLONASS, Galileo, and BeiDou) and operate on dual-frequency bands (L1 - 1575.42 MHz / L2 - 1227.60 MHz), enhancing satellite signal reception and reducing interference (Rodriguez et al. 2021). The main difference between these two modules lies in their functionality within a dGNSS

setup. SparkFun units with a ZED-F9R are designed solely for use as rover units and can only receive corrections to enhance their position accuracy. Additionally, they feature an embedded display that allows for monitoring the accuracy of the rover unit (SparkFun, 2023a). The SparkFun units equipped with the ZED-F9P module do not have the display, but they can both send or receive corrections, allowing them to work as base or rover units, respectively.

The SparkFun unit features an SMA port for connecting an L1/L2 GNSS antenna, and two USB-C ports, which allow for changing the configuration or charging the units. It also includes a radio port that enables sending or receiving correction data to enhance the unit's accuracy. The unit is equipped with a 1300 mAh battery, consuming approximately 240 mA; it has a micro-SD socket that allows for SD cards with a capacity of up to 32 GB to record GNSS data. The units record time, number of satellites in view, longitude, latitude, geocentric coordinates (X, Y, and Z), height above mean sea level (MSL), height above ellipsoid (HAE), as well as horizontal and vertical accuracy. The SparkFun unit's main hardware architecture is shown in Figure 3.4.

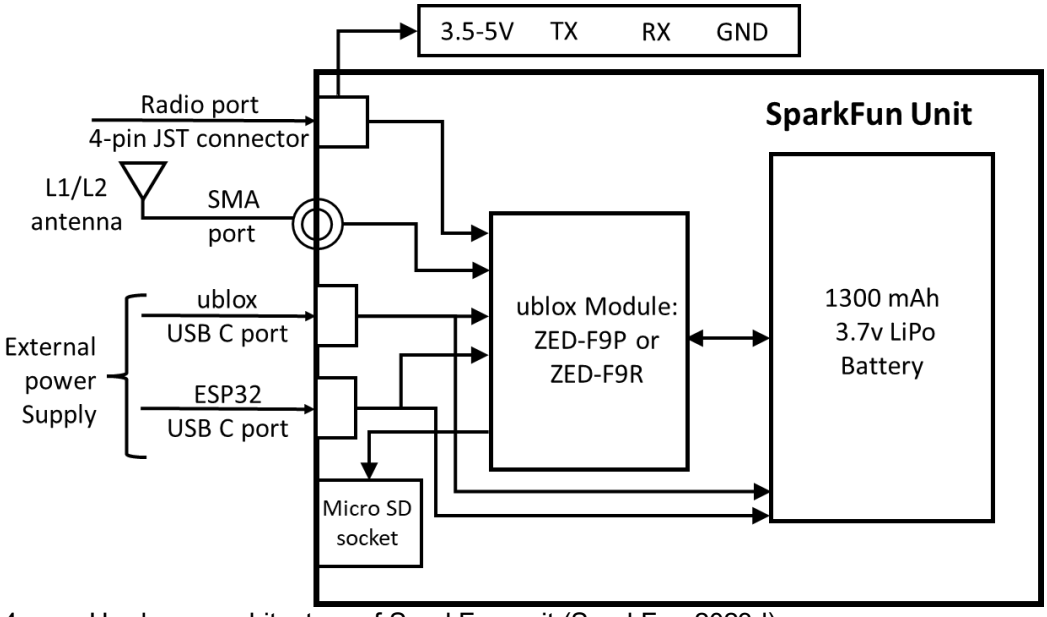

Figure 3.4 Hardware architecture of SparkFun unit (SparkFun 2023d)

The SparkFun units can be configured using the open access software U-center (Ublox 2023c), via WIFI or through a terminal window, such as Tera Term (SparkFun 2023e). To configure the

unit using U-center, the SparkFun unit needs to be connected by a USB cable to a computer using the ublox port (Figure 3.4). For the Tera Term terminal, the ESP32 port is used (Figure 3.4). The configuration of a SparkFun unit centers around six key settings: configuring transmission ports, initiating an in-process survey to estimate the base position, setting ports for receiving or sending corrections (enabling correction transmission), storing monitoring parameters, adjusting monitoring rates, and configuring logging time. The SparkFun units do not require the settings to be uploaded every time the unit is powered on or off. The system automatically utilizes the most recent settings saved on the microSD card (Berru et al. 2023). Additionally, the configuration can be saved in text (.txt) format and uploaded to the units via U-center, which helps to prevent potential misconfigurations in future deployments. For a more detailed explanation of the configuration, please refer to Ublox (2022, 2023d).

The SparkFun units can achieve a manufacturer accuracy of 30 cm upon powering them on (SparkFun 2023a). However, when the GNSS SparkFun units operate as a dGNSS setup (base and rovers), the horizontal and vertical accuracy of the system can be improved to 14 mm (SparkFun 2023a). As a dGNSS setup, the SparkFun system requires additional components that are acquired separately and added to the SparkFun units. A schematic showing the link between different components of the SparkFun units to form a differential GNSS system is presented in Figure 3.5.

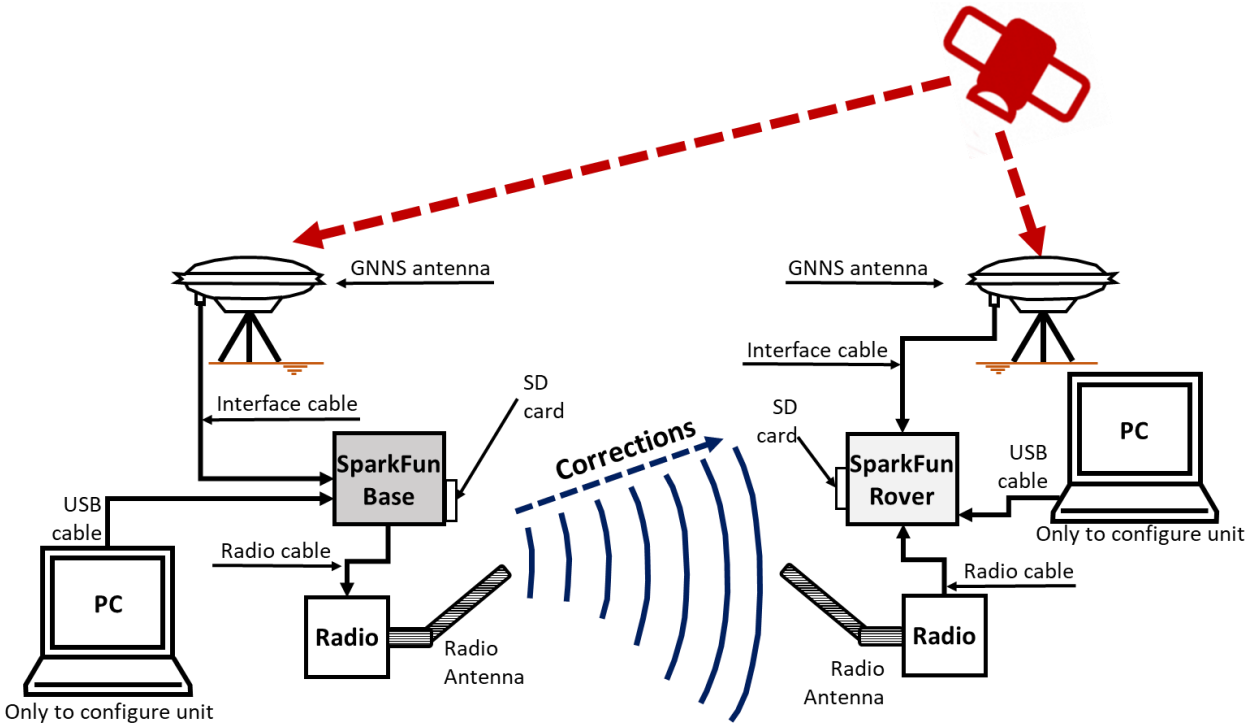

Figure 3.5 Schematic of SparkFun differential GNSS System

The additional components, connected to one SparkFun unit as shown in Figure 3.5,are described as follows:

- A GNSS antenna that receives the L1/L2 bands for the four constellations, and an interface cable that connects the antenna to the SparkFun unit.
- A radio that sends corrections, which can be point-to-point (one base and one rover) or point-to-multipoint (one base and multiple rovers), depending on the project requirements. The radio should operate at licensed frequencies in the country where the project is based. For the present research the radio operates at a frequency of 915 MHz for use in Canada and has a baud rate of 57 600 bps.
- USB cables to configurate and power the GNSS SparkFun Unit or charge the integrated battery.
- A micro-SD Card with a maximum capacity of 32 GB, formatted for FAT 32, is used to save the monitoring data. (SparkFun 2023a, b and c)

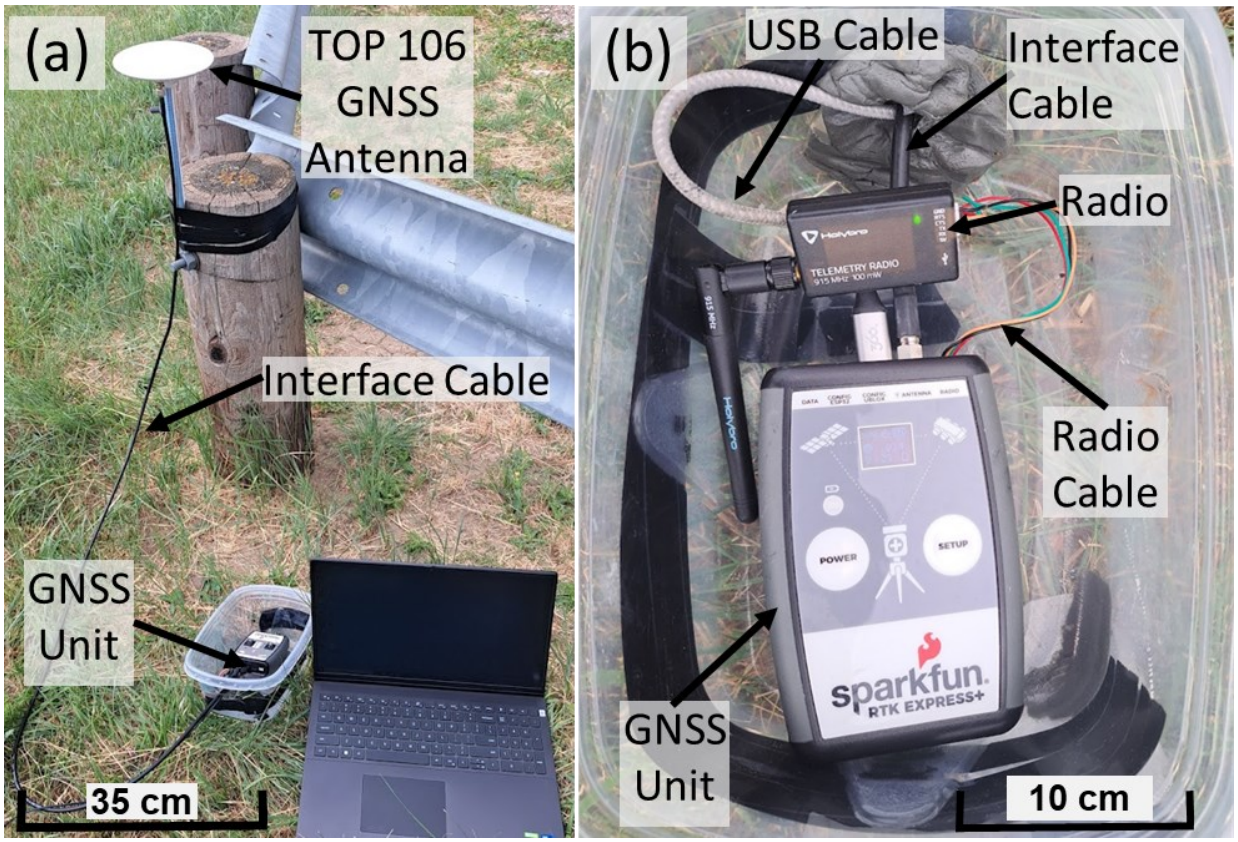

Figure 3.6 GNSS SparkFun unit Setup for just one SparkFun unit

3.4 dGNSS SparkFun System Tests and Data Processing Method

3.4.1 Pre-Deployment Tests

Four SparkFun units, one base and three rovers, were pre-tested before being deployed at the Chin Coulee landslide. The pre-tests focused on: (1) Configuring the units to allow sending and receiving corrections; (2) Ensuring uninterrupted transmission and reception of corrections through the radios and evaluating their operational range; (3) recording key parameters for landslide monitoring displacements; and (4) evaluating the SD storage capacity of the SparkFun units.

Several pre-deployment tests were conducted, with three considered crucial: Test A, conducted in an urban environment (longest test), Test B, pre-test conducted at the landslide site (Shortest test), and Test C, second urban test to evaluate new radios for the SparkFun units and a new antenna for the base. The three rovers were labeled as rover 949E, 9532 and 9562 following the

manufacturer-assigned codes. The unit responsible for transmitting corrections was referred to as the base. The characteristics and the arrangement of the pre-tests are presented in Figure 3.7 and Table 3.1.

Test A and C focused on evaluating the capacity to maintain the RTK connections between the units for long periods, rather than evaluating the radio range. During these tests, the SparkFun units were exposed to wind, rain, and snow; and were tapped and lightly shaken to test the robustness of connections. Test B, on the other hand, focused on assessing sky visibility, radio range, and the capacity to receive corrections at the monitoring site, before the deployment took place.

Table 3.1 Pre-Deployment Test Characteristics and Results

Item	Test A	Test B	Test C
		Pre -Tests Characteristics	
Location	Edmonton, Alberta	Chin Coulee Landslide, Taber, Alberta	Edmonton, Alberta
GNNS Unit Base	SparkFun RTK Surveyor (ZED-F9P module)		
GNNS Unit Rovers	SparkFun RTK Express Plus (ZED-F9R module)		
Rover and base radios	Telemetry radio (1)	Telemetry radio (1)	XBP9X radio (2)
Rovers Antenna	GNSS Multi-Band L1/L2 Antenna		
Base Antenna	GNSS Multi-Band L1/L2 Antenna	GNSS Multi-Band L1/L2 Antenna	GNSS Multi-Band Magnetic Mount Antenna
Testing time	7 days	Four hours	5 days
Data Recording rate	Every minute	Every second Every minute	Every minute
SD Storage		32 Gb	
Distance between Rover and Base	< 2 m.	~1.1 Km	< 2 m.

Notes: (1) Sik Telemetry radio range is above 300 m, frequency range 915 MHz and built to work as point-to-point and (2) XBP9X radio range is up to 2.5 km, frequency range from 902 to 928 MHz, and work as point-to-multipoint.

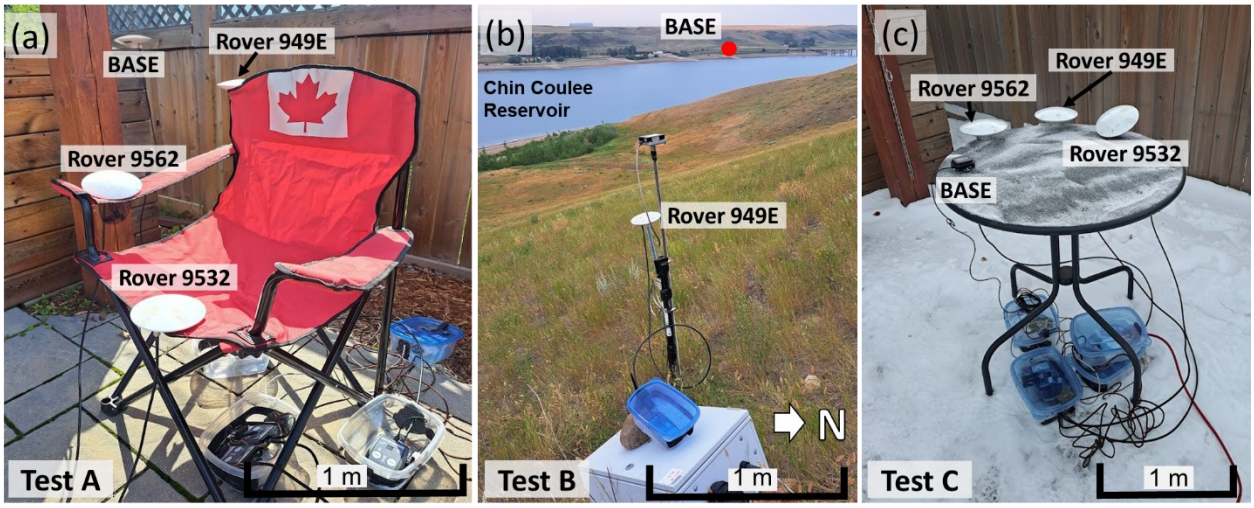

Figure 3.7 Pre-tests arrangement: (a) Test A, (b) Test B and (c) Test C

3.4.2 Chin Coulee Landslide Deployment

Three GNSS SparkFun units, one base and two rovers, were deployed in November 2022 to assess the reliability and accuracy of the SparkFun system in monitoring landslide displacements. The SparkFun base was installed in a stable area across the landslide (Figure 3.7b and Figure 3.8). The two rovers, designated rover 949E and rover 9532, were respectively installed near Geocubes SM22-06 and SM22-09 within the sliding mass (Figure 3.8). The rovers' locations were selected for two main reasons: (1) These Geocubes registered the largest displacements within the sliding mass (Rodriguez et al. 2021) and (2) to use the Geocubes' power supply.

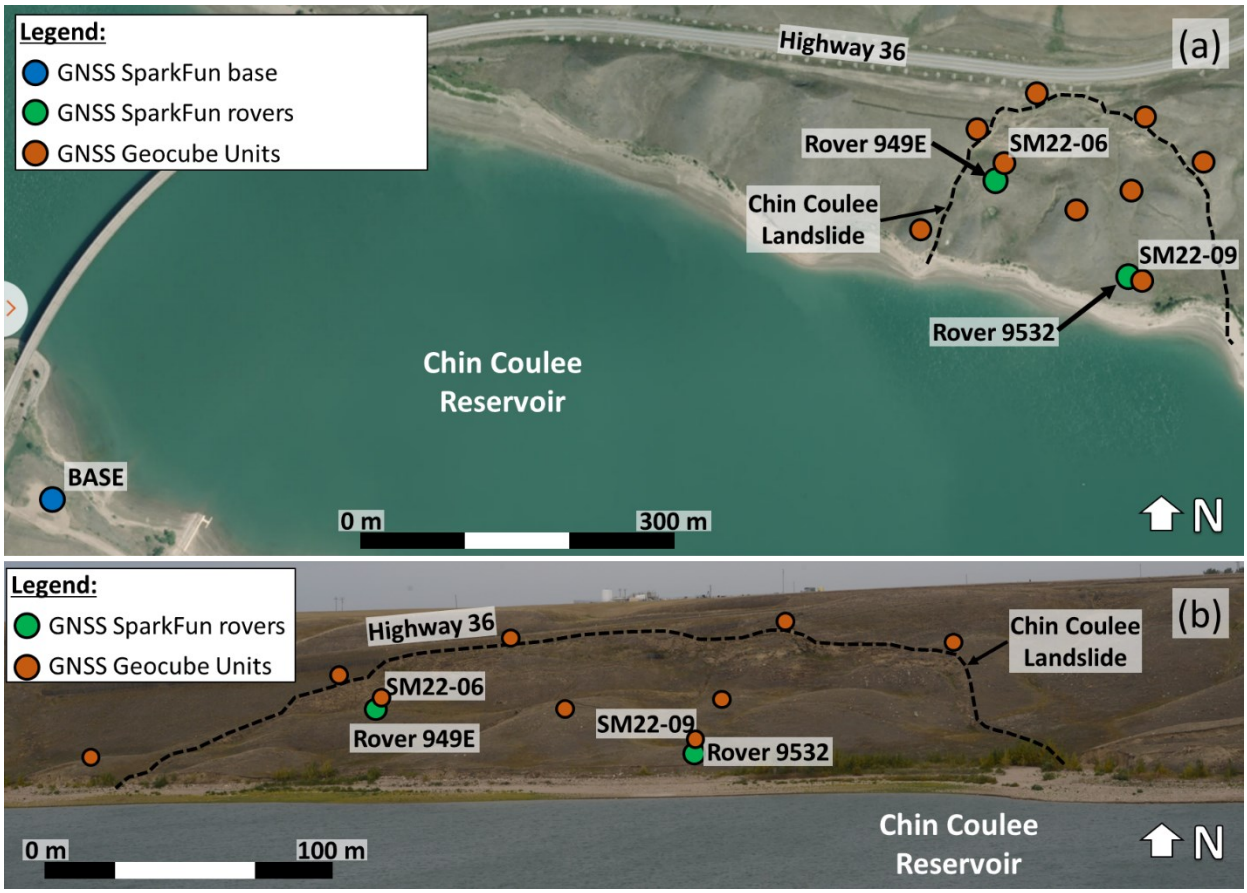

Figure 3.8 (a) Plan view and (b) frontal view of GNSS SparkFun units' locations at Chin Coulee landslide ((a)'s Right photo: Ophelia Sensors))

The Sparkfun base was installed at a pump house to ensure an uninterrupted power supply. The base satellite antenna was mounted on the Geocubes antenna support (Figure 3.9c), while the XBP9X radio's antenna was mounted on the pumping house's far end to establish an unobstructed line of sight with the rover's radio (Figure 3.9a). The SparkFun base and the XBP9X radio are stored inside a plastic box (Figure 3.10b).

The GNSS antennas for the SparkFun rovers were mounted on steel rods. The rods were embedded 0.5 m into the ground and connected to square steel tubes, driven 0.8 m into the ground, using brackets to add stability and prevent inclination. The XB9X radios' antennas were connected to the rods above ground to ensure a clear line-of-sight to the base radio's antenna and accommodate snow accumulation in the winter (Figure 3.11a, b).

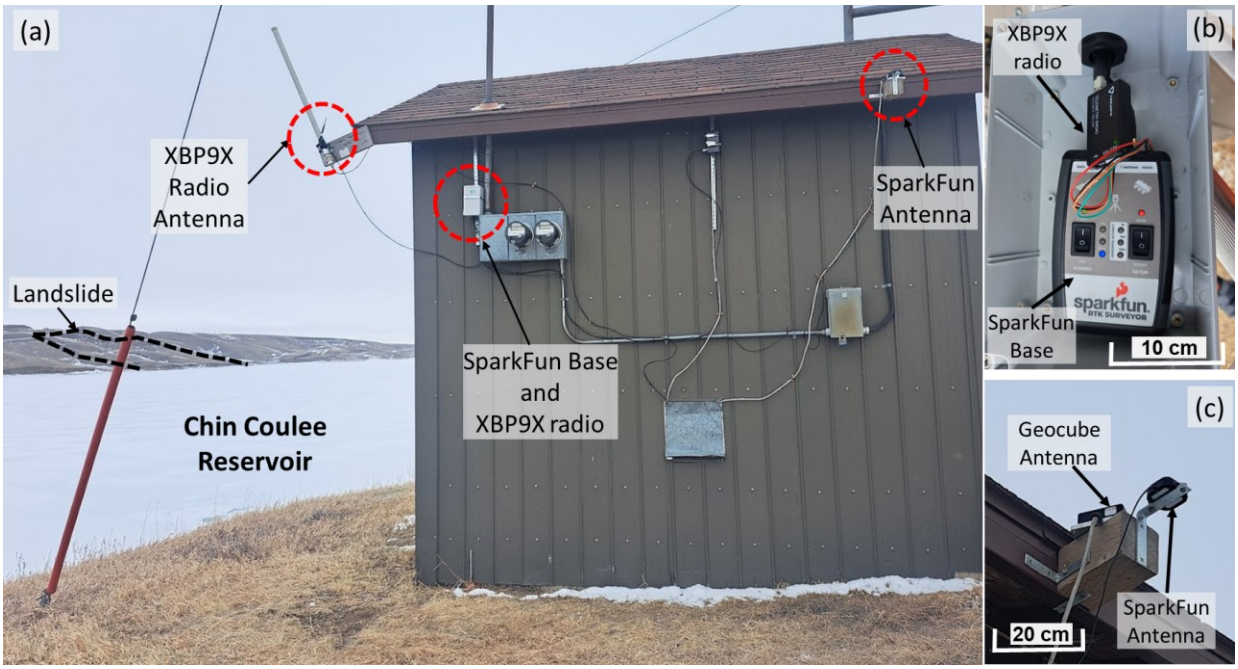

Figure 3.9 (a) Base SparkFun Installation arrangement, (b) SparkFun unit and (c) Satellite antenna

The rovers are powered by the Geocubes' power supply system, consisting of two 12-volt, 100 Ah batteries, a 10-watt solar panel, and a solar charge controller (Figure 3.10b). The rovers and the XBP9X radios are connected to the charge controller via a USB plug designed specifically for this purpose (Figure 3.11c). The SparkFun rovers and the XBP9X radios are stored inside an aluminum battery box (Figure 3.11a, and Figure 3.10). After the installation, the SparkFun differential GNSS system was set up to collect data every minute.

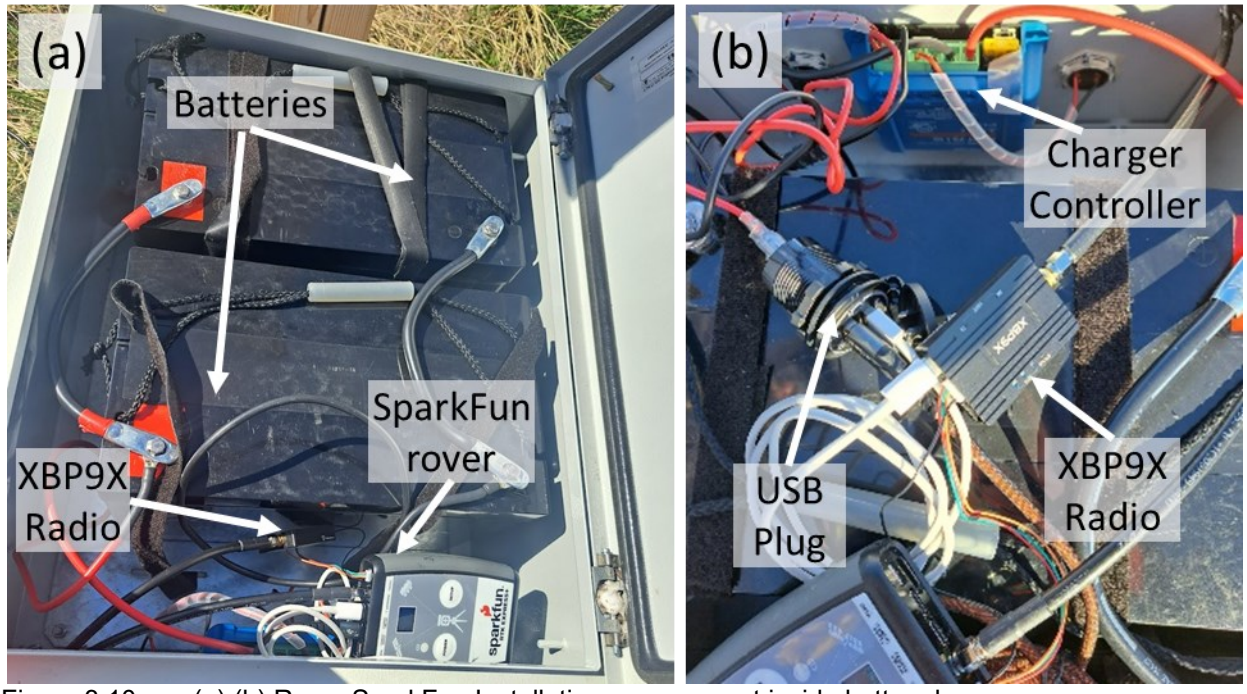

Figure 3.10 (a) (b) Rover SparkFun Installation arrangement inside battery box

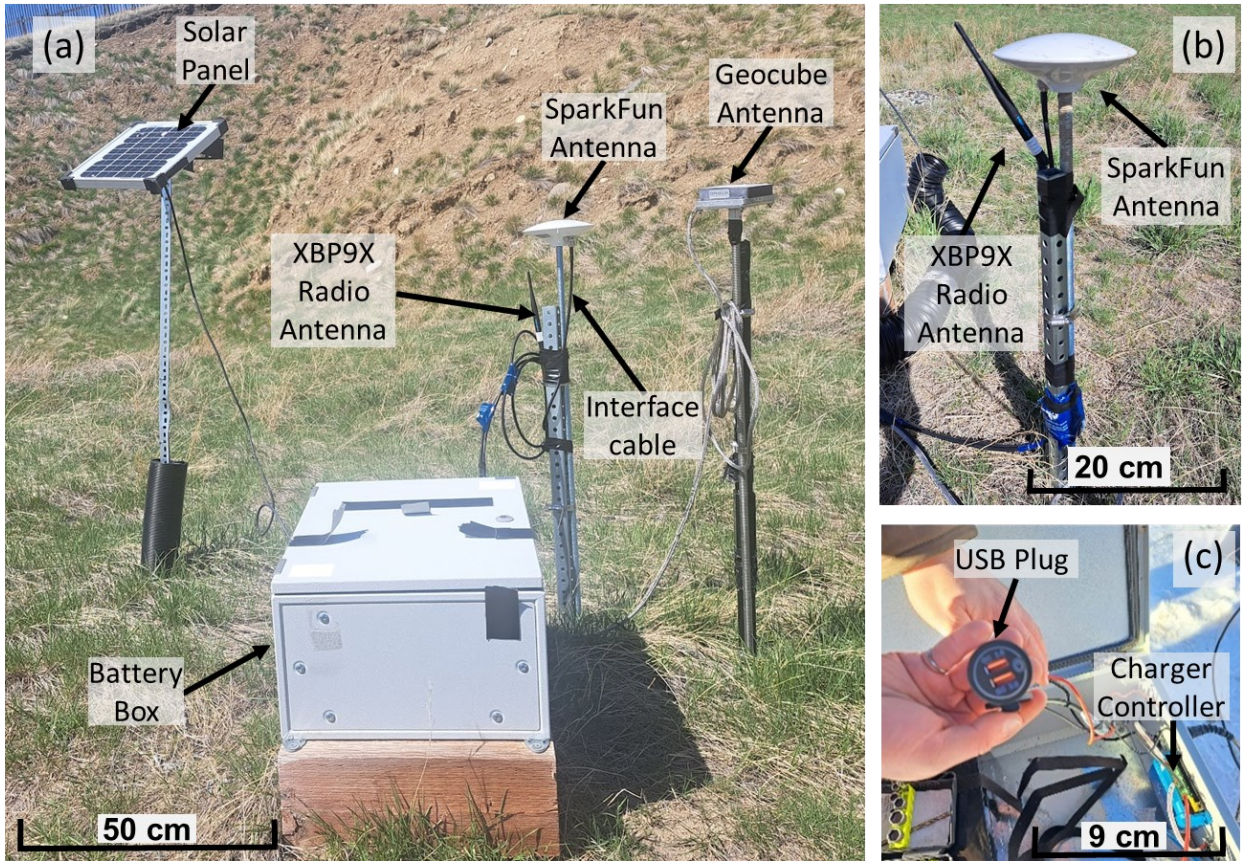

Figure 3.11 (a) Rover SparkFun Installation arrangement, (b) Steel rods, GNSS antenna and XBP9X antenna (c) USB plug.

The capital cost of this deployment (three SparkFun units) was approximately $5,765 USD, which is around $1930 USD per unit. This cost includes expenses related to the SparkFun unit ($750 USD), as well as radio equipment, protection, and power supply (Table 3.2). The costs associated with assembly, planning, installation time, data retrieval, and data processing will vary depending on specific project requirements and are not included in the capital costs.

Table 3.2 dGNSS SparkFun system costs at Chin Coulee landslide

Components	Description	Cost (USD)
Three SparkFun units	One base and Two rovers	$2230
Radio System	XBP9X radio, cables, and antennas	$740
Protection	Battery boxes and plastic boxes	$1040
Mounting Equipment	Steel rod, square tube, pole mount support for solar panel	$485
Power Supply System	Batteries, USB cable, USB plug, solar charge controller, solar panel	$1270
	Total Capital Cost	$5765

3.4.3 Data Processing Method

The collected monitoring data is stored in an ubx format, a proprietary binary protocol. The u-blox software converts the data a xls format and organizes the data in columns and rows, where each column corresponds to a monitoring parameter, and the rows represents the collected data at one-minute intervals (Table 3.3) (Ublox 2023c).

Table 3.3 Monitoring data arrangement using U-blox software

Index	SVs Used (1)	UTC (2)	Lat (3)	Lon (4)	Alt (HAE) (5)	PACC H (6) (m)	PACCV (7) (m)
0	28	5/2/2023 16:03	49.60501963	-112.180339	865.115	0.014	0.01
1	28	5/2/2023 16:04	49.60501961	-112.180339	865.105	0.014	0.01
2	28	5/2/2023 16:05	49.60501963	-112.180339	865.114	0.014	0.01
3	30	5/2/2023 16:06	49.60501966	-112.180339	865.11	0.014	0.01
4	30	5/2/2023 16:07	49.60501963	-112.180339	865.111	0.014	0.01
5	30	5/2/2023 16:08	49.60501959	-112.180339	865.109	0.014	0.01

Notes: (1) Number of satellites captured, (2) Coordinated Universal Time (UTC), (3) Latitude, (4) Longitude, (5) Height above ellipsoid, (6) Achieved horizontal accuracy (m) and (7) Achieved vertical accuracy (m)

A Python-based code was developed to facilitate the post-processing of data. The code first converts Universal Time (UTC) to Mountain Standard Time (MST), which is the time zone at the

project location. The code then transforms the longitude and latitude data to the Universal Transverse Mercator (UTM) coordinate system. After these two first steps, a preliminary filtering process is applied to the data to discard measurements outside the manufacturer accuracy thresholds of 14 mm horizontally and 10 mm vertically.

The Hampel filter (Hampel 1971) is used as a second preliminary filter to eliminate outliers, which are unusual discrepancies compared to most observations in a randomly sampled dataset (Sharifi et al. 2022; Zimek and Filzmoser 2018). This filter is applied to the UTM coordinates, as well as altitude (HAE) within 24-Hrs time intervals. Outliers in the data are identified as points deviating from the median by three times the median absolute deviation (Sharifi et al. 2022; Davies and Gather 1993; Pearson 2002; Liu et al. 2004; Yao et al. 2019), and these outliers are replaced with the median value within the same 24-Hrs intervals. After applying the Hampel filter, the Python code processes the data to generate graphs representing the number of satellites vs. time, horizontal and vertical accuracy vs. time and percentage of data remaining after the filtering process.

Typically, GNSS unit data does not exhibit a visual trend upon initial analysis unless the displacement rate is significant compared with the accuracy of the system (Macciotta et al. 2016 and Deane 2020). To enhance the interpretation of landslide displacements, kernel filters (simple moving average (SMA) and Gaussian-weighted moving average (GWMA)) or regression filters (Savitzky-Golay (S-G)) can be applied to reduce data scatter and the errors of the GNSS system. Both types of filters have demonstrated effectiveness for time-domain datasets (Sharifi et al. 2022). However, the GWMA filter has been shown to effectively reduce the scatter, while maintaining the genuine displacement pattern (Sharifi et al. 2022).

The GWMA filter uses a constant window size (bandwidth) for the entire dataset, but the window size can be adjusted near the boundaries depending on the available data points (Sharifi et al. 2022). Within this window, the filter assigns weights to the data points, giving the highest weight

to the measurement closest in time to the calculation point. As the time difference from the current calculation point increases, the weight assigned to each data point decreases. This weighting approach ensures that the data point closest in time to calculation point receives the greatest influence during the filtering process (Sharifi et al. 2022). The weights are determined based on the Gaussian (normal) distribution as follows:

Equation 3.1 $$\widehat{y_i} = \sum_{i-\frac{p-1}{2}}^{i+\frac{p-1}{2}} w_i * y_i$$

where $\widehat{y_i}$ is the filtered value at the time i, y_i is the unfiltered value, p is the window size, w_i is the weight coefficient based on the Gaussian distribution.

The GWMA filter is applied to UTM coordinates and altitude (HAE). After the GWMA filter, the cumulative displacement is calculated based on the distance between the positions at the desired time and the initial time (Deane 2020). This approach is taken to avoid overestimation of cumulative displacement measurements since both negative and positive displacements (displacements towards and away from the initial position) are recorded in the dataset without differentiation (Deane 2020). The equation for calculating cumulative displacement is shown below:

Equation 3.2 $$D_i = \sqrt{(X_i - X_0)^2 + (Y_i - Y_0)^2}$$

where D_i is the cumulative displacement at the time i, X_i is the east coordinate at time i, X_0 is the east coordinate at time zero, Y_i is the north coordinate at time i and Y_0 is the north coordinate at time zero.

The cumulative elevation is calculated by subtracting the filtered elevation at the desired time from the filtered elevation at the initial time, as follows:

Equation 3.3 $$E_i = Z_i - Z_0$$

where E_i is the cumulative elevation at the time i, Z_i is the elevation at time i, X_0 is the elevation at time zero.

The displacement rate is estimated by subtracting the cumulative displacement at the desired time from the cumulative displacement at one minute before, as the data is recorded every minute. To enhance the interpretation of the displacement rate, this parameter is also filtered using the GWMA filter.

Equation 3.4 $$\overline{D}_i = D_i - D_{i-1}$$

where $\overline{D}_i$ is the velocity at the time i, D_i is the cumulative displacement at time i, D_{i-1} is the cumulative displacement at time i minus 1 minute.

3.5 dGNSS SparkFun System Results

3.5.1 Pre-Deployment Tests Results

The SparkFun units were pre-tested independently and as part of a dGNSS setup. In both approaches, the units successfully captured satellite signals, recorded their positions, and maintained a consistent number of satellites throughout all three pre-tests. When assessed as individual units, they achieved an accuracy of up to 0.30 m, as specified by the manufacturer. In the dGNSS setup, the base achieved a fixed position and initiated the transmission of corrections to the rovers.

During Tests A and B, the rovers' radio inconsistently receive the corrections, resulting in horizontal and vertical accuracies ranging from 11 mm to 5 m (Figure 3.12). Test A's data showed that horizontal accuracies under 17 mm constituted 50% of the overall data, while for Test B, it represented approximately 60%. The lower percentage of data within the specified accuracy was attributed to the use of "Sik telemetry radios" during these tests. These radios are small, inexpensive, open-source platforms designed exclusively to function as pairs (one base and one

rover). However, Test B demonstrated that they can effectively transmit and receive corrections within a range of approximately 1 km (Figure 3.7).

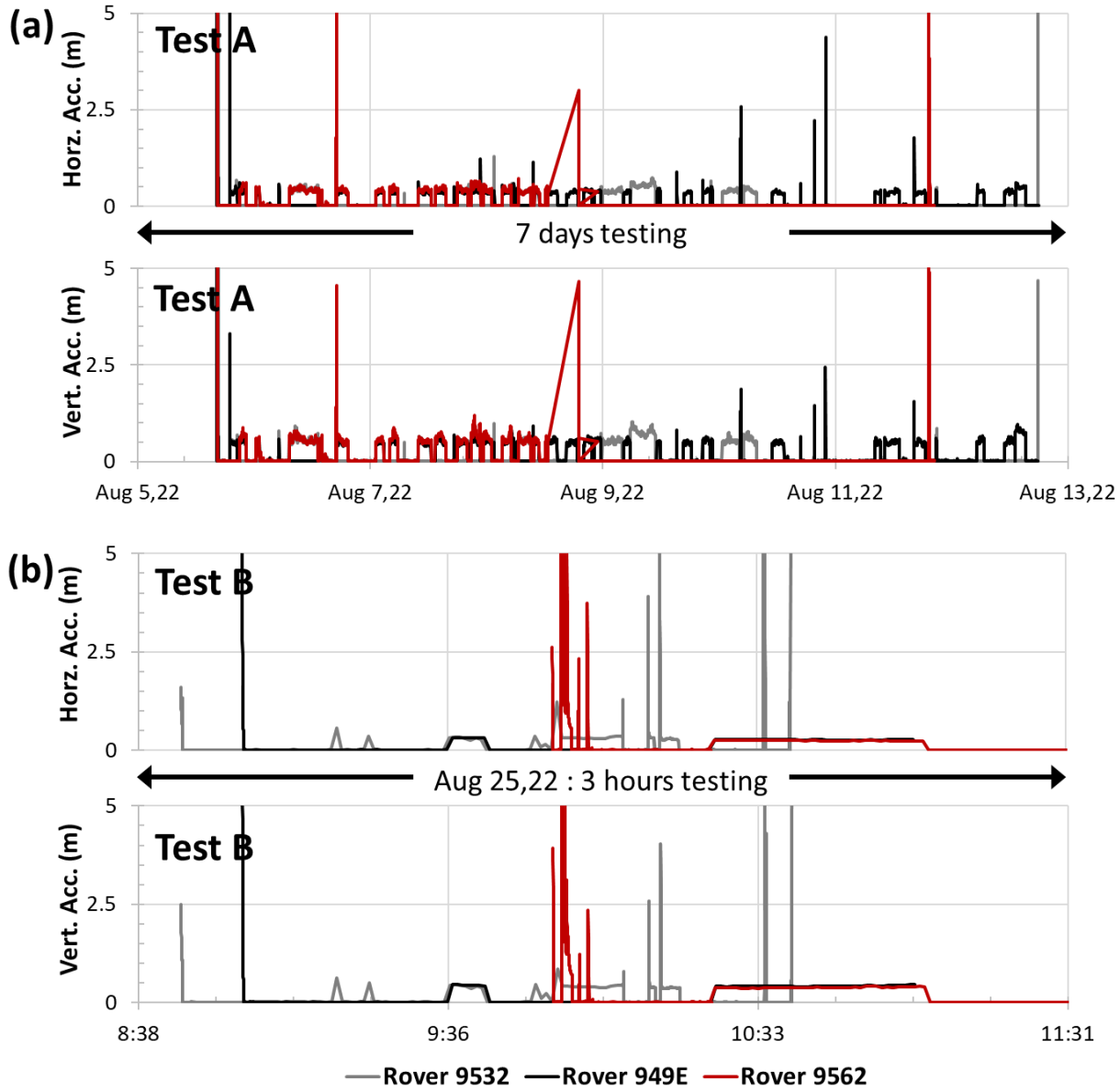

Figure 3.12 Horizontal and Accuracy (m): (a) Pre-test A (7 days testing) and (b) Pre-test B (3 hours testing)

For Test C, XBP9X radios were used which work in a point-to-multipoint configuration. The results indicated an improvement in both horizontal and vertical accuracy, with measurements ranging from 10 mm to 20 mm (Figure 3.13). Horizontal accuracies less than 16 mm represented approximately 95% of the total data.

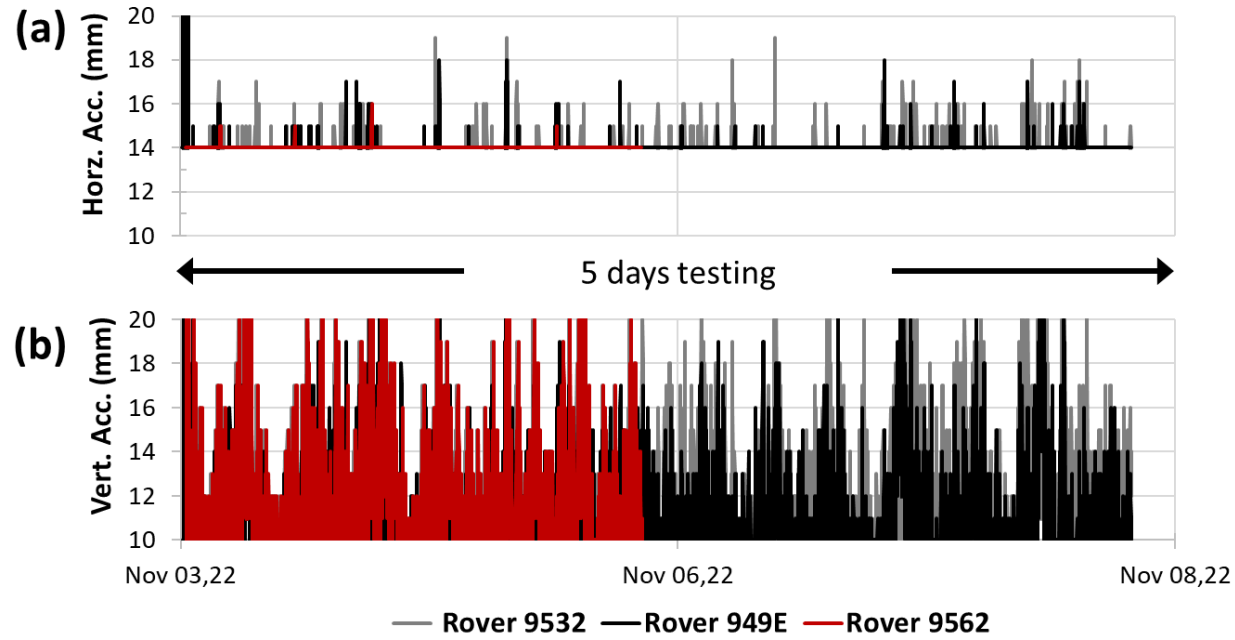

Figure 3.13 Pre-test C: (a) horizontal and (b) vertical accuracy (mm)

During pre-testing, the SparkFun units' storage capacity over time was assessed by gathering data at two recoding rates: one point per minute and one point per second. Results showed that at a one-minute recording rate, a 32 GB microSD card can store data for around 2.5 years. However, at a one-second recording rate, this capacity reduces to just 3 months (Figure 3.14).

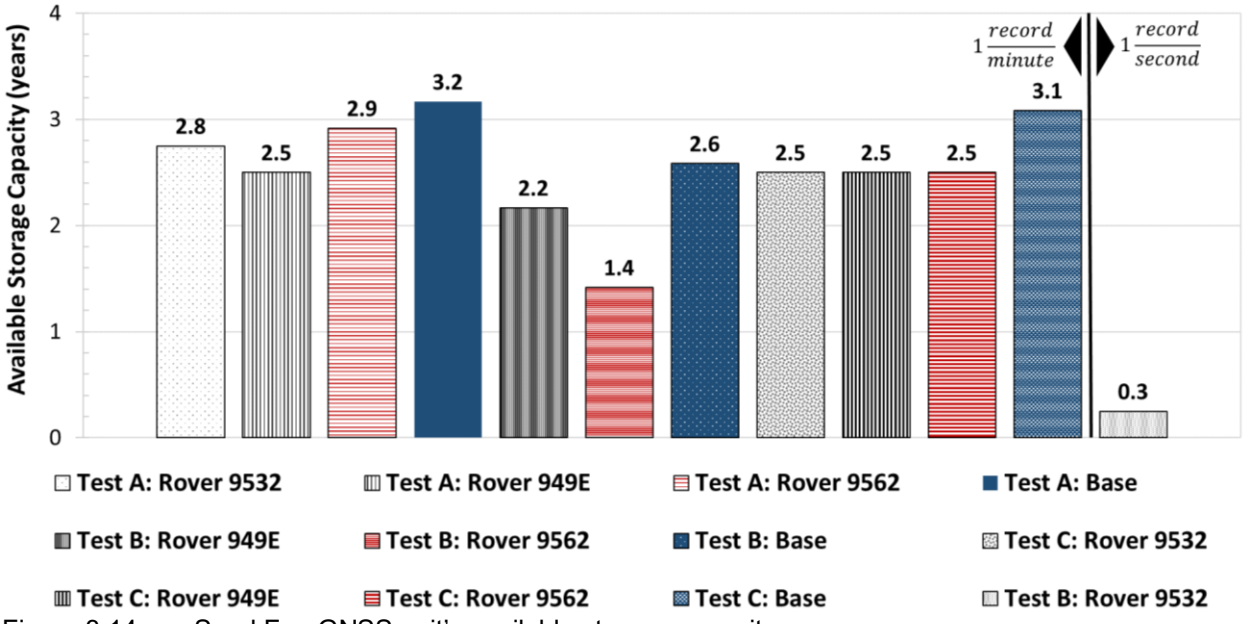

Figure 3.14 SparkFun GNSS unit's available storage capacity

3.5.2 Chin Coulee Landslide Deployment Results

The dGNSS SparkFun setup (the base and rovers 9532 and 949E) collected data at 1-minute intervals for approximately six months, from November 18th, 2022, to June 6th, 2023. Data gaps during the monitoring period were mainly due to power supply issues and equipment damage caused by extreme cold temperatures in winter (December to March), reaching as low as -32°C, as indicated by data from the Alberta Climate Information Service (ACIS 2023). The following observations were made:

- Connection issues between the USB plug and the charger controller (Figure 3.10) affected the power supply to the SparkFun units. Initially, this affected the radios, which failed to process corrections transmitted from the base. Ultimately, it resulted in a complete shutdown of the SparkFun units. Throughout these periods, data exceeding the accuracy threshold was recorded or no data was captured.
- The lack of insulation in the storage boxes affected the SparkFun units' hardware. Rover 949E's data recording stopped after 10 days due to a potential misconfiguration in the logging time, likely caused by damage to the SparkFun board. Similarly, the base unit discontinued correction transmission after 13 days of operation due to a damaged SD card, impacting both the base's configuration and correction transmission capacity.

When the dGNSS SparkFun setup worked smoothly, the SparkFun rovers tracked a varying number of satellites, ranging from 16 to 32. This occurred even in instances when corrections were temporarily lost, highlighting excellent satellite visibility. In the absence of corrections, horizontal accuracies ranged between 0.25 m and 1.3 m (Figure 3.15), with vertical accuracies reaching up to 1.5 m for both rovers.

Upon receiving corrections, the SparkFun rovers had horizontal accuracies from 14 mm to 19 mm and vertical accuracies between 10 mm and 19 mm for both rovers (Figure 3.16). These results suggest that the XBP9X radios effectively transmitted and received corrections across a distance

exceeding 1 km. Furthermore, the selected installation locations exhibited an unobstructed line of sight between them and the base.

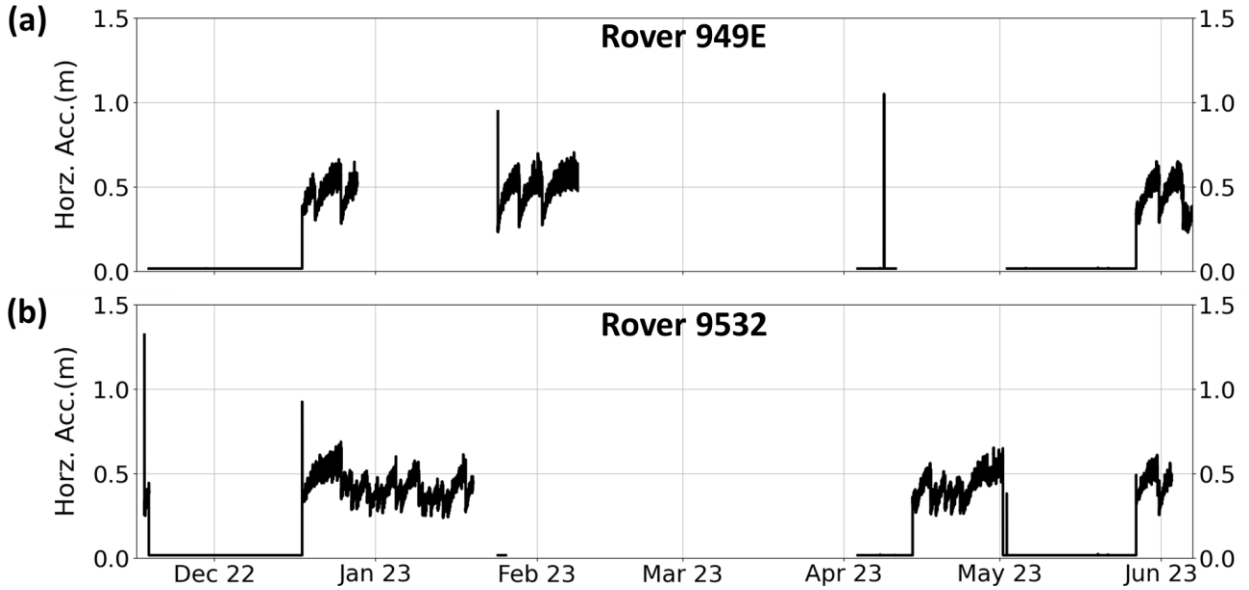

Figure 3.15 Horizontal (Horz.) accuracies vs. time: (a) Rover 949E and (b) Rover 9532

Data outside the manufacturer's accuracy thresholds was removed, discarding 40% of the data for rover 949E and 45% for rover 9532 due to extended intervals without corrections caused by power system failures. However, if only the period with corrections is considered, data with 14 Accuracy (m): (a) Pre-test A (7 days testing) and (b) Pre-test B (3 hours testing)mm horizontal accuracy and 10 mm vertical accuracy represent 95% for rover 949E and 96% for rover 9532. Post-Hampel filter, the outliers constituted only 1% for rover 949E and 2% for rover 9532. The data remaining after applying both preliminary filters represent 59% for rover 949E and 53% for rover 9532 of the entire raw data sets. This suggests that enhancing the power supply and robustness against winter weather conditions can allow the use of approximately 95% of the data.

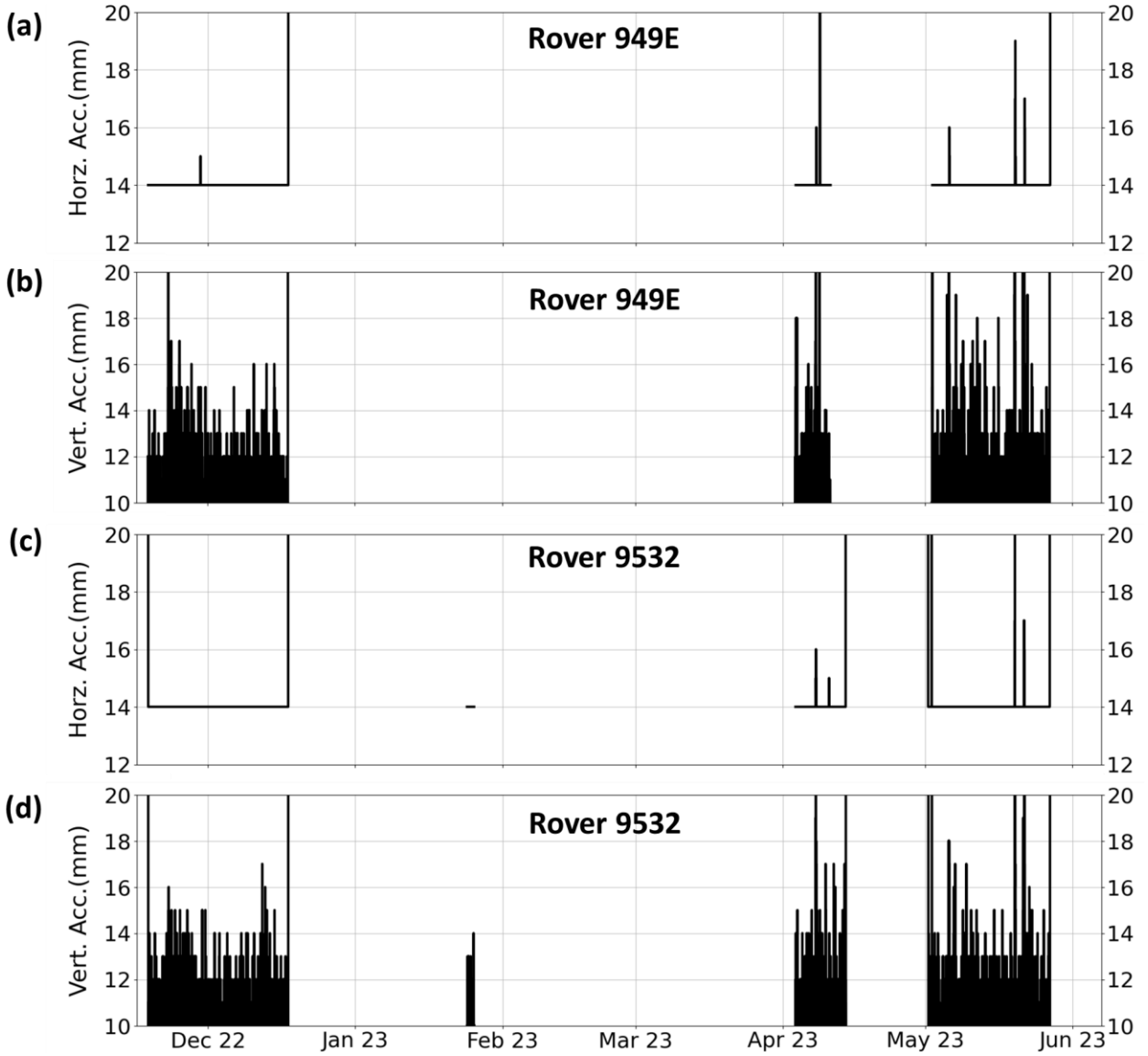

Figure 3.16 Horizontal (Horz) and vertical (Vert) accuracies after first filter: (a)(b) Rover 949E and (c)(d) Rover 9532

The SparkFun GNSS units' position variability was assessed using the standard deviation of the filtered data over a 24-Hrs period following Macciotta et al. (2016) and Deane (2020). Both rovers exhibited horizontal standard deviations (σ) below half of the manufacturer's estimate (14 mm), indicating positional errors within the expected range for SparkFun GNSS units. Vertical σ ranges from 3.2 to 12.2. Approximately 45% of the data for rover 949E and 42% for rover 9532 exceeded the vertical manufacturer's specifications (10 mm).

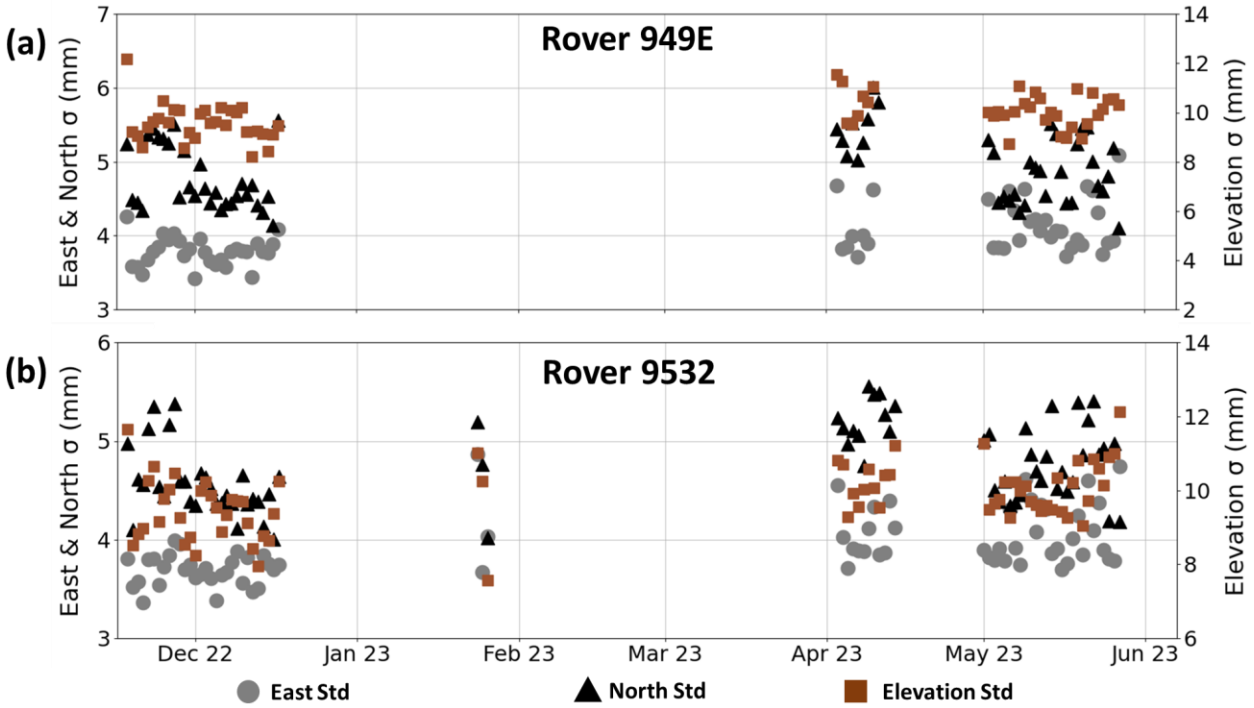

Figure 3.17 Standard deviation (σ) vs. time: (a) Rover 949E and (b) Rover 9532

3.5.3 Interpretation of Results of dGNSS SparkFun

To understand variations in displacement rates, such as seasonal periods of acceleration and deceleration, landslide monitoring data should be gathered over extended periods (Deane E. 2020). In prior studies conducted in the area, data was recorded for 1.2 years (July 2018 to September 2019), indicating that displacement rates are influenced by reservoir drawdown effects (Maximum and minimum reservoir elevation are 847.9 m and 834.7 m, respectively) (Drawdown rate ranging from 0.04 m/day to 0.19 m/day), leading to episodes of landslide acceleration (Rodriguez et al. 2021, Deane 2020).

Currently, the SparkFun monitoring data does not span a one-year period, however, it provides valuable insights into the potential suitability of the dGNSS SparkFun setup for landslide monitoring. The raw data was pre-filtered using accuracy thresholds and the Hampel filter, removing measurements without corrections and outliers. Subsequently, the pre-filtered data for both east and north coordinates was subjected to the GWMA filter, using a 3-day window size,

which balances timely landslide deformation information, scatter removal, and preservation of short-term displacement events (Deane 2020).

Rover 949E initially decreased in elevation by -6.7 mm, followed by a subsequent increase of 2.1 mm, resulting in a cumulative elevation change of approximately -4.6 mm over a 6-month period (Figure 3.18). Meanwhile, rover 9532 exhibited an elevation spike, reaching an average cumulative elevation of 16.5 mm between December 2022 and January 2023, followed by a decrease of approximately 7.1 mm, leading to a cumulative vertical displacement of 9.4 mm (Figure 3.18).

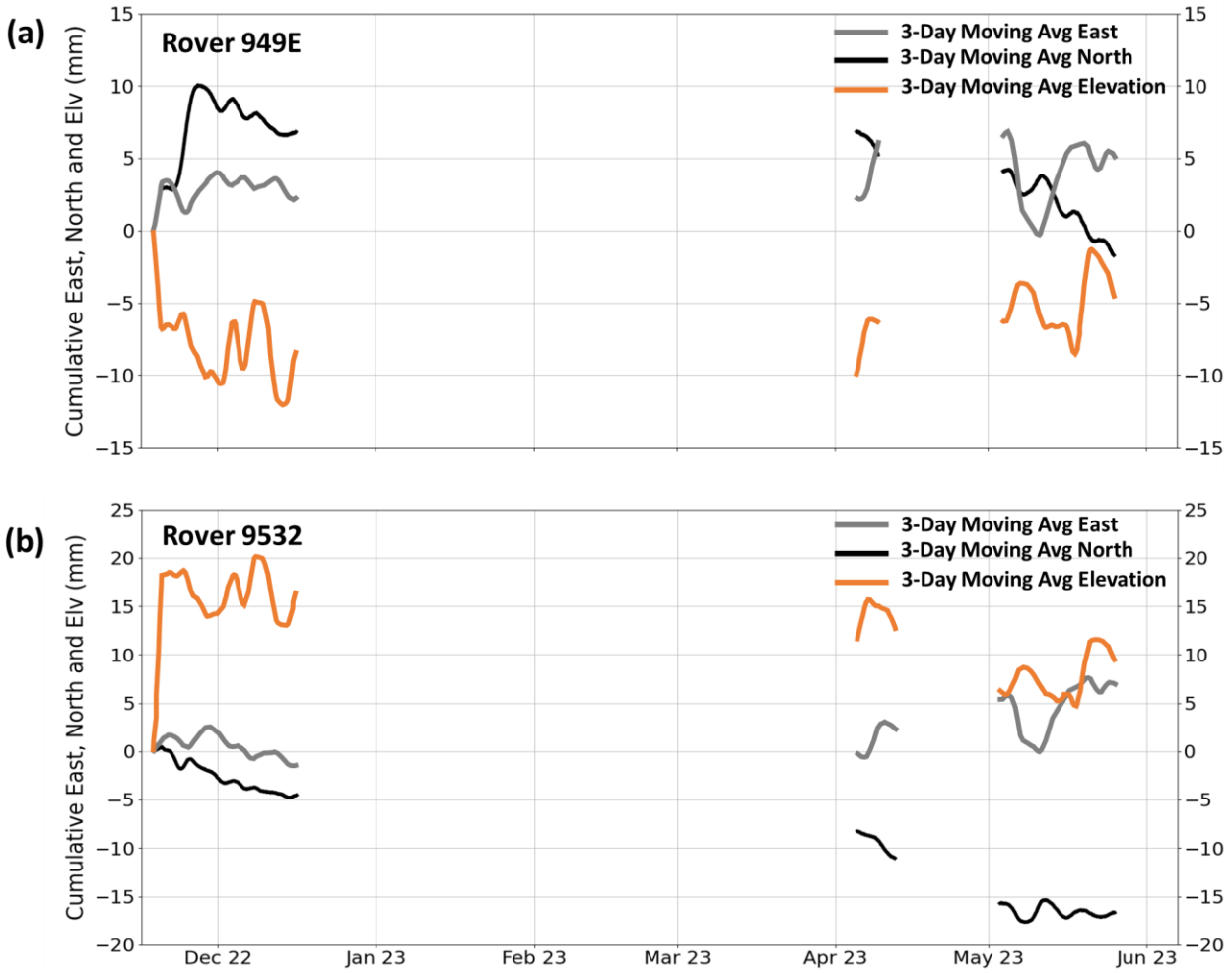

Figure 3.18 Cumulative east, north and elevation: (a) Rover 949E and (b) Rover 9532 (Note: Elv = Elevation (mm))

In Deane's 2020 study, the Geocube near rover 949E exhibited a cumulative vertical displacement of -5.2 mm over a six-month period and -11 mm over one year. The Geocube near rover 9532 recorded a cumulative vertical displacement of 3.5 mm in six months, and an estimated total of 16 mm over one year. Furthermore, Geocubes near the SparkFun rover sites demonstrated a decline from December 2018 followed by an increase in March 2019. This pattern aligns with the experiences of both SparkFun rovers.

The cumulative displacements in the North and East directions (Figure 3.18) are used to generate horizontal cumulative displacements and displacement rates (Equation 3.2 Rovers 949E and 9532 had horizontal cumulative displacements of 5.3 mm and 18.5 mm, respectively, over the six-month monitoring period (Figure 3.19). In the initial month of monitoring, rover 949E exhibited an abrupt spike in the horizontal cumulative displacement trend after 10 days of monitoring. This sudden acceleration is likely unrelated to genuine ground movement, as indicated by the absence of similar behavior in the Geocubes installed in the area. However, the precise cause remains undetermined. One plausible explanation is interference from local wildlife.

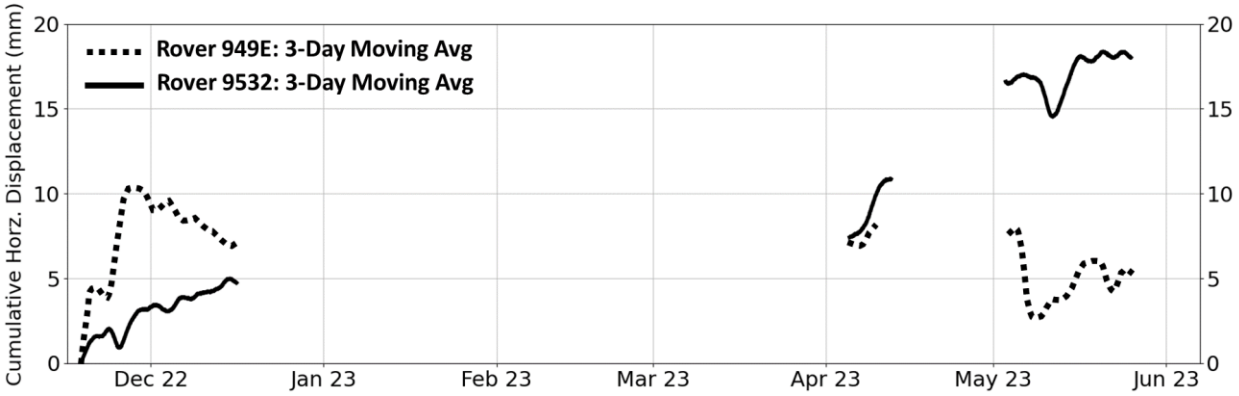

Figure 3.19 Cumulative horizontal displacements of Rover 949E and Rover 9532

Rover 949E experienced a horizontal displacement rate of 9.7 mm/year, while rover 9532 had a rate of 33.7 mm/year during the monitoring period. These estimated annual displacement rates might be higher, given the increase in displacement trend experienced by both rovers since May 2023 (Figure 3.19). The expected increase aligns with findings that indicate acceleration periods

during May to September, according to the 2018 -2019 monitoring campaign (From July 11, 2018, to July 30, 2019) (Rodriguez et al. 2021; Deane 2020; Rodriguez 2021). The horizontal direction of displacements observed in the SparkFun rovers (Rover 949E and 9532) over the 6-month period (Figure 3.20) differs from those reported by Deane (2020) in their 12-month monitoring period. However, it aligns with the results for the months of October to December 2018 and April to June 2019 as presented by Rodriguez et al. (2021) (Figure 3.20). Additionally, the direction of resulted displacement vector (Horizontal and vertical) of both SparkFun rovers correspond with Rodriguez et al. (2021) estimation (Figure 3.20).

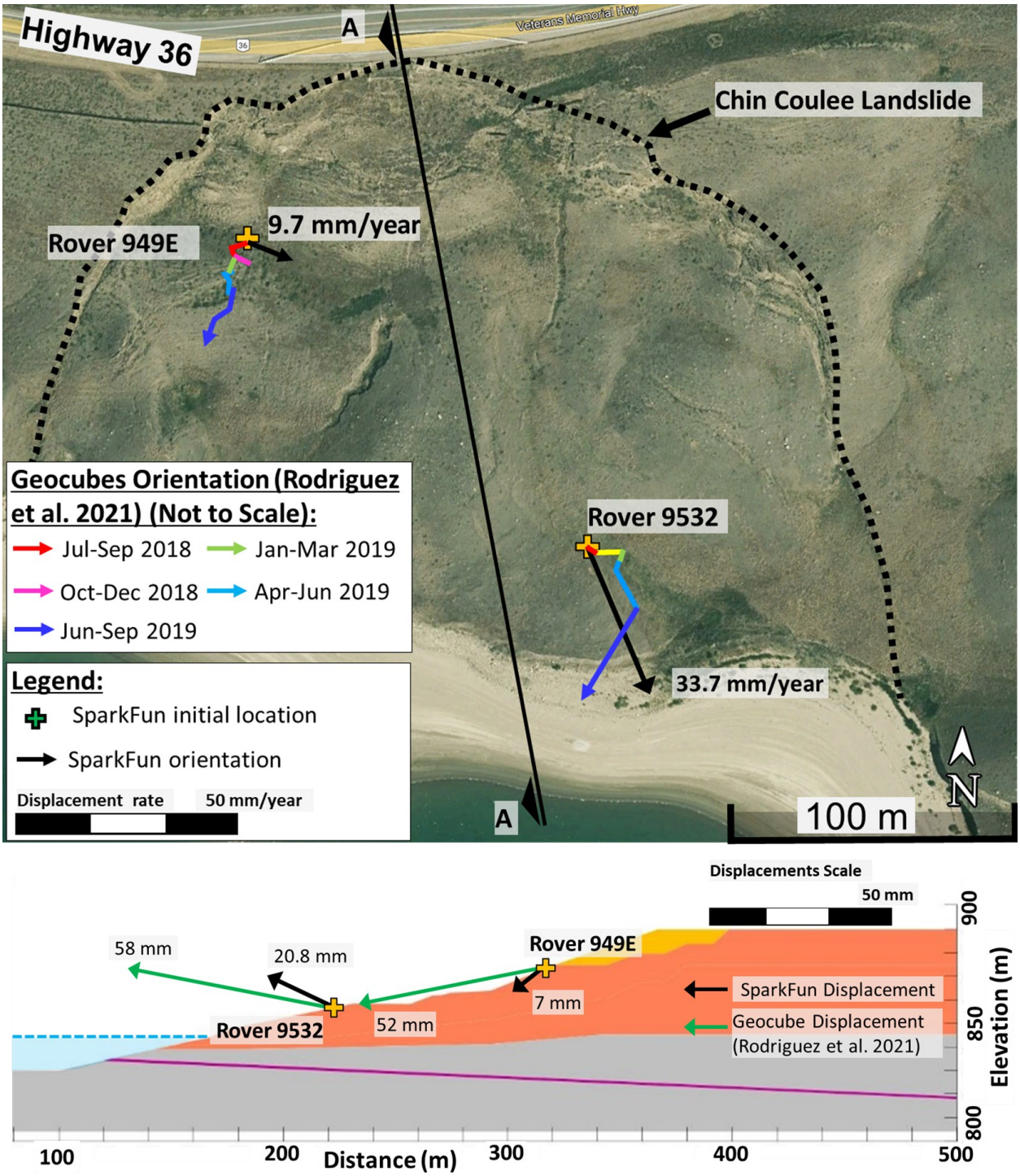

Figure 3.20 Cumulative horizontal and vertical displacement vectors of SparkFun units from November 2022 to June 2023 (Data is average using a 3-day moving average)

3.5.4 Results of dGNSS Geocubes

The Geocubes system monitored the landslide simultaneously with the SparkFun units. However, starting in January 2023, the Geocubes encountered diverse connectivity issues related to the

hardware and the RTK connectivity between the Geocube rovers and their base. This resulted in either no data recording or intermittent raw data (SM22-06). Consequently, for the analysis of landslide displacements, it is considered that reliable Geocube data was only recorded until this month.

For the current study, Geocubes SM22-06 and SM22-09 (Figure 3.2b and Figure 3.8) hold particular relevance due to their location for comparison with the SparkFun system. The Geocube raw data was presumed to meet the manufacturer's claimed accuracy of 2 mm or lower, thus just the Hampel filter was used to filter it (Ophelia, 2023). Ophelia did not provide accuracy information for the monitoring period. After filtering, 99% of the total dataset was retained, a 4% improvement over SparkFun, which retained 95% of the data after applying the Hampel filter.

A 24-Hrs standard deviation was estimated for the Geocubes in both the East and North coordinates, ranging from 0.5 mm to 2 mm, and reaching up to 4 mm on the elevation plane. Considering a 3-day moving average for the GWMA filter, Geocubes SM22-06 and SM22-09 exhibited cumulative vertical displacements of 0.4 mm and 1.32 mm, respectively. Both Rover 9532 and SM22-09 recorded upward movements, characterized by a declining trend.

The estimated cumulative horizontal displacements for Geocube SM22-06 and SM22-09 are 5.6 mm and 6.2 mm, respectively (Figure 3.21) up to December 2022, corresponding to displacement rate of 60.2 mm/year and 66.6 mm/year for Geocube SM22-06 and SM22-09, respectively. By considering only the cumulative displacement from unprocessed intermittent data, Geocube SM22-06 had a cumulative displacement of 19 mm over 6-months (Figure 3.21) which represents a displacement rate of 39.5 mm/year. This cumulative displacement is 13.7 mm greater than the displacement recorded by the SparkFun rover 954E.

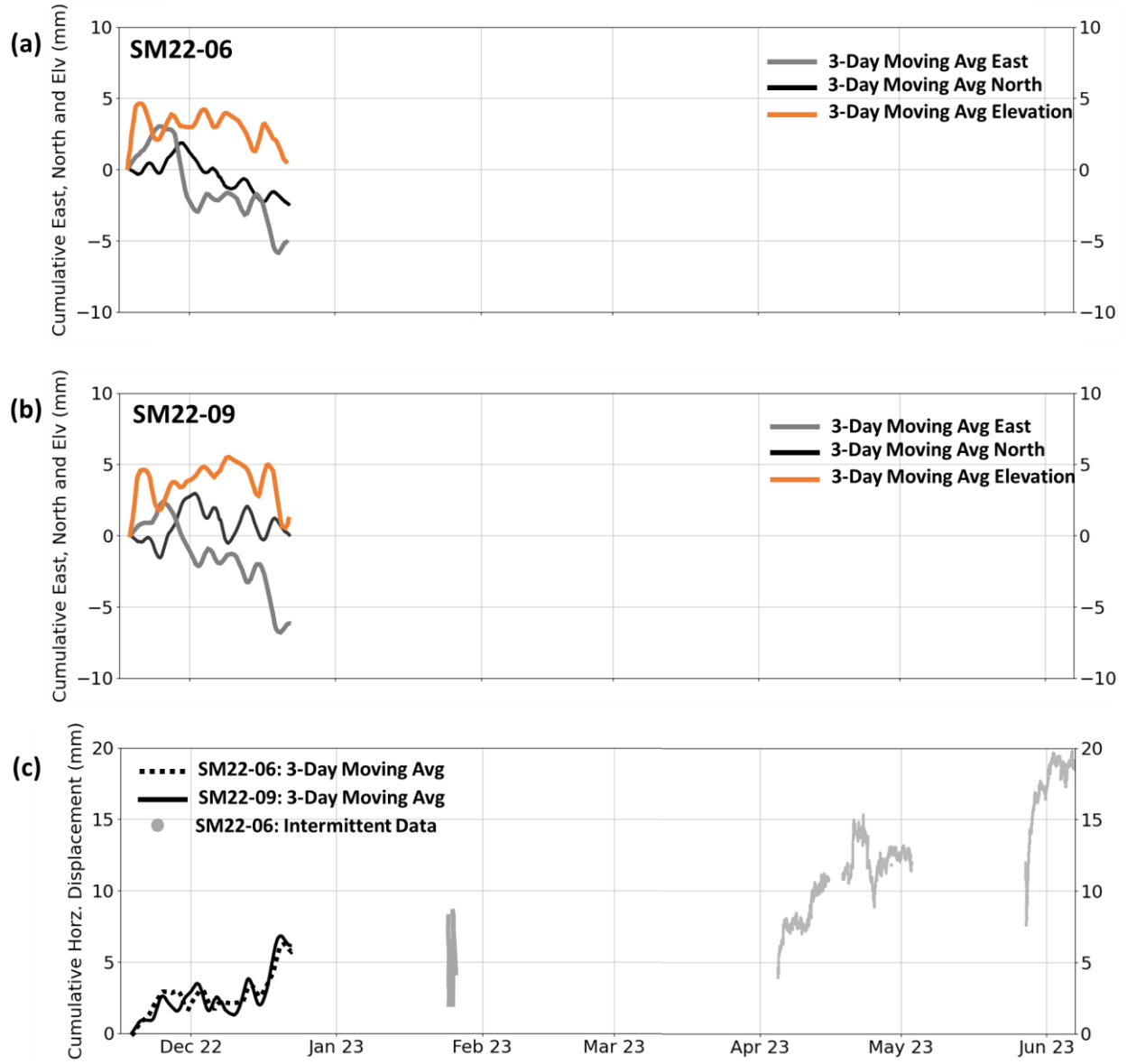

Figure 3.21 Cumulative east, north, elevation displacements: (a) Geocube SM22-06 and (b) SM22-09; and horizontal displacements: (c) Geocubes SM22-06 and SM22-09

3.5.5 SparkFun and Geocubes Systems

The cumulative horizontal displacements and elevations between the SparkFun units and the Geocubes until December 2022 are shown in Figure 3.22. Both technologies exhibited similar horizontal displacements until this month. For instance, rover 949E and Geocube SM22-06 have a difference of 1.5 mm, while the difference between rover 9532 and Geocube SM22-09 is 1.36 mm.

In the vertical direction, there is no clear alignment. Rover 949E and Geocube SM22-06 showed agreement in the displacement trend, but the rover 949E recorded higher increases in the vertical direction. For rover 9532, the results are opposite, with the rover 9532 indicating a decrease in elevation while its corresponding Geocube (SM22-09) recorded a slight increase in elevation of 0.8 mm.

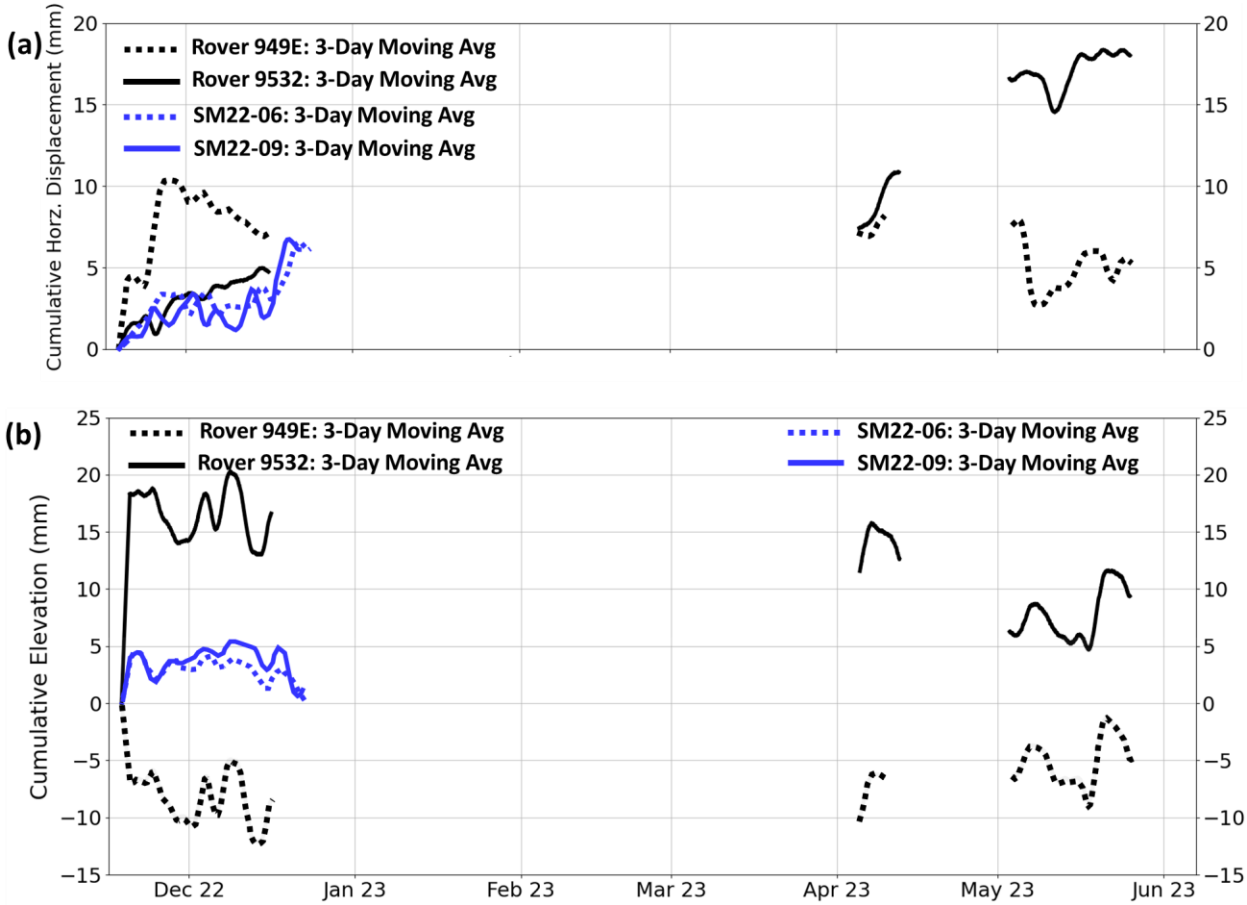

Figure 3.22 Comparison of (a) cumulative horizontal displacements and (b) elevation between SparkFun and Geocube systems

The total displacement and the displacement rates estimated for the SparkFun and the Geocubes are shown in Table 3.4. The difference in horizontal displacement rates between the two technologies can be attributed to the monitoring period duration. Sparkfun system's monitoring period extends up to June, but Rodriguez et al. (2021) suggested that the predominant displacements occurred from July to September, a period not currently included in the assessment. However, both technologies indicate greater displacement in the area where rover

9535 is located; and when examining the displacement trend, the SparkFun data aligns with the documented seasonal behavior of the landslide.

Table 3.4 SparkFun and Geocube system results

GNSS Technologies	SparkFun System		Geocube System			
	2022-2023 Chin Coulee		2022-2023 Chin Coulee (2)		Rodriguez et al. 2021(3)	
	Rover 949E	Rover 9532	SM22-06	SM22-09	SM22-06	SM22-09
Horizontal Displacement (mm)	5.3	18.5	5.6	6.2	-	-
Total Displacement (mm)	7	20.8	5.7	6.3	52	58
Horizontal Displacement Rate (mm/year)	9.7	33.6	60.2	66.6	45.3	89.8

Notes: (1) SparkFun rovers 949E and 9532 are paired with Geocube SM22-06 and SM22-09, respectively; (2) Geocube monitoring data spans from November 2022 to June 2023 (1-month monitoring period); (3) Rodriguez et al. (2021) reported Geocube monitoring data from July 11, 2018, to September 19, 2019.

The SparkFun and Geocubes dGNSS networks experienced power supply issues, resulting in inconsistent monitoring times. However, despite this limitation, the alignment in displacement trends, such as the increase in displacement since May (Figure 3.19), and directional accuracy, including the identification of the graben and horst area in the landslide (Figure 3.20), consistent with previous studies, demonstrated the promising performance of the SparkFun system at half the cost of the Geocubes. A comparison between the two technologies is presented in Table 3.5.

Table 3.5 SparkFun and Geocubes systems performance comparison

	SparkFun System	Geocube System
Constellation	GPS, GLONASS, BeiDou, Galileo	GPS, GLONASS, BeiDou, Galileo
Frequency	Dual frequency	Single frequency
Data collection rate	60 s (Up to 1 s)	60 s
Unit cost	$1930 USD (1)	~$4500 CAD (2) (Currently ~$3925 USD)
Data Storage	SD (Up to 32 Gb)	Requires phone signal for data upload to Ophelia server.
Data storage maintenance cost	No	Yes
Distance between base and rovers	Based on radio specifications (Chin coulee tested for ≤1.1 km)	≤2 km
External antenna	Yes	Integrated
RTK mode	Yes	Yes
Manufacturer accuracy in RTK mode	10 mm - 14 mm	1 mm – 2 mm
Position variability	Horizontal ≤7 mm (3)	Horizontal ≤2 mm (3)

	SparkFun System	Geocube System
	Vertical ≤12 mm (3)	Vertical ≤4 mm (3)

Notes: (1) Detailed cost in section 3.4.2, (2) Based on Rodriguez (2021) and Berru et al.(2023), and (3) Estimated position variability using 24-Hrs standard deviation (See sections 3.5.2 and 3.5.4)

3.6 Summary and Conclusions

The description, assembly, and testing of a cost-effective dGNSS monitoring system, known as the SparkFun system, are presented in this paper. We assessed its performance for 6 months and compared it with another dGNSS system, Geocubes, at a landslide site in Western Canada. The findings lead to the following conclusions:

- The SparkFun units as a dGNSS consistently achieved the specified manufactured accuracy (14 mm horizontally and 10 mm vertically) for over 95% of the testing time for the pre-tests and at the Chin Coulee landslide test when the appropriate components were added to the SparkFun units. This demonstrates good reliability in forming the dGNSS system required for monitoring landslides.
- At the Chin Coulee landslide, data outliers represent up to 2%, resulting in 93% of the total raw data being reliable. The system's level of errors, represented by a 24-Hrs standard deviation (σ), ranged from 2.5 mm to 6.2 mm in the East and North coordinates and from 9 mm to 12.5 mm in the vertical plane (Figure 3.17). These error ranges can be considered comparable to the Geocubes, and they demonstrate high precision at a lower cost.
- The field deployment of the SparkFun system revealed a need to enhance the power supply system and to improve the overall system's robustness and insulation to withstand the harsh Canadian winter.
- During periods when the SparkFun system did not encounter issues related to environmental factors, it provided results consistent with previous monitoring dGNSS campaigns at the area and the known landslide deformation behavior. For example, the SparkFun units exhibited vertical displacement alignment with Deane (2020) and Rodriguez et al. (2021) (Figure 3.20). Regarding horizontal displacements, the system indicated an increase in displacement since

May, corresponding to the period when landslide movement intensifies. However, the detailed assessment of displacement magnitude was limited due to the duration of the monitoring period.

- The results indicate that the SparkFun system shows promise as a GNSS system. However, a more extended monitoring period, along with the need to enhance assembly robustness, is necessary for a comprehensive evaluation. This would confirm its suitability as a cost-effective alternative to existing monitoring strategies for landslide characterization.

3.7 Acknowledgement

This research was made through a collaboration with Alberta Transportation and Economic Corridors (TEC) and Klohn Crippen Berger (KCB). I'd also like to extend a special thank you to Jorge Rodriguez, Aden Shipton and Katrina Cereno for helping me install the GNSS system at the Chin Coulee landslide.

3.8 References

Alberta Climate Information Service (ACIS) (2023) Current and Historical Alberta Weather Station Data Viewer. https://acis.alberta.ca/acis/weather-data-viewer.jsp. Accessed 11 November 2023

Amec Foster Wheeler (2015) Southern region geohazard assessment 2015 annual inspection report site S5: Highway 36:02, Chin Coulee. Calgary, Alberta

Berru, Macciotta R, Gräpel C, Rodriguez J, Skirrow R, Tappenden K (2023) Cost-effective dGNSS system for landslide monitoring: system description, deployment, and initial findings at the Chin Coulee Landslide. GeoSaskatoon 2023

Benoit L, Briole P, Martin O, Thom C, Malet JP, Ulrich P (2015a) Monitoring landslide displacements with the Geocube wireless network of low-cost GPS. Eng Geol 195:111–121

Benoit L, Dehecq A, Thai Pham H, Vernier F, Trouvé E, Moreau L, Martin O, Thom C, Pierrot-Deseilligny M, Briole P (2015b) Multi-method monitoring of Glacier d'Argentière dynamics. Ann Glaciol 56:118–128. https://doi. Org/ 10. 3189/ 2015A oG70A 985

Caldera S, Barindelli S, Sansò F, Pardi L (2022) Monitoring of Structures and Infrastructures by Low-Cost GNSS Receivers. Appl. Sci. 2022, 12, 12468. https://doi.org/10.3390/app122312468

Chae B, Park H, Catani F (2017) Landslide prediction, monitoring and early warning: a concise review of state-of-the-art. Geosci J 21, 1033–1070 (2017). https://doi.org/10.1007/s12303-017-0034-4

Cina A, Piras M (2015) Performance of low-cost GNSS receiver for landslides monitoring: test and results, Geomatics, Natural Hazards and Risk, 6:5-7, 497-514, DOI: 10.1080/19475705.2014.889046

Cruden DM, Varnes DJ (1996) Landslide Types and Processes; in Landslides: Investigation and Mitigation, (ed.) A.K. Turner and R.L. Schuster; U.S. Transportation Research Board, Special Report, no. 247, p. 36-75.

Davies L, Gather U (1993). The identification of multiple outliers, J. Am. Stat. Assoc., 88, 782–792, 1993.

Deane E, Macciotta R, Hendry M, Gräpel C, Skirrow R (2019) The use and limitations of modern technologies for slow, vegetated landslide monitoring – Chin Coulee landslide. In: 72nd Canadian Geotechnical Conference, Geo St. John's 2019. St. John's, NL, Canada

Deane E (2020) The Application of Emerging Monitoring Technologies on Very Slow Vegetated Landslides. Master's Thesis, University of Alberta, Edmonton, Canada, 2020. https://era.library.ualberta.ca/items/a669ecdc-4535-4145-8684-c071729875e3

Deane E, Macciotta R, Hendry M, Gräpel C, Skirrow R (2020) Leveraging historical aerial photographs and digital photogrammetry techniques for landslide investigation—a practical perspective. Landslides 17, 1989–1996 (2020). https://doi.org/10.1007/s10346-020-01437-z

Doberstein D (2012) Fundamentals of GPS Receivers. Springer, Nipomo, CA, USA

Emlid (2020) Single-band vs Multi-band. https://docs.emlid.com/reach/tutorials/basics/single-multi/

Gili J, Corominas J, Rius J (2000) Using Global Positioning System techniques in landslide monitoring, Engineering Geology, Volume 55, Issue 3, 2000, Pages 167-192, ISSN 0013-7952. https://doi.org/10.1016/S0013-7952(99)00127-1.

Golder and Associates (1998) Geotechnical investigation – site S5: highway 36:02 – November 1998 Report Geotechnical Risk Management Plan

Hamza V, Stopar B, Sterle O, Pavlov˘ci˘c-Prešeren P (2023) A Cost-Effective GNSS Solution for Continuous Monitoring of Landslides. Remote Sens. 2023, 15, 2287. https://doi.org/10.3390/rs15092287

Harris S (2023) Global Navigation Satellite System (GNSS) and Satellite Navigation Explained. https://www.advancednavigation.com/tech-articles/global-navigation-satellite-system-gnss-and-satellite-navigation-explained/

Liu H, Shah S, Jiang W (2004) On-line outlier detection and data cleaning, Comput. Chem. Eng., 28, 1635–1647, 2004.

Macciotta R, Hendry M, Martin CD (2016) Developing an early warning system for a very slow landslide based on displacement monitoring. Nat Hazards 81:887–907. https:// doi. org/ 10. 1007/ s11069- 015- 2110-2

Malet J, Maquaire O, Calais E (2002) The use of global positioning system techniques for the continuous monitoring of landslides: Application to the Super-Sauze earthflow (Alpes-de-Haute-Provence, France). Geomorphology 43: 33 – 54.

Manzini N, Orcesib A, Thom C, Brossaultd M-A, Bottone S, Ortiz M, Dumouling J (2022). Performance analysis of low-cost GNSS stations for structural health monitoring of civil engineering structures. Structure and Infrastructure Engineering. 2022, VOL. 18, NO. 5, 595–611. https://doi.org/10.1080/15732479.2020.1849320

Miller S, Zhang X, Spanias A (2015) Multipath effects in GPS receivers: a primer. Morgan & Claypool. https:// doi. org/ 10. 2200/ S0068 2ED1V 01Y20 1511C OM011

Ophelia-Sensors (2019) Geocube. https://ophelia-sensors.com/geocube-solution

Pearson RK (2002) Outliers in process modeling and identification, IEEE Trans. Contr. Syst. T., 10, 55–63, 2002.

Rodriguez J, Hendry M, Macciotta R, Evans T (2018) Cost-effective Landslide Monitoring GPS System: Characteristics, Implementation and Results. Geohazards 7, Proceedings Paper, 8 p

Rodriguez J (2021) Assessing The Benefits of Cost-Effective Monitoring Technology on Unstable Slopes Sensitive to Weather. Doctoral's Thesis, University of Alberta, Edmonton, Canada, 2021. https://era.library.ualberta.ca/items/3b6c65a4-7842-419e-82b1-49ba578c9d04

Rodriguez J, Deane E, Hendry M, Macciotta R, Evans T, Gräpel C, Skirrow R (2021). Practical evaluation of single-frequency dGNSS for monitoring slow-moving landslides. Landslides 18, 3671–3684 (2021). https://doi.org/10.1007/s10346-021-01737-y

Sharifi S, Hendry M, Macciotta R, Evans T (2022) Evaluation of filtering methods for use on high-frequency measurements of landslide displacements, Nat. Hazards Earth Syst. Sci., 22, 411–430, https://doi.org/10.5194/nhess-22-411-2022, 2022.

Shen N Chen L, Liu J, Wang L, Tao T, Wu D, Chen R (2019) A Review of Global Navigation Satellite System (GNSS)-Based Dynamic Monitoring Technologies for Structural Health Monitoring. Remote Sensing. 2019; 11(9):1001. https://doi.org/10.3390/rs11091001

Smethurst J, Smith A, Uhlemann S, Wooff C, Chambers J, Hughes P, Lenart S et al. (2017) Current and future role of instrumentation and monitoring in the performance of transport infrastructure slopes. Q J Eng Geol Hydrogeol 50:271–286. https:// doi. Org/ 10. 1144/ qjegh 2016- 080

SparkFun (2023a) About us. https://www.SparkFun.com/about_SparkFun

SparkFun (2023b) SparkFun RTK Surveying Kit. https://www.sparkfun.com/products/17370

SparkFun (2023c) SparkFun RTK Express Plus Kit. https://www.sparkfun.com/products/18589

SparkFun (2023d) SparkFun Schematic. https://cdn.sparkfun.com/assets/c/1/b/d/8/SparkFun_RTK_Surveyorv13.pdf?_gl=1*1pwu48q*_ga*MTk4NjE3MzQyOS4xNjc4MTE4OTA2*_ga_T369JS7J9N*MTY5NDY1MTc5OS4zMi4xLjE2OTQ2NTEMDQuNTUuMC4w

SparkFun (2023e) Serial Terminal Basics. https://learn.SparkFun.com/tutorials/terminal-basics/tera-term-windows

SparkFun RTK Surveyor. (n.d.). GPS-18443 – SparkFun Electronics. https://www.SparkFun.com/products/18443

Tagliavini F, Mantovani M, Marcato G, Pasuto A, Silvano S (2007) Validation of landslide hazard assessment by means of GPS monitoring technique – A case study in the Dolomites

(Eastern Alps, Italy). Natural Hazards and Earth System Science (European Geosciences Union) 7 (1): 185-193.

Takasu T, Yasuda A (2009) Development of the low-cost RTK GPS receiver with the open source program package RTKLIB. International Symposium on GPS/GNSS. International Convention Centre Jeju, Korea, 2009

Ublox (2022) ZED-F9P: u-blox F9 high precision GNSS module.https://content.u-blox.com/sites/default/files/ZED-F9P_IntegrationManual_UBX-18010802.pdf

Ublox (2023a) ZED-F9P module - u-blox F9 high precision GNSS module .https://www.u-blox.com/en/product/zed-f9p-module#tab-documentation-resources

Ublox (2023b) ZED-F9R module - u-blox F9 high precision dead reckoning module. https://www.u-blox.com/en/product/zed-f9r-module

Ublox (2023c) u-center - GNSS evaluation software for Windows. https://content.u-blox.com/sites/default/files/u-center_Userguide_UBX-13005250.pdf

Ublox (2023d) ZED-F9R High precision sensor fusion GNSS receiver. https://content.ublox.com/sites/default/files/ZED-F9R_Integrationmanual_UBX-20039643.pdf

Xue C, Psimoulis P, Meng X (2022). Feasibility analysis of the performance of low-cost GNSS receivers in monitoring dynamic motion. Measurement. https://doi.org/10.1016/j.measurement.2022.111819

Yao Z, Xie J, Tian Y, Huang Q (2019) Using Hampel identifier to eliminate profile-isolated outliers in laser vision measurement, J. Sensors, 2019, 3823691, https://doi.org/10.1155/2019/3823691, 2019.

Zimek A, Filzmoser P (2018) There and back again: Outlier detection between statistical reasoning and data mining algorithms, WIREs Data Min. Knowl., 8, 1280, https://doi.org/10.1002/widm.1280.

4 METHOD FOR ESTIMATING LANDSLIDE STABILITY UNDER FUTURE DRAWDOWN SCENARIOS DUE TO CLIMATE CHANGE - CHIN COULEE LANDSLIDE

A version of this chapter has been submitted to the journal *Landslides* under the title “Method for Estimating Landslide Stability under Future Drawdown Scenarios due to Climate Change - Chin Coulee Landslide”.

Abstract

The effects of climate change in Canada are evident through rising temperatures, earlier snowmelt, and drier summers. This has led to an increased demand for reservoir water, especially in Alberta, due to its distance from large water bodies, a declining trend in precipitation, and the necessity for irrigation water. Fluctuations in reservoir water levels indirectly measure the demand for reservoir water. Drawdown, a critical phenomenon influencing slope stability, has the potential to reactivate old landslides, trigger new ones, or intensify existing movements. Alberta's geology is characterized by materials with low shear strength such as coal seams and bentonitic layers with low residual strength when disturbed. Therefore, it is crucial to evaluate the stability of landslides near rivers or reservoirs under varying drawdown rates, especially when considering extreme cases of drawdown related to climate change. This research develops a systematic methodology to assess the current stability condition of a landslide under existing drawdown scenarios and explore changes in stability under potential future drawdown scenarios caused by climate change. The practicability of the methodology was assessed at the Chin Coulee landslide, located in southern Alberta, which has been affected by the reservoir drawdowns during the summer. The methodology agrees with the observed failure mechanisms and mechanical properties of the soil, as well as a decrease in stability as the drawdown rates increased. The method includes a practicable simplified approach to estimate the change in drawdown magnitude and rate because of climate change.

Keywords

Climate change, Drawdown rates, Landslide, Modelling, Strain-softening

4.1 Introduction

Landslides occur across various geographical regions impacting various types of infrastructure in Canada (Guthrie 2013). Sudden and catastrophic landslide events, triggered by factors such as heavy rainfall, stream erosion, earthquakes, and snowmelt are often perceived as the most critical case (Porter et al. 2019). However, landslides classified as slow to extremely slow (Cruden and Varnes 1996) can have a significant economic impact. In Canada, Porter et al. (2019) estimated an annual cost between $281 and $450 million, impacting communities, farmlands, highways, and railway infrastructure, among others due to landslides movement.

Landslide risks in Canada are commonly managed through monitoring, stabilization, or protection works (Macciotta et al. 2016a, Macciotta et al. 2016b, Carlà et al. 2017, Journault et al. 2017, Macciotta et al. 2019, Woods et al. 2020, 2021, Rodriguez et al. 2020, Macciotta and Hendry 2021, Soltanieh and Macciotta 2022). However, understanding the trigger factors driving the movement is critical for landslide risk management. Studies have starter to assess the effect of extreme weather conditions, related to climate change, with landslide movement (Hendry et al. 2015, Mirhadi and Macciotta 2023, Macciotta 2019, Pratt et al. 2019, Macciotta et al. 2017, Macciotta et al. 2015).

Slow-moving landslides on valley walls are frequent in the Prairie region in Western Alberta. The geology in the area is commonly comprised of a combination of glacial tills (tills) and sedimentary bedrocks. These bedrocks usually consist of clay shales interbedded with siltstones, sandstones, and coal seams. They are often highly fractured, thrust, and already deformed due to glacial overriding (Biagini et al. 2022), resulting in reduced shear strength, thereby increasing the potential for landslide occurrences. The Alberta Geological Survey has classified nearly every significant river valley and its tributaries in the region as susceptible to some degree of landslide activity (Pawley et al. 2018).

The unique geological characteristics of the region in western Alberta have been shaped by continuous erosion of the soft sedimentary bedrock, sculpting the main river valleys, and forming numerous coulees and ravines (Lalonde et al. 2005). These formations have allowed to build storage reservoirs for diverse purposes such as irrigation and agriculture, hydropower development, flood control, fishing, and household water supply (Alberta 2023a). Currently, the Alberta Government owns and operates approximately 130 reservoirs in the province (Alberta 2023b). In southern Alberta, there are 14 onstream reservoirs and 32 off stream reservoirs. This demand for reservoirs is driven by agriculture, which is fundamental for Alberta's economy. However, it's essential to recognize that, due to geological settings, landslide activity can be present in or around reservoirs banks.

Over the past decades, climate change and global warming have been significant concerns, with rising temperatures attributed to greenhouse gas emissions (Bo et al. 2008). The warming rate is anticipated to range from 0.3°C to 0.8°C per decade, with greater increases towards the poles, reaching up to 8°C, affecting greatly to countries in high latitudes, such as Canada (Bo et al. 2008). For example, the most recent report from Environment and Climate Change Canada (ECCC) forecasted a temperature increase of 6.5°C for the Canadian Prairies, including Alberta (Bush et al. 2019, Muhammad et al. 2020). According to Clark et al. (2017), climate change is projected to reduce the availability of industrial water supply in the Canadian prairie area by 26%. Additional studies suggest earlier snowmelt due to rising temperatures are causing drier late summer conditions (Joyse et al. 2016, St-Jacques et al. 2018), thereby increasing dependency on reservoirs to irrigate the farmlands (Alberta 2023c), leading to a greater decrease in reservoirs water levels (Wada et al. 2014, Kraemer et al. 2020, Lewis et al. 2023). Reservoir and river fluctuations globally have been linked to the reactivation of existing landslides and the initiation of new ones (Hendry et al. 2015, Yin et al. 2016, Macciotta et al. 2016b). The drawdown, when

reservoir water levels decrease, affects partially or entirely submerged slopes, including reservoir banks where landslides may occur in Alberta.

Drawdown significantly impacts slope stability, especially soils with low permeability which are prevalent in the region, such as tills or weak clay shales. These soils do not allow the dissipation of induced pore water pressure at the same rate as the drawdown. Additionally, drawdown reduces the external force exerted by reservoir water on the slope, acting as a buttress (Bo et al. 2008, Alonso and Pinyol 2009, Hendry et al. 2015).

In Southern Alberta, a slow-moving landslide, named the Chin Coulee landslide, has been subjected to drawdown from the Chin reservoir, particularly in the summer as demand for irrigating surrounding farmlands increases, resulting in increased displacements during these periods. This off-stream reservoir is located approximately 20 km south of Taber and serves as a water source for irrigating nearby farmland (Deane 2020). The annual average drawdown rates exhibit an increasing trend based on Chin reservoir water levels provided by Alberta Environment and Parks (AEP) (Figure 4.1). This trend has the potential to significantly impact the stability of the Chin Coulee landslide and other reservoir banks in the Chin area that are on the verge of instability.

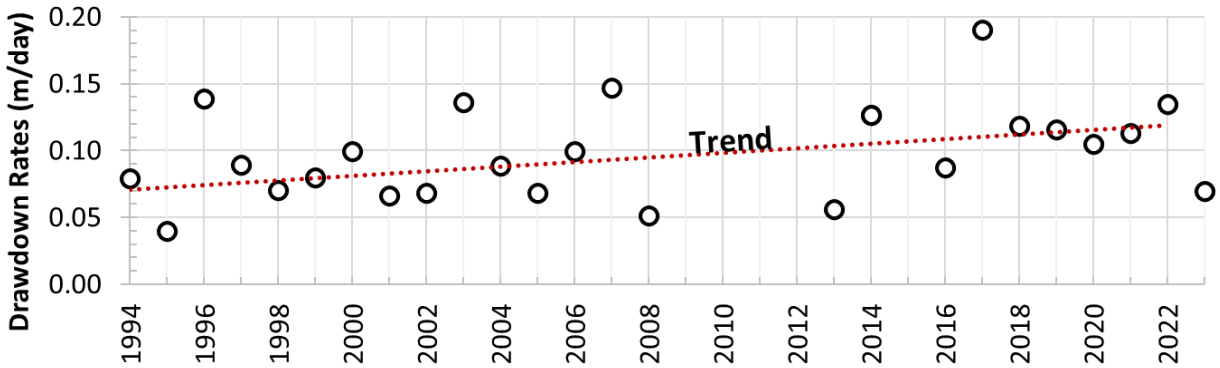

Figure 4.1 Chin reservoir annual average drawdown rates

With the continued change in climate and the need for sustainable economic growth, estimating landslide hazard changes due to climate change becomes important. This paper presents an approach to estimate changes in the landslide's stability under possible reservoir drawdown

scenarios due to climate change, illustrated by a case study. Three major steps are proposed: (1) a seepage back analysis, (2) a stability back analysis and (3) future drawdown analyses. A factor of Safety (FoS) equal to one was assumed for the stability back analysis, following Cartier and Pouget (1988) and Hendry et al. (2015), representing the current landslide condition (Baseline scenario). The stability back analysis results were used to estimate the impact of projected drawdown scenarios on changes in landslide stability. The change in the percentage of FoS relative to the baseline scenario indicates an increase or decrease in the future stability.

4.2 Chin Coulee Landslide

4.2.1 Location, Site Investigations, and Instrumentation Campaigns

The Chin Coulee landslide is located on the northern bank of the Chin Reservoir and adjacent to the south shoulder of Highway 36 (Rodriguez et al. 2021; Deane et al. 2019, Deane 2020) (Figure 4.2). The overall slope inclination of the landslide ranges from 9º to 13º, but near the headscarp, it steepens to approximately 20º (Rodriguez 2021). The landslide has a width of approximately 350 m and a height of 50 m from the reservoir level to the headscarp, resulting in an estimated volume of 2 Mm^3 (Deane et al. 2019) (Figure 4.2).

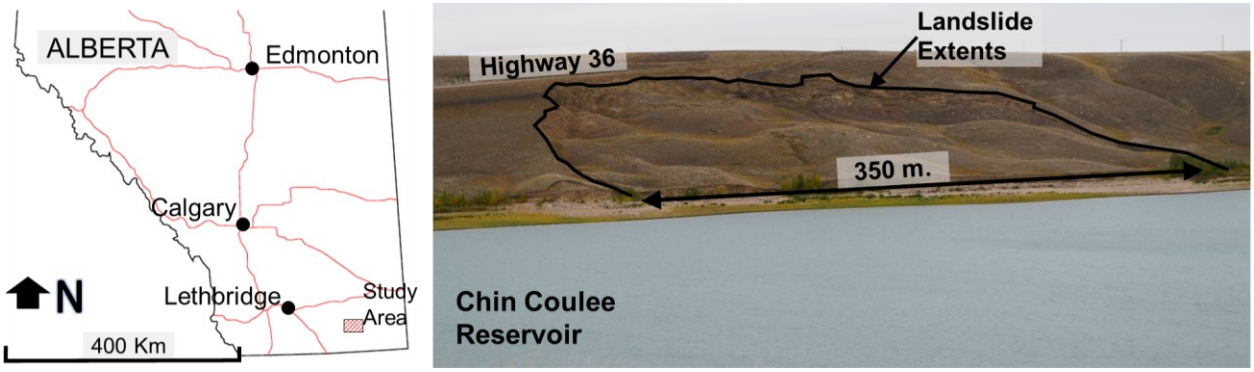

Figure 4.2 Chin Coulee landslide location and geometry characteristics

Alberta Transportation and Economic Corridors (TEC) has conducted several site investigations and instrumentation campaigns to characterize the landslide stratigraphy and identify its failure mechanism. Between 1998 and 2015, piezometers and slope inclinometers (SI) were installed;

however, they ceased working for various reasons, such as being sheared off or damaged during the 2016 highway realignment construction work. Soil samples were collected for laboratory tests (Golder 1998, Amec 2002, 2015; Deane et al. 2019; Deane 2020) in 2015. In 2018, TEC completed an additional site investigation to monitor retrogressive displacements that could affect Highway 36, installing four vibrating wire piezometers (VWPs) and two slope inclinometers (SI) (Deane 2020). Additionally, nine GNSS devices were installed, with four on the moving mass and the remaining five around the landslide perimeter (KCB 2018, Berru et. al. 2023). These devices, known as Geocubes, monitored surficial displacements between 2018 and 2023, until they were decommissioned from the site. Based on the Geocubes monitoring records, the landslide exhibits cycles of movement and inactivity, with displacements ranging from 17 mm to 107 mm in the sliding mass over a one-year period (Deane et al. 2019; Rodriguez et al. 2021). A plan view of the drill holes and instrument locations is in Figure 4.3.

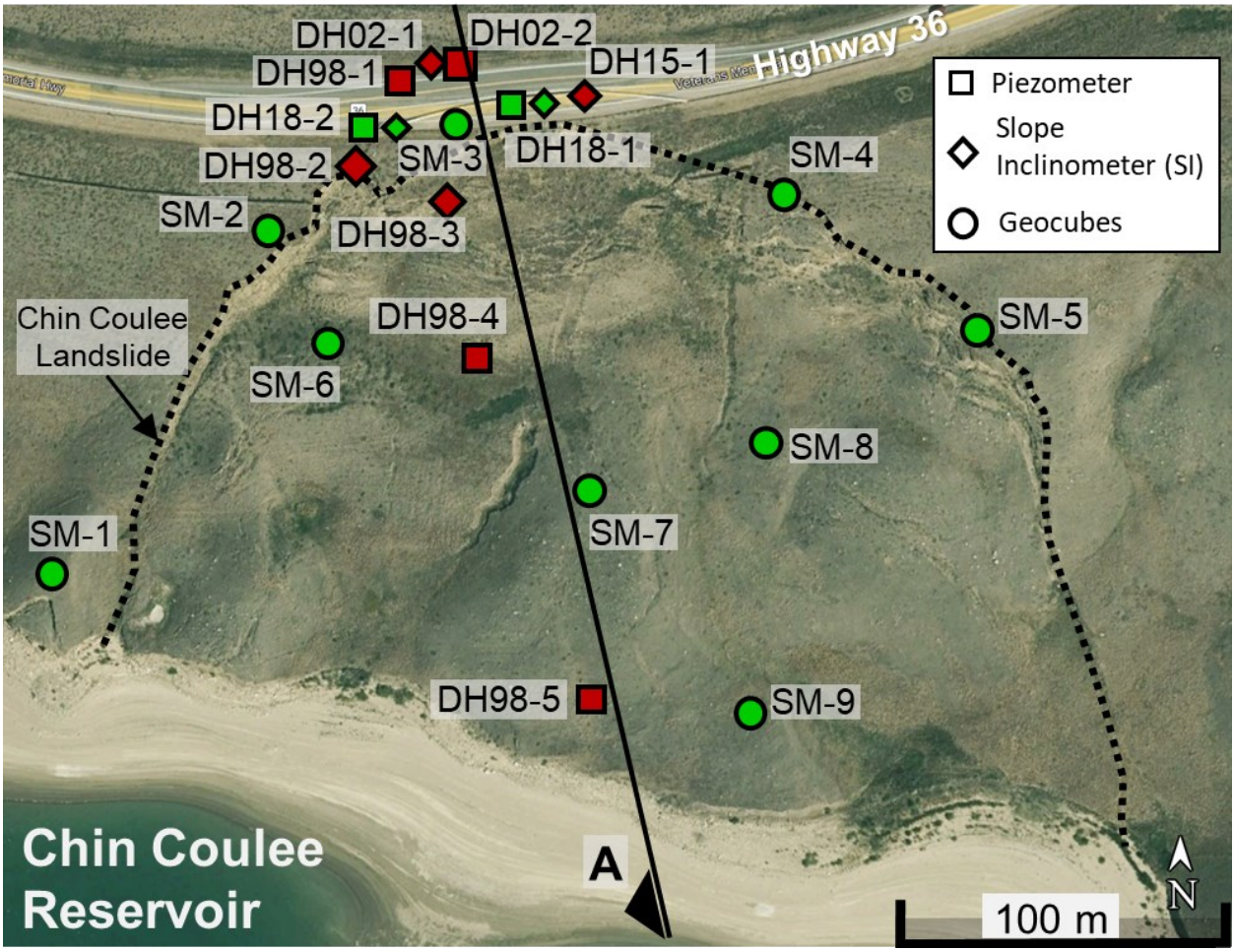

Figure 4.3 Drillholes and Instruments locations (DH (Drillhole) (Installation year)) (Green indicates operational, red indicates non-operational) Geocubes are a GNSS monitoring system (Photo right: S. Alberta MDs and Counties, Google Earth Image)

4.2.2 Landslide Stratigraphy and Groundwater Conditions

Site investigations identified an overlaying fill layer of stiff to very stiff silty clay with low to medium plasticity, which is 5 m to 10 m thick, resulting from Highway 36 construction work (Deane et al. 2019). Beneath the fill, a till layer is present, divided into two units with different degrees of weathering, consistent with regional soils' stratigraphy (Bayrocks 1963; Hendry 1980, 1982). The upper till layer, extending to approximately 15 m depth, is very stiff, weathered, brown, and exhibits low to medium plasticity due to oxidation (Hendry 1980). Meanwhile, the lower till consists of a very stiff to hard, unweathered, dark grey till with low plasticity up to 45 m below ground surface.

The bedrock comprises discontinuous layers of non to low plasticity grey siltstones, non to low plasticity grey sandstone, and medium to high plasticity weak clay shales (Deane et al. 2019, Rodriguez et al. 2021). A 1 m thick coal seam was found within the clay shales at elevations approximately 830 m and 827 m in boreholes DH-98-5 and DH98-4, respectively (Deane et al. 2019). Sandstone was inferred to lay beneath the coal seam according to borehole logs. A typical cross section showing the landslide stratigraphy is presented in Figure 4.4

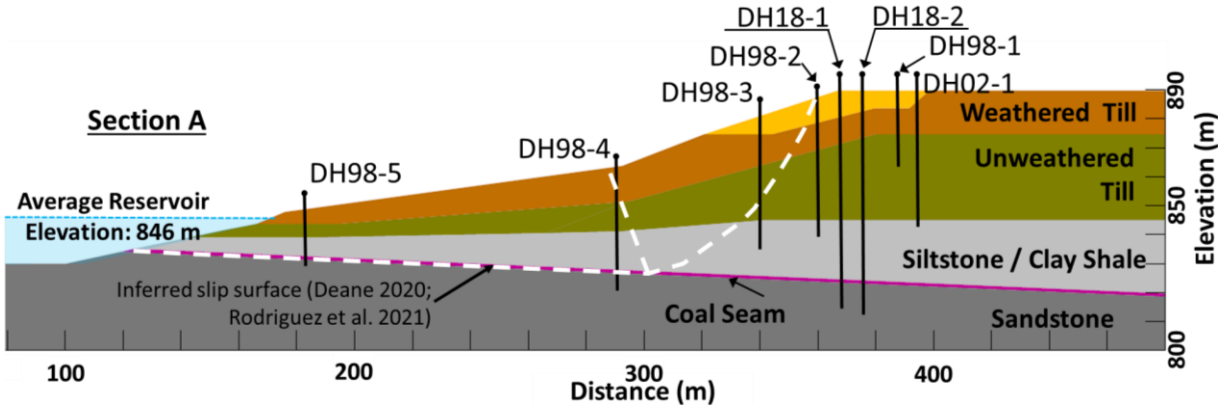

Figure 4.4 Chin Coulee landslide's Stratigraphy

During drilling, groundwater was encountered at the landslide crest in the upper till. Amec (2015) observed groundwater at an elevation of 878.9 m, while DH98-1 standpipe piezometer indicated levels ranging from elevations 877 m to 886.3 m. The 2018 VWP records have suggested stable groundwater levels between elevations 869.5 m to 877.5 m (KCB 2022) throughout the year (Figure 4.5), with no discernible seasonal or rainfall-related fluctuations. However, the infrequent readings do not allow assessing small-scale fluctuations (KCB 2022).

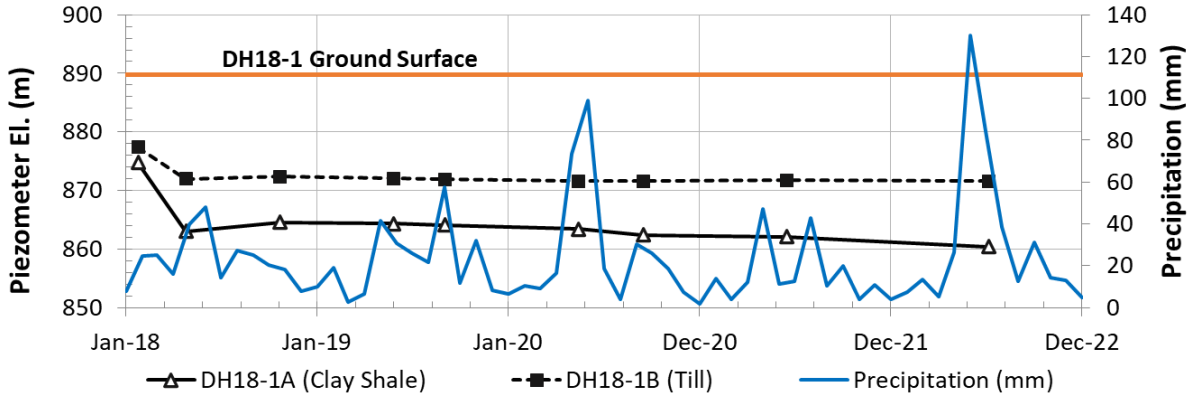

Figure 4.5 DH18-1 VWP record and precipitation (El. = Elevation, precipitation based on Wrentham Station)

Deane (2020) identified the unweathered till (Figure 4.4) as the key material influencing groundwater at the landslide. DH98-5 and DH98-4 piezometers installed at the landslide toe had provided relatively constant groundwater levels over time, excluding the first four measurements, which appear to be inaccurate as the piezometers were still stabilizing (Figure 4.6), indicating that this material exhibited higher permeability at the landslide toe (Deane 2020; Golder 1998). Green vegetation observed also in this area may indicate shallow groundwater (Golder 1998).

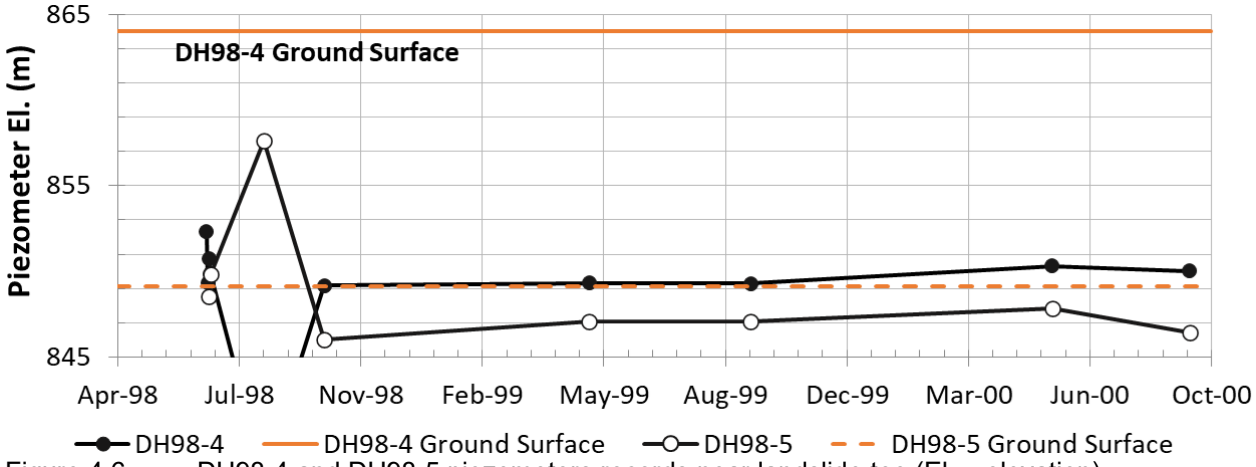

Figure 4.6 DH98-4 and DH98-5 piezometers records near landslide toe (El. = elevation)

4.2.3 Failure Mechanism and Triggering Factors of the Chin Coulee Landslide

Golder (1998) suggested that the failure surface may be located on the weak shale/coal seam. Amec (2015) conducted two stability analyses, one considering a slip surface along the coal seam and the other along the contact of the bedrock and the till. Their findings indicated that the

landslide is primarily driven by deep-seated movement on the weak shale/coal seam, exhibiting retrogressive behavior towards the north.

Deane (2020) analyzed the landslide evolution and identified two primary factors contributing to its displacements: (1) the realignments of Highway 36, and (2) the filling of the reservoir. He also noted that that increasing reservoir water usage in the summer causes drawdown periods, further exacerbating the displacements. He concluded that the Chin Coulee landslide is characterized by a compound failure mechanism involving a combination of translational rotational sliding and lateral spreading. Rodriguez (2021) analyzed the landslide mechanism using Geocubes. Geocube SM-6, installed in the upper area, showed a downward component of movement, consistent with its location identified as a graben area, while SM-7 and SM-9 units installed at the landslide middle and toe areas recorded slightly upward movements (Figure 4.7). The small upward component of movement at the toe suggests a possible rotational movement near the toe to allow the kinematical feasibility of the displacements, increasing the complexity of the deformation mechanism (Rodriguez 2021). Rodriguez et al. (2021) also observed greater displacement trends due to reservoir drawdown.

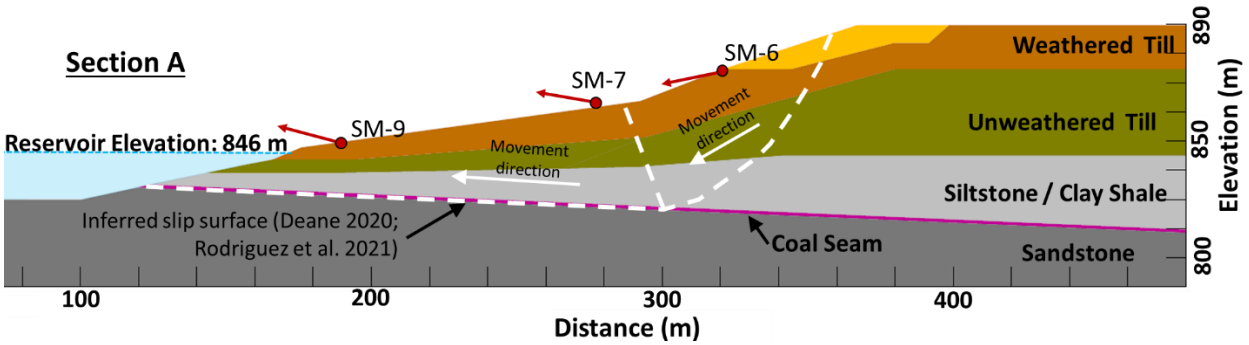

Figure 4.7 Chin Coulee landslide estimated failure mechanisms (After Deane (2020) and Rodriguez et al. (2021))

4.2.4 Common Landslide Behaviour in Western Canada

The Chin Coulee landslide exhibits an instability mechanism commonly observed in weak bedded rock slopes in western Canada (Renani and Martin 2018), characterized by a translational movement over a weak layer (coal seam). These weak rocks and overconsolidated soils, such as

the siltstones, shales and tills typically exhibit a progressive decrease in shear strength through continuous slow movements (Skempton 1964, Hettler and Vardoulakis 1984, Renani and Martin 2018, 2019). This behaviour is commonly known as strain-weakening or strain-softening (Terzaghi 1936). Renani and Martin (2019) illustrated this behaviour in examples from Buchberg sandstones and Walton's Wood clay (Kovari 1977, Skempton 1964, Renani and Martin 2019). Both materials showed that the residual is significantly lower than the peak shear strength, but the slopes of their strength envelopes are almost identical (Figure 4.8), indicating a gradual loss of cohesion due to strain, while the friction angle is relatively maintained (Renani and Martin 2019).

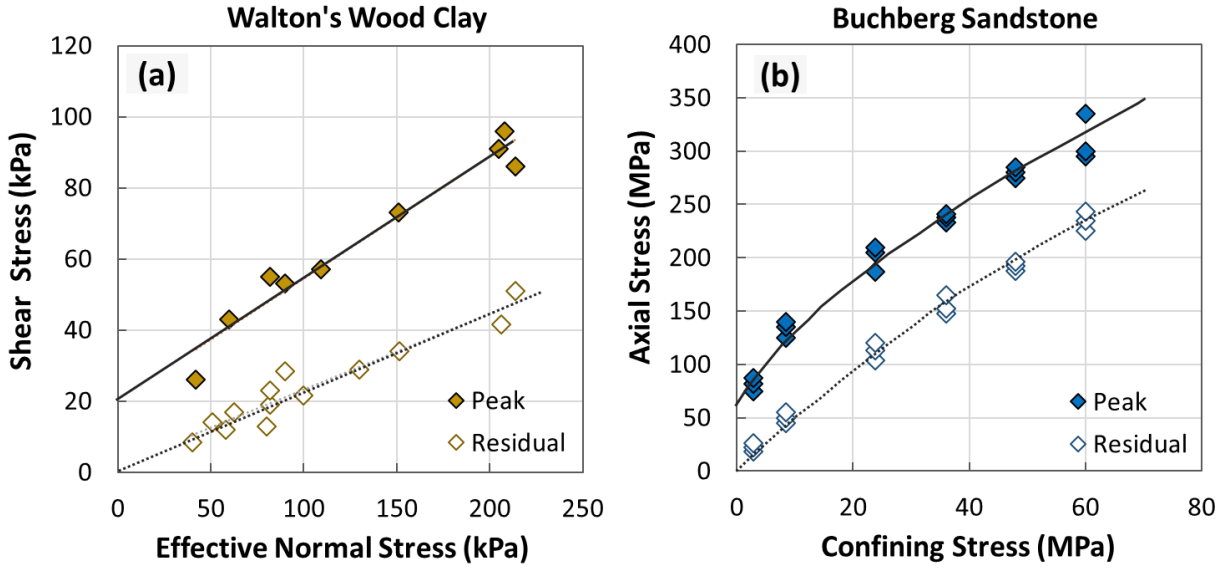

Figure 4.8 Strength envelopes at peak and residual states: (a) Walton's Wood clay and (b) Buchberg sandstone (Kovari, 1977, Skempton, 1964, Renani and Martin 2019)

Renani and Martin (2019) suggested describing the strain-softening behaviour using the Mohr-Coulomb (M-C) criterion with linearly degrading strength parameters (Potts et al. 1997, Troncone 2005, Conte et al. 2010, Renani and Martin 2019, 2020) (Figure 4.9). This criterion considers an immediate and total loss of cohesion following failure (Cr= residual cohesion = 0 kPa) (Figure 4.9b). This aligns with cases presented by Renani and Martin (2019), illustrating that the residual strength envelopes of soils displaying strain-softening behavior intersect at the origin (Figure 4.8 and Figure 4.9b) (Renani and Martin 2019). The clay shales and tills at the Chin Coulee landslide

site are likely to exhibit similar behaviour because of their low liquidity index (LI) (<0.5), suggesting an overconsolidated and fissured state (Morgenstern 1967; Tweedie 1976).

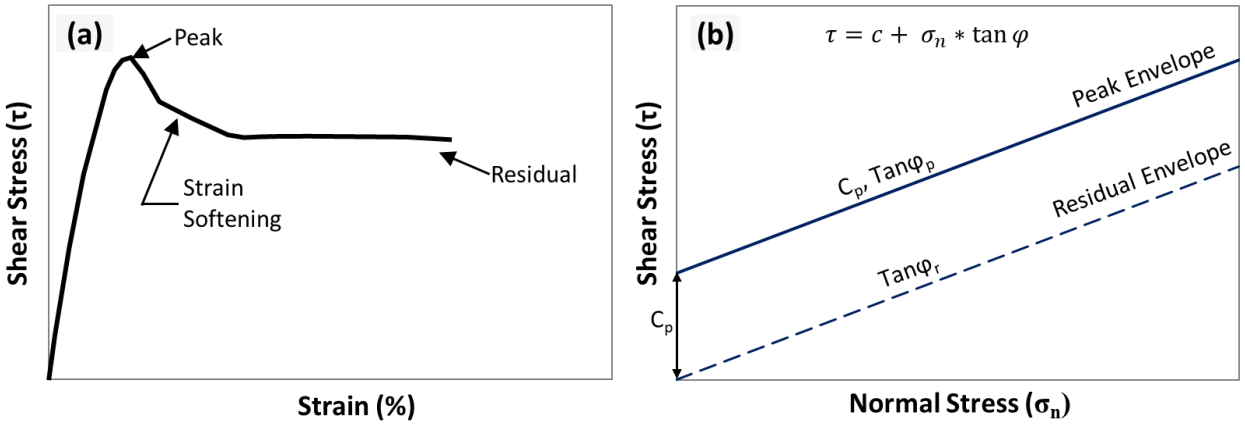

Figure 4.9 (a) Shear stress vs strain and (b) peak and residual strength envelopes in a linear degradation (Renani and Martin 2019) (Cp=peak cohesion, ϕp = peak friction angle, Cr= residual cohesion, ϕr = residual friction angle

where τ is the shear stress, σ_n is the effective normal stress, c is the cohesion, φ is the friction angle. Cohesion is generated by apparent cementation and intergranular bonds, while friction angles are related to the soil's fabric and the confining stress (Renani and Martin 2019, 2020).

4.3 Drawdown Stability Analysis Methodology

The methodology presented aims to assess the current and future landslide stability under drawdown scenarios due to climate change (Figure 4.1). The methodology comprises three principal steps: (1) a steady- state seepage back analysis that determined the landslide permeability that reflect the measured pore water pressures, (2) a drawdown stability back analysis to assess the residual strength parameters for the mobilized materials (Figure 4.4) and to define the current conditions (baseline scenario). This stability considered a critical drawdown rate, estimated based on reservoir water levels, previously estimated permeabilities, and deformation and shear strength parameters; and (3) future drawdown scenarios assessment relative to the baseline scenario.

A two-dimensional model was created, which considered the landslide section nearest to the drilled boreholes and instruments for a better representation of the stratigraphy and the current

conditions (Figure 4.3 and Figure 4.4). The seepage back analysis used the Slide2 software (Rocscience Inc., version 9.028), while the stability back analysis employed FEM model using RS2 software (Rocscience Inc., version 11.019). RS2 software allowed for the consideration of strain softening of the tills and clay shales using the M-C constitutive model with linearly degrading strength (Mebrahtu et al. 2022, Zhang et al. 2013). A uniform mesh comprising triangular nodal elements was used to discretize the landslide. The boundary conditions assumed for the seepage model were based on reservoir water levels, drilling observations and instruments records. The FEM model boundaries consisted of fully fixed nodes at the sides and base, allowing free movement on the landslide slope. A flow chart illustrating the steps for the assessment is presented in Figure 4.10, Figure 4.11 and Figure 4.12.

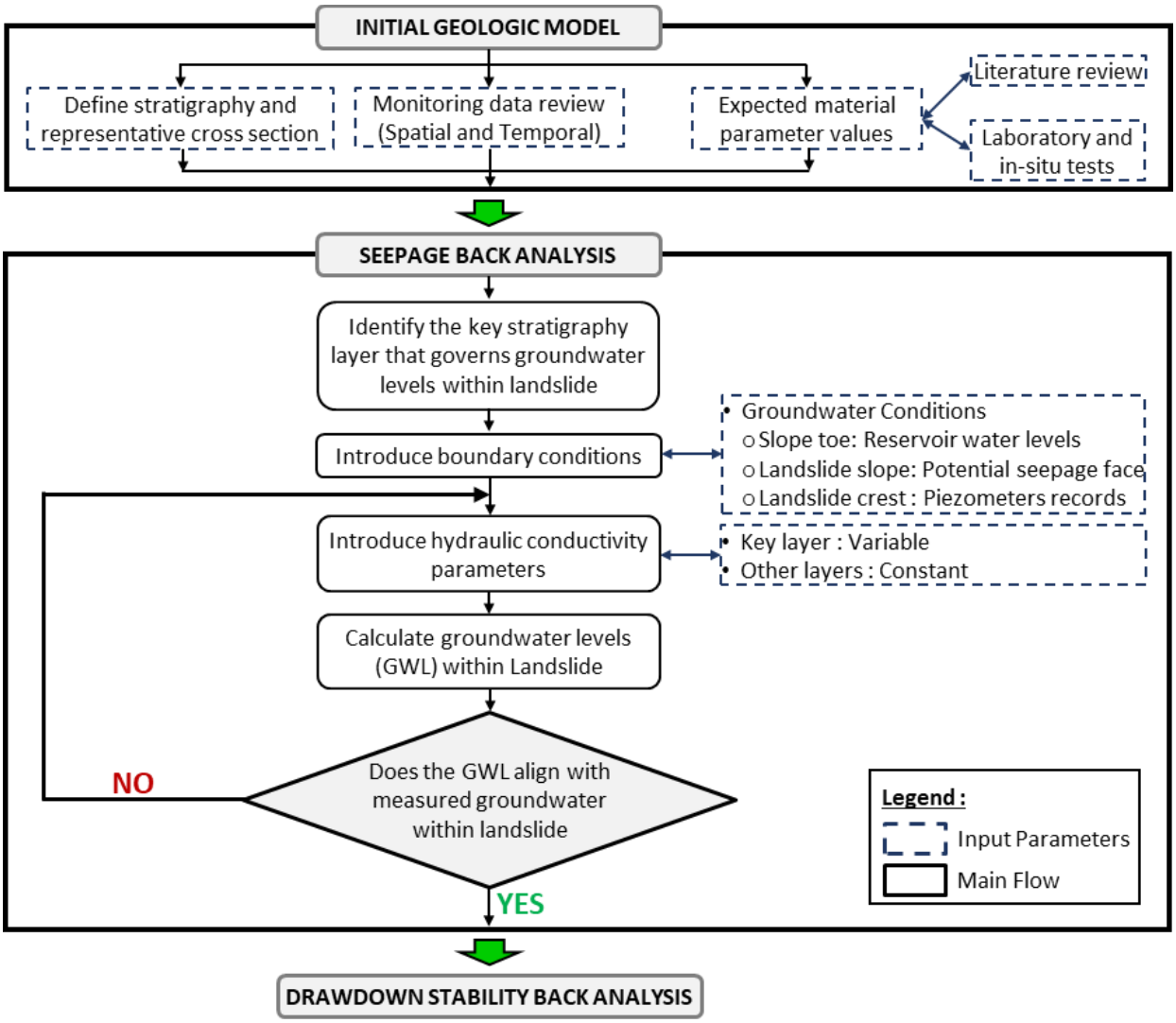

Figure 4.10 Drawdown back analysis flow chart: Initial Geologic model and Seepage Back Analysis (1 of 3)

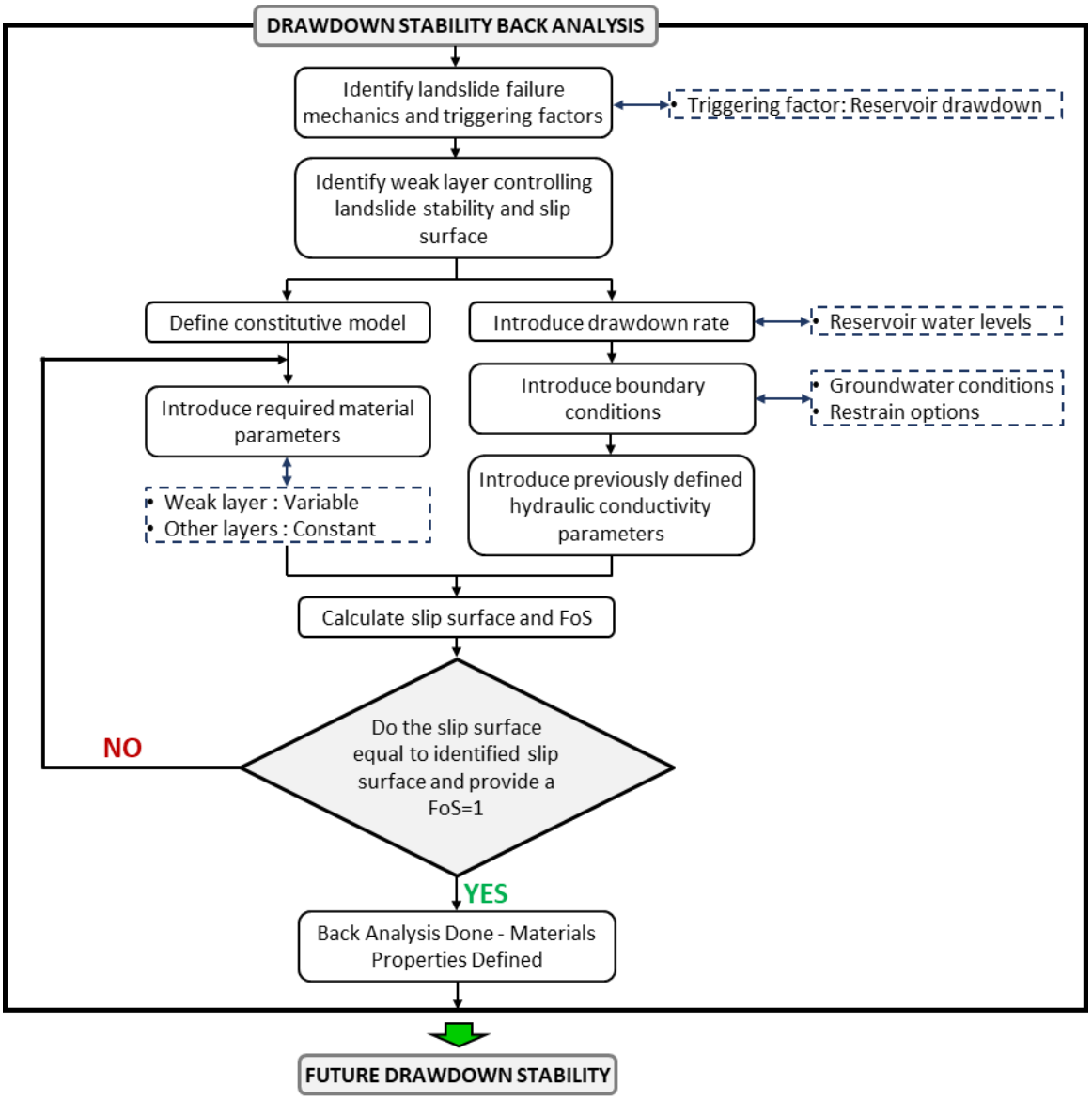

Figure 4.11 Drawdown back analysis flow chart: Drawdown back analysis (FoS= Factor of Safety) (2 of 3)

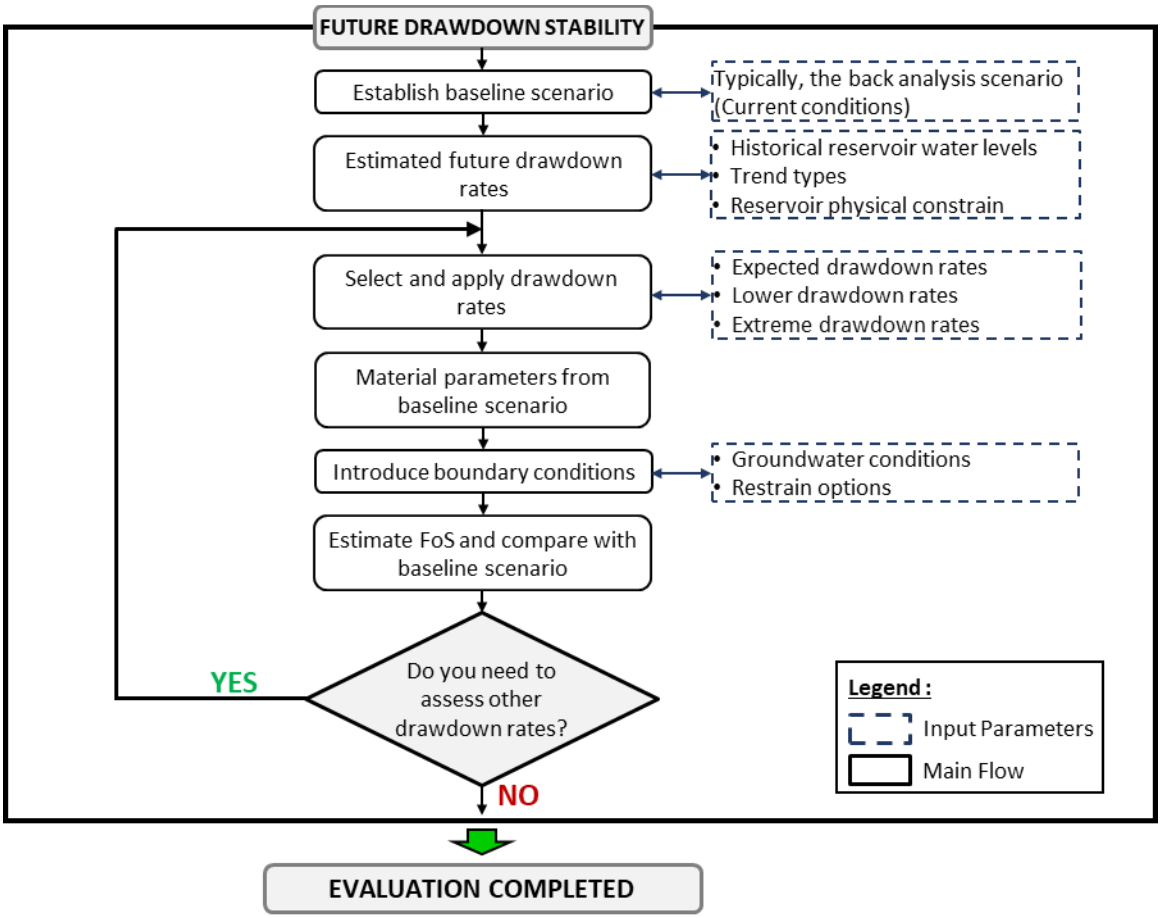

Figure 4.12 Drawdown back analysis flow chart: Future drawdown stability (FoS= Factor of Safety) (3 of 3)

A Shear Strength Reduction (SSR) analysis was used to solve the back analysis FEM model. This analysis consisted of employing different trial strength reduction factors (SRFs) on shear strength parameters until the slope reached the point of failure, preventing numerical convergence. This critical failure point is identified as the Critical SRF which is equivalent to a FoS in Limit equilibrium method (Renani and Martin 2019). This SRF value serves as a stability index, for example, a SRF greater than one can indicate a reduction in the required mobilized strength compared to the observed current strength (Hendry et al. 2015), or it can suggest an increase in stability relative to the current conditions. In the M-C criterion (Figure 4.9b), cohesion and effective friction angle are reduced by applying the SRF (Troncone 2015; Renani and Martin 2019).

Equation 4.1 $$C^{trial} = \frac{c}{SRF}$$

Equation 4.2 $$\tan \varphi^{trial} = \frac{\tan \varphi}{SRF}$$

Where C^{trial} and $\tan \varphi^{trial}$ are the trial values of cohesion and effective friction angle associated with a specific SRF.

As previously mentioned, the M-C with linear degrading was applied to the clay shales and the tills. For the fill and the coal seam, and elasto-perfect plastic behavior was assumed, resulting in equal peak and residual shear strength. This model was applied to the coal seam, assuming it is at its residual shear strength, which is typically common in bedding planes. The sandstone was considered to have elastic behavior for model simplification.

4.3.1 Shear Strength, Stiffness, and Permeability Properties

4.3.1.1 Shear Strength

Consolidated undrained triaxial tests (CUTX) on the fill provided an effective friction angle (ϕ') of 27.5º and cohesion (c') of zero. Amec (2015) estimated a ϕ' between 22º to 25º and zero cohesion. Chan and Morgenstern (1987) proposed a ϕ' of 25º for a silty clay fill at the Edmonton. A ϕ' of 25º and a c' of 0 kPa were considered representative of both peak and residual shear strength (Figure 4.13a).

Direct shear tests (DS) on till samples at elevation 877 m, indicated a ϕ' of 25.6º and c' of 21.5 kPa. Golder (1998) estimated a ϕ' of 18º and a c' of 5 kPa. Amec (2005) suggested a c' of 30 kPa and a ϕ' of 18º. However, in 2015 Amec proposed a ϕ' between 25º to 27.5º and zero c'. Hayley (1968) characterized the tills in Northern Alberta with a ϕ' of 27º and a c' of 14.4 kPa. Triaxial test on tills from Edmonton CN Tower showed a ϕ' of 24º and a c' of 14 kPa (DeJong and Harris 1971, Elwood and Martin 2010). Medeiros (1979) characterized tills with a ϕ' of 40º based on CUTX from Churchill and Central LRT Stations in Edmonton (Elwood and Martin 2010). Wittebolle (1983) estimated a ϕ' between 31.5º to 33.5º, and c' between 15 kPa to 25 kPa (Elwood and Martin 2010) based on till samples from Nipawin Dam foundation in Saskatchewan and the

Epcor building in Edmonton (Elwood and Martin 2010). Elwood (2015) constructed a M-C failure envelope based on data from Mederios (1979) and Wittebolle (1983), resulting in a ϕ' of 49.9º and a c' of 38.3 kPa. Overconsolidated tills from Toronto indicated a ϕ' ranging from 31º to 45º (Average of 33º) and a c' between 0 kPa to 50 kPa (Average of 10 kPa) (Manzari et al. 2014). Elwood (2015) estimated the residual ϕ' ranges from 89% to 99% of the peak friction angle. A ϕ' of 26º and a c' of 25 kPa were considered suitable for the peak shear strength for both unweathered and weathered till (Figure 4.13b, c). This simplification was made due to the limited laboratory tests performed and to avoid overcomplicating the model.

Golder (1998) and Amec (2005) considered a ϕ' of 25º and a c' of 50 kPa for the clay shale, while Amec (2015) proposed ϕ' from 30º to 35 º with no cohesion. Deane (2020) suggested ϕ' of 30º for the clay shale. Locker J. (1969) conducted DS on siltstones from Edmonton and the Paskapoo formation in central Alberta. The siltstones exhibited ϕ' between 35 º to 40º and c' between 140 kPa to 420 kPa (Thomson and Morgenstern 1979). Based on triaxial laboratory tests from the Leseur slide in Edmonton, Thomson (1971) determined a ϕ' = 24º and c' = 65 kPa for the clay shale (Thomson and Morgenstern 1979). Eigenbrod and Morgenstern (1972) proposed a ϕ' = 33º and c' = 9.5 kPa for the weathered clay shales of the Devon slide located in Edmonton. Chan and Morgenstern (1987) recommended ϕ' of 21º and c' of 48 kPa for the clay shale. Davachi et al. (1991) conducted direct shear tests at the Oldman River dam site in southwest Alberta, suggesting ϕ' = 35º and c' = 200 kPa for unweathered siltstones, with zero cohesion for weathered siltstones. Renani and Martin (2020) proposed a ϕ' = 35º and c' = 250 kPa for clay shales in western Alberta (Cornish and Moore 1985). A ϕ' of 30º and a c' of 100 kPa was considered for the clay shale, based on these literature review (Figure 4.13d, e)

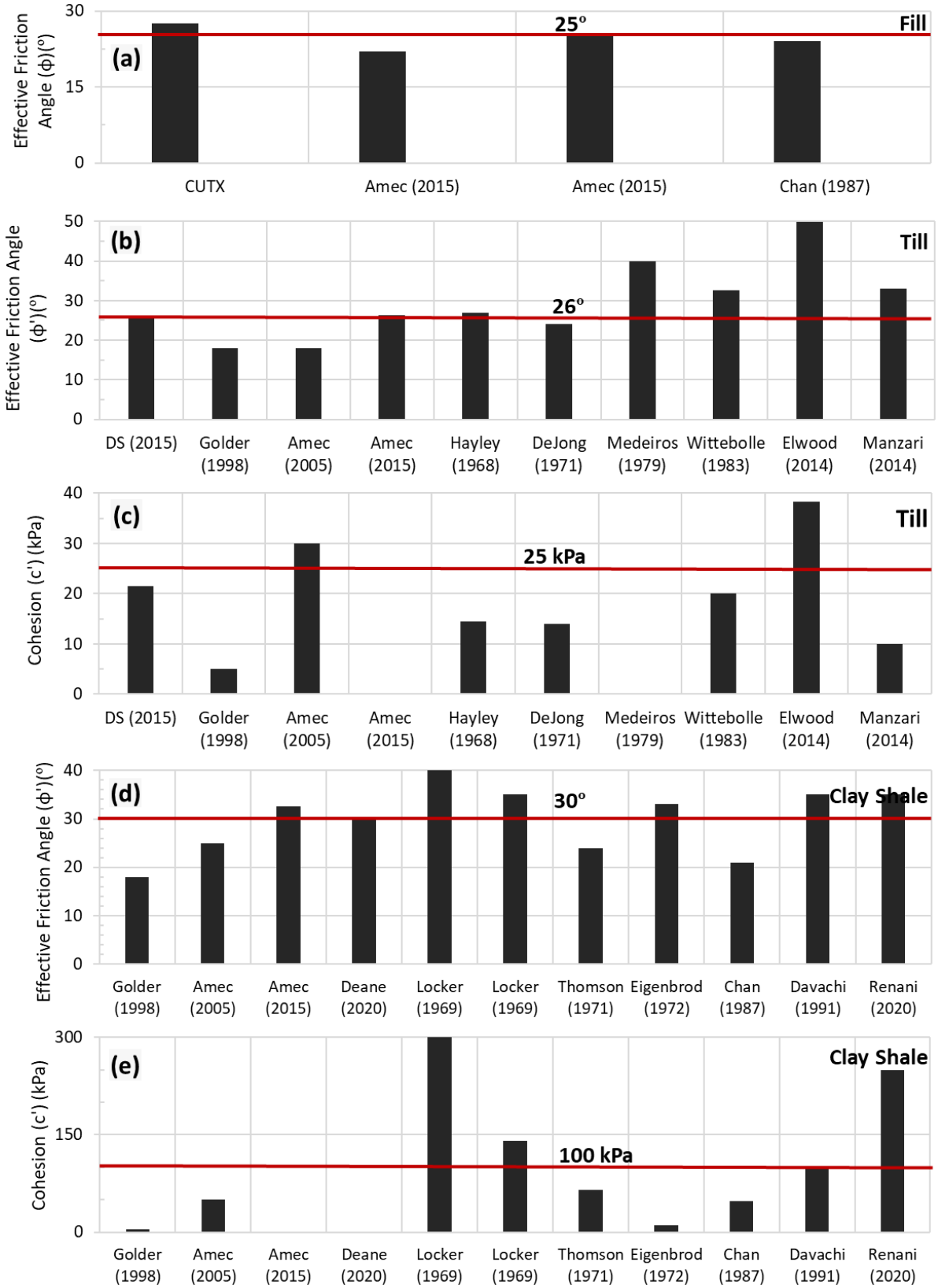

Figure 4.13 Initial shear strength parameters for (a) fill material, (b)(c) glacial till and (d)(e) clay shale (CUTX = Consolidated undrained triaxial test and DS= Direct shear test)

Golder (1998) and Amec (2005) proposed a ϕ' between11º to 16º for the coal seam, while Amec (2015) suggested a ϕ' between 8 º to 9.5º. Ringheim (1964) estimated ϕ' = 9º for soft shales based on back analyses. Hayley (1968) determined that clay shales of the Little Smoky River landslide was at its residual strength with ϕ' = 14º and c' = 0 kPa. Eigenbrod and Morgenstern (1972) determined a ϕ' = 8º with no cohesion for bentonite seams. Cornish and Moore (1985) reported a ϕ' of 9 º for bedding planes in Western Alberta (Renani and Martin 2020). Davachi et al. (1991) recommended a ϕ' between 10º to 16º for bedding planes. For the coal seam, ϕ' values between 8º to 12º, with no cohesion were evaluated to determine the value that provides an SRF equal to 1 (Figure 4.14).

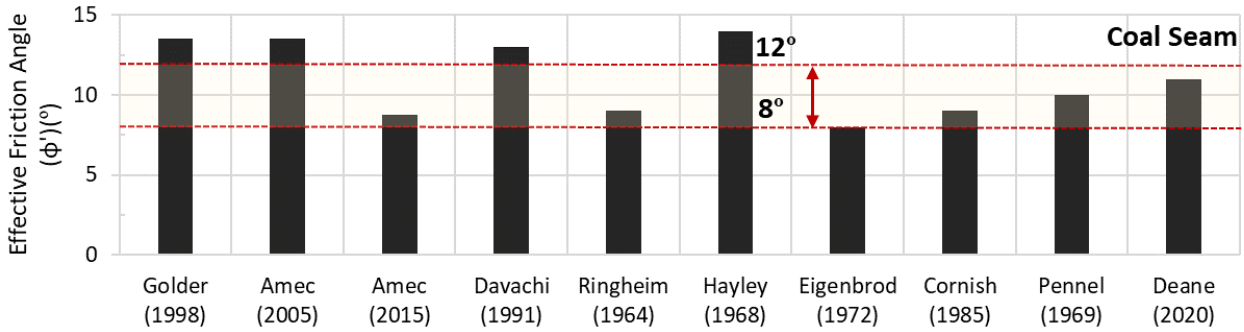

Figure 4.14 Initial shear strength parameters for coal seam

Golder (1998) and Amec (2005) proposed a ϕ' = 40º and c' = 200 kPa for the sandstone. Locker J. (1969) suggested a ϕ' = 35º and a c' = 140 kPa for the claystones (Thomson and Morgenstern 1979). Davachi et al. (1991) recommended a ϕ' of 60º for sandstones. For the sandstone a ϕ' equal to 40º and a cohesion of 100 kPa was considered. The initial shear strength parameters for the back analysis are in Table 4.1.

4.3.1.2 Stiffness

Chan and Morgenstern (1987) proposed an elastic modulus (E) of 25 MPa for the silty clay fill. Pressuremeter tests on Edmonton tills provided E between 125 MPa to 140 MPa (Eisenstein and Morrison 1973). Medeiros (1979) determined tills' E between 142 MPa to 164 MPa, while Chan and Morgenstern (1987) suggested a value of 92 MPa. Elwood and Martin (2010) statistically

estimated the average E of tills as 197 MPa, combining results from DeJong and Harris (1971), Medeiros (1979), and Eisenstein and Morrison (1973). Elwood (2015) suggested that E between 125 MPa to 200 MPa and a Poisson's ratio (υ) of 0.325 for tills based on in-situ and laboratory tests in Edmonton. It was considered a E of 120 MPa for the tills (Figure 4.15).

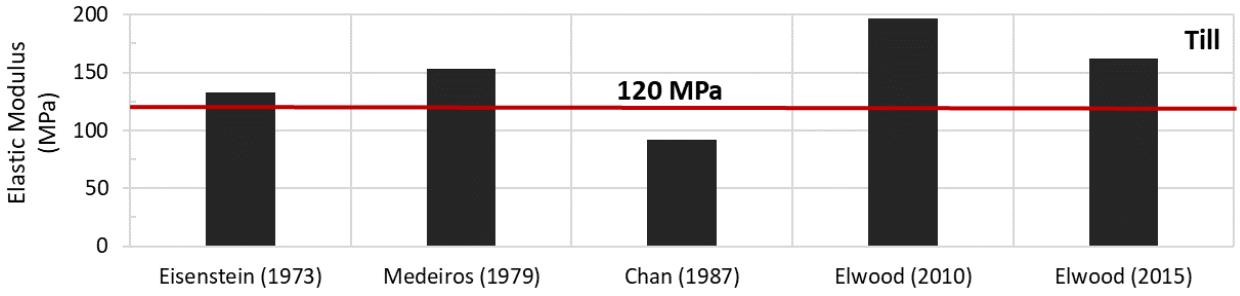

Figure 4.15 Initial elastic modulus for glacial till

Chan and Morgenstern (1987) proposed a minimum E of 138 MPa and a υ of 0.40 for clay shales, based on back analyses of excavation projects. Renani and Martin (2020) considered an E of 400 MPa for clay shales and 100 MPa for bedding planes in western Canada, with a υ of 0.25 for both materials. Morrison (1972) conducted pressuremeter tests on clay shales in Edmonton, estimating E between 87 MPa to 900 MPa (Average of 500 MPa). Elwood (2015) recommended an E of 425 MPa and a υ of 0.35, for the Edmonton bedrock, comprising sandstones, siltstones and claystones. For this study, E of 140 MPa was considered for the clay shale, following Chan and Morgenstern (1987). An E of 100 MPa and 400 MPa were considered for the coal seam the sandstone, respectively, based on Renani and Martin (2020). Plaxis (2021) recommends a υ less than 0.35 to ensure accurate computational outcomes, hence, a υ of 0.30 was considered for all materials. The initial shear strength and stiffness parameters for the back analysis are in Table 4.1.

Table 4.1 Initial shear strength and stiffness parameters for back analysis

Stratigraphy Unit	γ (kN/m^3)	Shear Strength				Stiffness	
		C_p (kPa)	ϕ_p (°)	C_r (kPa)	ϕ_r (°)	E (MPa)	υ
Clay Fill	21	0	25	0	25	25	0.3
Till: Weathered and Unweathered	22	25	26	0	26	120	

Stratigraphy Unit	γ (kN/m^3)	Shear Strength				Stiffness	
		C_p (kPa)	ϕ_p (º)	C_r (kPa)	ϕ_r (º)	E (MPa)	υ
Siltstone/Shale	22	100	30	0	20	140	
Coal Seam	21	0	8 / 9 /10 /11 /12	-	-	100	
Sandstone	22	100	40	-	-	400	

γ= unit weight, C_p= peak cohesion, ϕ_p = peak friction angle, C_r= residual cohesion, ϕ_r = residual friction angle, E = Elastic modulus, υ = Poisson ratio

4.3.1.3 Permeability Properties

Ameratunga (2016) suggested that fill materials have permeabilities (k) between 1x10-6 m/s to 1x10-9 m/s based on its Unified Soil Classification System (USCS), while Deane (2020) estimated a k of 1x10-7 m/s for this fill (Figure 4.16a).

Tills are considered a crucial material governing groundwater level (GWL) within the landslide, particularly the dual permeability unweathered till, with higher values close to the toe (Deane 2020). Hendry (1982) classified tills in southern Alberta into two hydrogeological units, suggesting a permeability of 2x10-7 m/s for upper weathered tills, while lower unweathered tills exhibited values between 1x10-10 m/s to 5x10-9 m/s. Deane (2020) proposed values below 1x10-7 m/s for all types of tills.

To accurately characterize this unweathered till, two permeabilities (1x10-6 m/s and 1x10-7 m/s) were evaluated near the landslide surface, and three (1x10-8 m/s, 1x10-9 m/s and 1x10-10 m/s) were assessed farther away from the slope (Figure 4.18) (Table 4.2). For the weathered till, a permeability of 1x10-7 m/s was assigned based on Deane (2020) (Figure 4.16b, c).

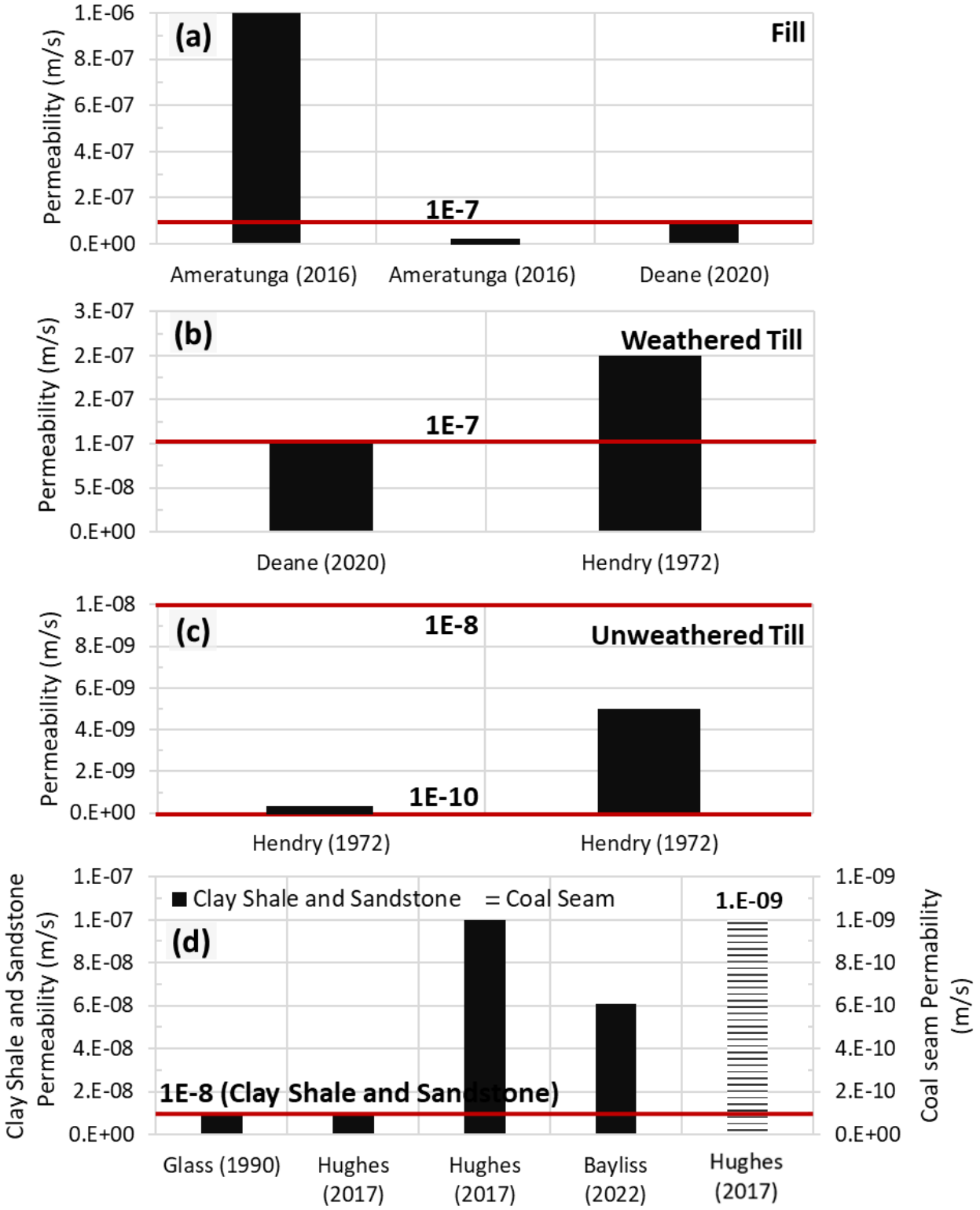

Figure 4.16 Selected permeabilities for (a) fill, (b)(c) glacial till, (d) sandstone, clay shale and coal seam

Permeabilities for sandstones in the Milk River Formation, similar to the Foremost Formation, range from 1x10-8 m/s to 3x10-6 m/s (Glass 1990, Lawrence 2011). The Porcupine Hills

Formation in southwestern Alberta exhibits diverse permeability, varying from low-permeability shales, siltstones, and mudstones to highly permeable sandstones, for instance, permeability within this formation varies from 6.5 x 10-5 m/s to 6.1 x 10-8 m/s (Bayliss 2022). In western central Alberta, the Paskapoo formation comprises siltstones, sandstones, and mudstones. The sandstone in this formation has permeabilities ranging from 1x10-8 m/s to 1x10-7 m/s, while the mudstones, siltstones and shales exhibit values around 1x10-9 m/s (Hughes et al. 2017). A permeability of 1x10-8 m/s was selected for the clay shale and the sandstones based on Glass (1990) and Hughes (2017), while for the coal seam a permeability of 1x10-9 m/s was considered based on Hughes (2017) (Figure 4.16d). The initial permeabilities for the back analysis are in Table 4.2.

Table 4.2 Initial permeabilities for seepage back analysis

Stratigraphy Unit	Permeability K_H (m/s)	K_H/K_V
Clay Fill	1x10-7	
Weathered Till	1x10-7	
Unweathered Till (near slope)	1x10-6 / 1x10-7	
Unweathered Till (away from slope)	1x10-8 / 1x10-9 /1x10-10	1
Siltstone/Shale	1x10-8	
Coal Seam	1x10-9	
Sandstone	1x10-8	

K_H = Horizontal permeability, K_H/K_V = Horizontal permeability/Vertical permeability

4.3.2 Seepage Back Analysis

The seepage back analysis initially considered permeability parameters from Table 4.2. These parameters were then refined, considering that the appropriate permeabilities should provided with a groundwater level within the limits of piezometers records (Figure 4.18).

Three hydraulic boundary conditions were assumed for the calibration of the seepage model. The boundary condition at the landslide toe was defined based on historical reservoir levels from Alberta Environment and Parks (AEP), with an average level of 844.2 m considered representative (Figure 4.17).

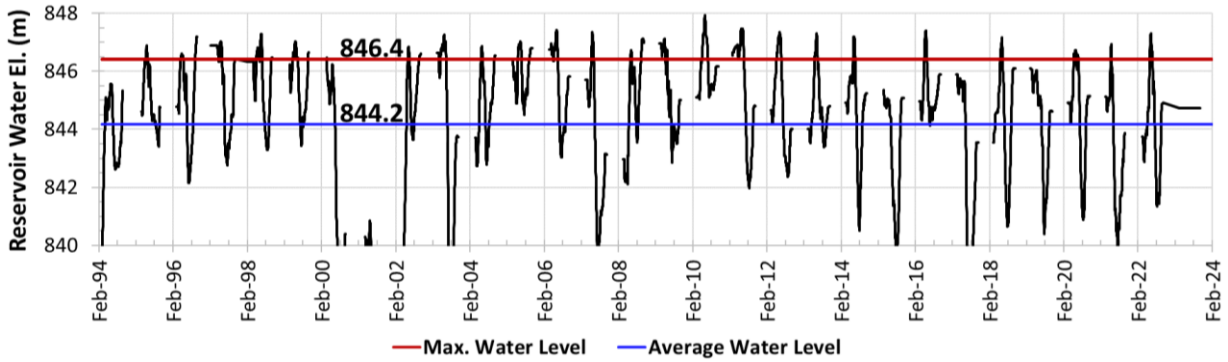

Figure 4.17 Historical reservoir water level

At the slope crest, boundary conditions are estimated based on observations during drilling and piezometer records. The GWL at the crest is assumed to be at elevation 878 m (12 m deep) (See section 4.2.2). On the landslide surface slope, a 'Seepage Face Condition' was applied to prevent the total head from exceeding the elevation head (Figure 4.18).

Upper and lower limits of groundwater elevations within the landslide, corresponding to the maximum and minimum observed piezometer records, were established for comparison with computed values. Currently, there are only piezometer records at the landslide crest (2018 VWP), however due to constant and stabilized measurements in the 1998 toe piezometer records (Figure 4.6). The 2018 VWP data with the 1998 piezometer records were merged to establish groundwater limits for the seepage model. The boundary conditions and piezometer limits are shown in Figure 4.18 and Table 4.3.

Table 4.3 Piezometer Upper and Lower Limits

Piezometer	1998 Piezometers		2018 VWP		
	GA98-5	GA98-4	VW18-02B	VW18-01B	2018 Combined
Location	Near landslide toe		At the crest		
Lower Limit (m)	845.4	849.2	859.7	871.6	859.7
Upper Limit (m)	847.2	850.3	871.1	872.3	872.3

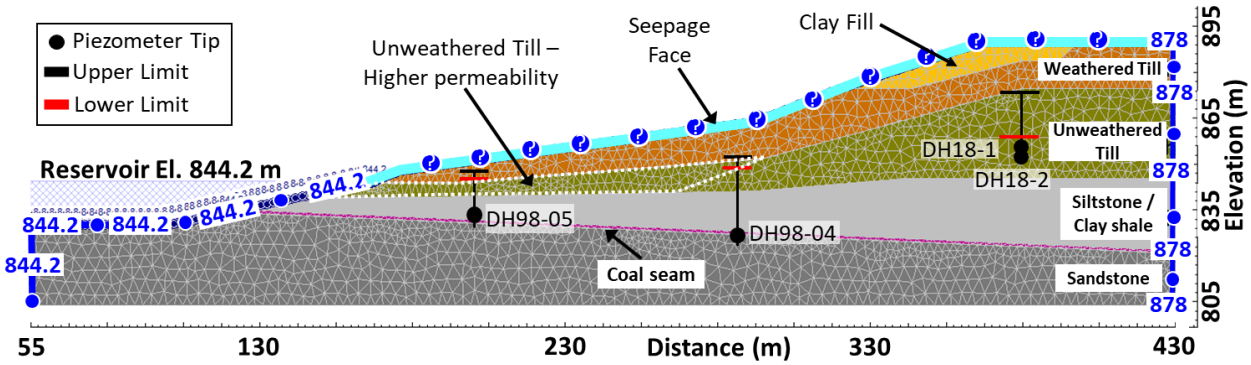

Figure 4.18 Boundary conditions and piezometer limits for seepage analysis

4.3.3 Drawdown Back Analysis Modelling under Observed Conditions (Baseline scenario)

Drawdown rates are influenced by factors like water demand and the physical characteristics of the reservoir. Water demand depends on factors such as climate, land use and demographics. However, reservoir water level fluctuations (Δ) can offer an indirect measurement of this demand. For this study, reservoir water level fluctuations are calculated as the difference between the highest levels observed at the end of the rainy season, just before peak demand, and the lowest level at the end of the dry season. This approach considers that landslide stability is most critical when fluctuations are at their highest. The annual reservoir water fluctuations, along with its calculation example for year 2019, are presented in Figure 4.19.

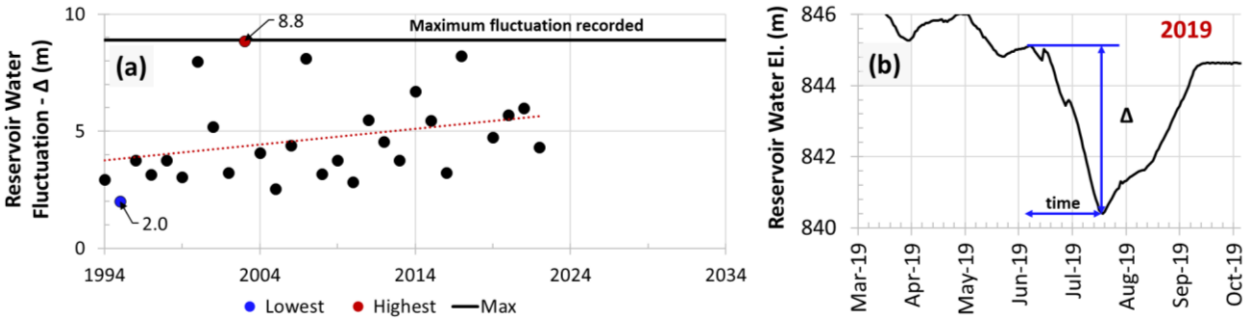

Figure 4.19 (a) Annual reservoir water fluctuation and (b) 2019 Fluctuation calculation

The annual drawdown rate is calculated by dividing the annual reservoir water fluctuation by the time it takes for this fluctuation (Equation 4.3). The highest estimated drawdown rate was 0.19 m/day in 2017, corresponding to a water fluctuation of 8.2 m (drawdown time ≈ 43 days)

(Figure 4.20). This scenario, representing the worst-case, is the one evaluated for the drawdown back analysis.

Equation 4.3 $$Drawdown\ rate = \frac{Water\ fluctuation\ (\Delta)}{time} = \frac{Reservoir\ El_{max} - Reservoir\ El_{min}}{time}$$

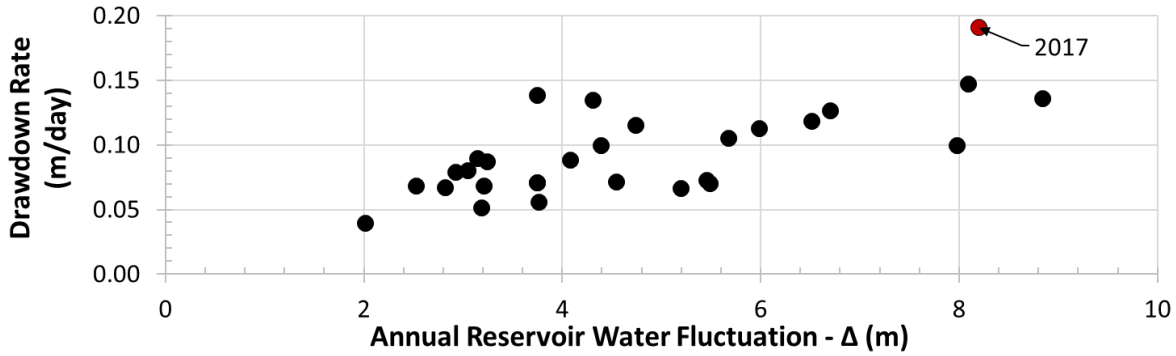

Figure 4.20 Drawdown rate vs reservoir water fluctuation

At the crest, the piezo elevation was initially set at 878 m, then reduced to 877.1 m. An average variation of 0.9 m was adopted based on 2018 VWP records (one year after the critical scenario), showing the ground water level at the crest varies from 0 m to 2 m in the till. At the slope's toe, it was considered a reservoir water elevation of 845.7 m, decreasing to 837.5 m based on the 2017 reservoir water records. The initial and final hydraulic boundary conditions for the back analysis are in Figure 4.21.

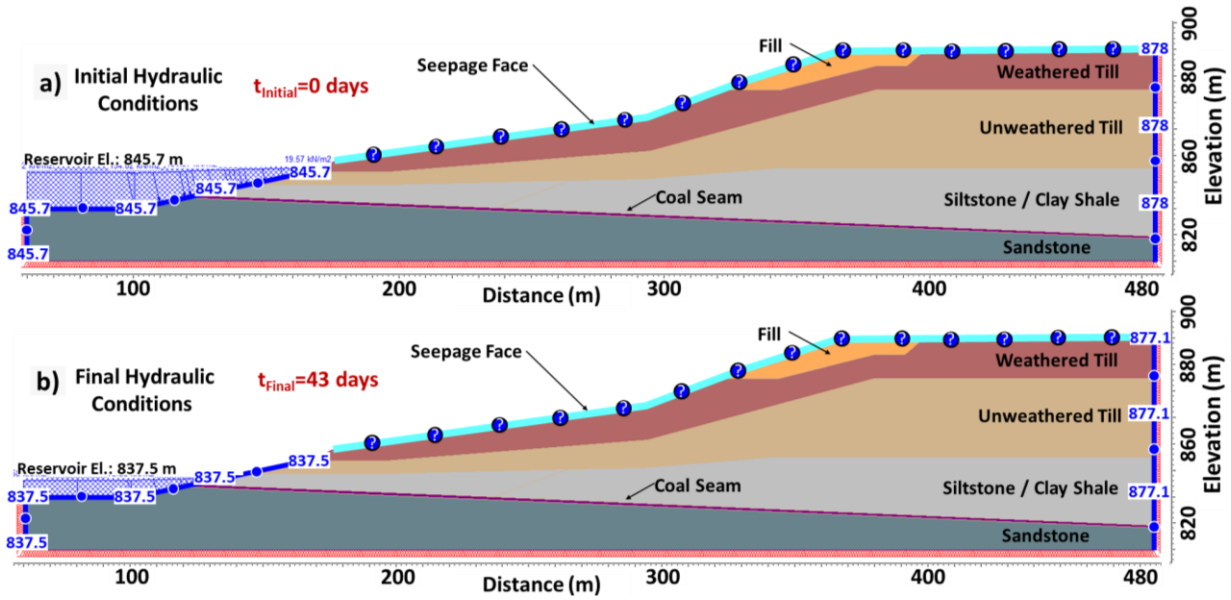

Figure 4.21 Hydraulic boundaries before and after drawdown period

4.3.4 Possible Drawdown Scenarios due to climate Change

Reservoir water fluctuations and drawdown rates exhibit an upward trend (Figure 4.1 and Figure 4.19a) potentially impacting landslide stabilities. When grouping some years, three distinct trends emerged corresponding to low, average, and maximum values (Figure 4.22). These trends also exhibited an increasing pattern which appear to be influenced by climate change, the reservoir water supply system and equipment leading to a significant increased demand for irrigation in the dryer years.

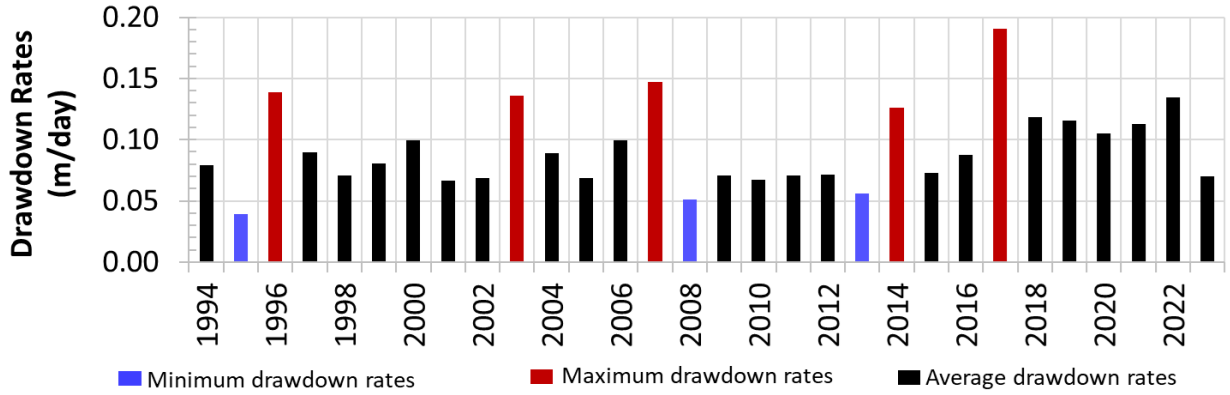

Figure 4.22 Low, average, and high drawdown rate trends

Due to the uncertainty in forecasting the increasing trend, a simple linear trend was employed for extrapolation to estimate the plausible scenarios for drawdown rates (Figure 4.23). Given the years of data available, forecasting beyond 2050 would be associated with excessive uncertainty. In this study, the drawdown stability analysis was conducted for year 2050's maximum rate (0.23 m/day in red in Figure 4.23). While not ideal, this rate was considered adequate to investigate the potential magnitude of drawdown rates and their effect in slope instability given the uncertainties associated with projecting climate change scenarios, and adequate to provide information for long term planning.

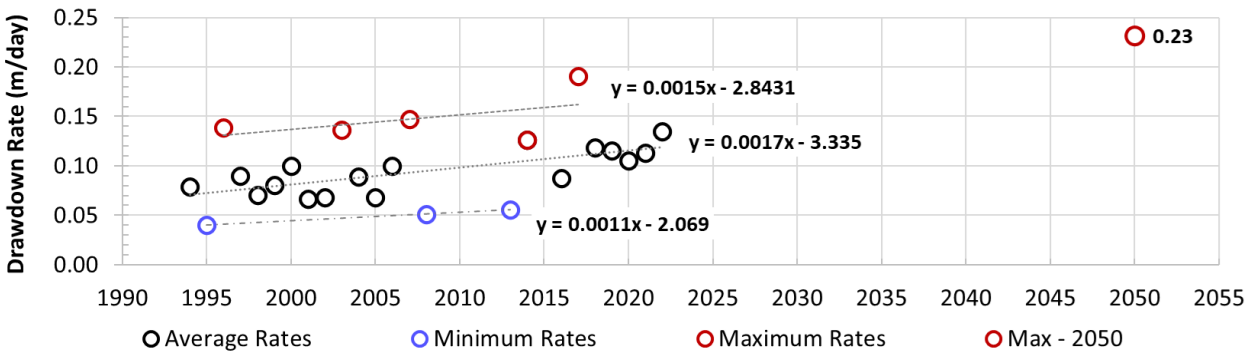

Figure 4.23 Drawdown rates trend

The water fluctuations would be limited by the required freeboard of the reservoir dam and the elevation of the outlet structure. Since there was no available data on these physical constraints, the model adopted the maximum historical fluctuation for the 2050 scenario equal to 8.8 m (Figure 4.19a), equivalent to a drawdown time of 38 days. For the future worst-case scenario modeling, the hydraulic boundary at the slope's toe considers the maximum historical average reservoir water level (Figure 4.17). At the crest, conditions resemble the 2017 scenario due to limited information on regional groundwater levels and data on their variation with precipitation or snowfall is unavailable.

Additional scenarios were evaluated to (1) assess whether a slower drawdown rate and shorter fluctuation improve stability compared to the 2017 scenario (baseline), and (2) explore the impact of extreme drawdown rates higher than the 2050 scenario on the landslide stability. For enhanced stability evaluation, an average drawdown rate of 0.09 m/day and an average fluctuation of 4.80 m were considered (drawdown time ≈ 53 days) (Figure 4.24). To explore potential further instability, two extreme drawdown rates— 0.3 m/day and 0.4 m/day —were selected, corresponding to drawdown times of approximately 29 days and 22 days, respectively. The boundary conditions for the extreme scenarios mirrored those of the 2050-year scenario. However, for the stability-increasing scenario, the initial reservoir water level was adjusted to the average reservoir water level of 844.2 m (Figure 4.17). The drawdown rates, drawdown times, fluctuations, and boundary conditions for all scenarios are summarized in Table 4.4.

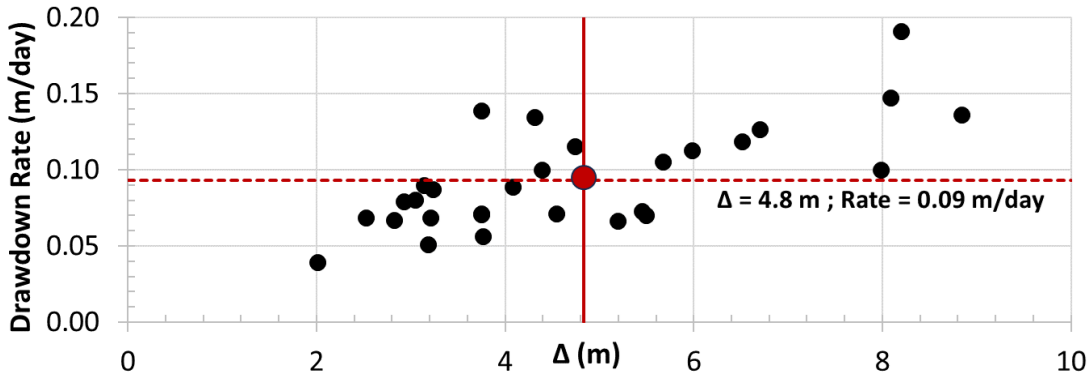

Figure 4.24 Additional scenario to compare increases in stability

Table 4.4 Drawdown rates, drawdown times, fluctuations, and Boundary conditions for scenarios

Item		Location	Drawdown Rate (m/day)				
			2017 scenario	2050 scenario	Further Instability scenario		Enhance stability scenario
			0.19	0.23	0.3	0.4	0.09
Reservoir Fluctuation (Δ) (m)			8.2	8.8	8.8		4.8
Drawdown Time (days)			43	38	29	22	53
Hydraulic Boundaries	Before Drawdown	Slope Toe	845.7		846.4		844.2
	After Drawdown		837.5		837.5		839.4
	Before Drawdown	Crest			878		
	After Drawdown				877.1		

4.4 Results

4.4.1 Seepage Analysis

For the weathered till, a permeability equal to 1x10-7 m/s showed a good agreement with the established piezometer limits and literature review (Figure 4.16b,c), while for the unweathered tills near the landslide surface values above 1x10-7 m/s caused the groundwater table to reach the surface, contrary to field observations. Unweathered tills far from the landslide surface showed that permeabilities below 1x10-8 m/s showed little variation, but at 1x10-9 m/s, the groundwater table fell within the middle of the piezometer limits and is consistent with the findings in Hendry (1982) (Figure 4.16b, c).

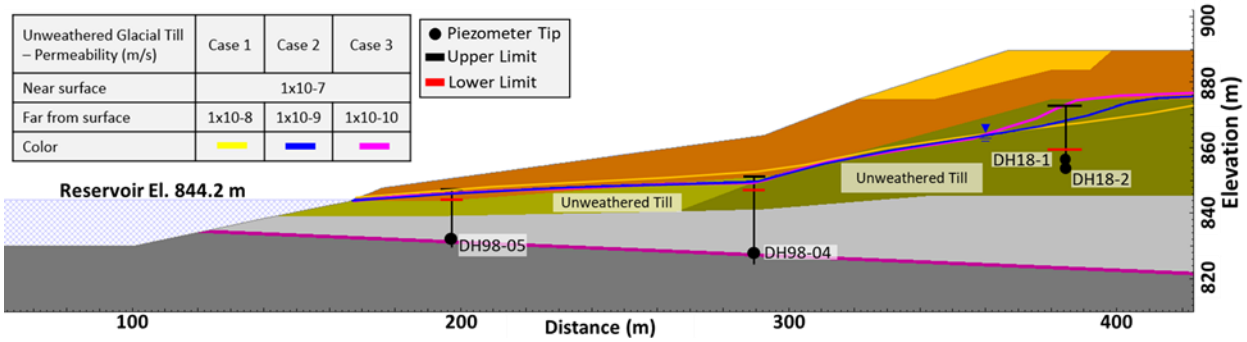

Figure 4.25 Seepage back analysis results

4.4.2 Baseline Drawdown Back Analysis

The baseline back analysis (drawdown rate of 0.19 m/day) provided a slip surface closely aligned with the observed failure mechanism (Figure 4.7 and Figure 4.26). The GWL falls within the limits of the piezometer records. The M-C criterion with linearly degrading strength successfully captured the development of a steep back scarp, the formation of a shear zone at the basal weak coal seam and continuing to the toe of the slope. This indicates a suitable balance between modeling practicability and capturing the failure mechanism. However, it was observed that the model did not clearly depict the formation of the shear zone separating the driving and passive wedges of the landslide. This could be attributed to the need for larger displacements to develop for internal shearing or the requirement to increase the brittleness of the till material. An ϕ' of 11° and no cohesion for the coal seam provided a Strength Reduction Factor (SRF) equal to unity. This shear strength aligns with Deane's (2020) findings and is within the observed range for this material type in Western Canada (Figure 4.14). The estimated landslide material properties align with values observed for similar stratigraphic units and, are in Table 4.5.

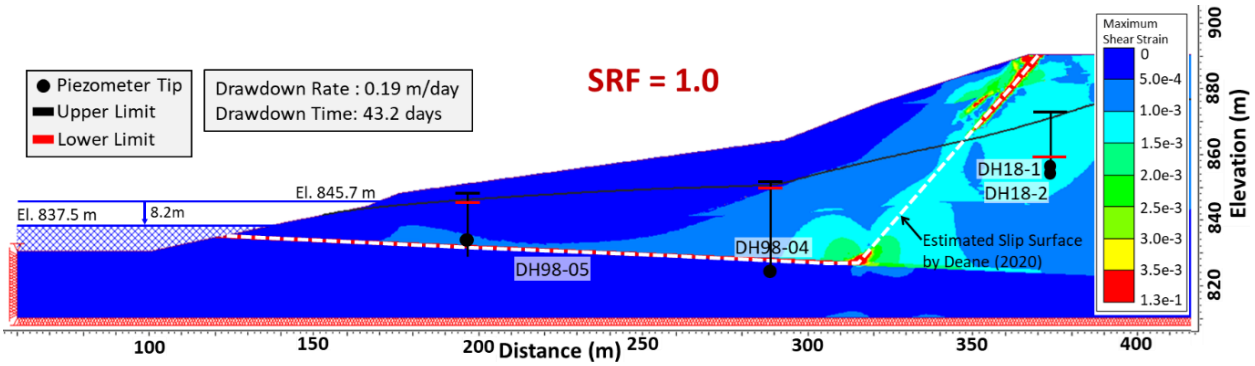

Figure 4.26 Back analysis: Critical SSR factor and slip surface obtained from SSR method

Table 4.5 Estimated landslide material parameters from back analysis

Stratigraphy Unit	γ (kN/m^3)	Stiffness E (MPa)	Stiffness υ	Shear Strength C_p (kPa)	Shear Strength ϕ_p (°)	Shear Strength C_r (kPa)	Shear Strength ϕ_r (°)	Permeability K_H (m/s)
Clay Fill	21	25		0	25	0	25	1x10-7
Weathered Till	22	120		25	26	0	26	1x10-7
Unweathered Till	22	120	0.3	25	26	0	26	1x10-7 (Near surface) 1x10-9 (Far from surface)
Siltstone/Shale	22	140		100	30	0	30	1x10-8
Coal Seam	21	100		0	11	-	-	1x10-9
Sandstone	22	400		100	40	-	-	1x10-8

γ= unit weight, E = deformation modulus, υ = Poisson ratio, C_p= peak cohesion, ϕ_p = peak friction angle, C_r= residual cohesion, ϕ_r = residual friction angle, K_H = Horizontal permeability

4.4.3 Possible Drawdown Scenarios due to climate Change

The drawdown analysis, considering a rate of 0.23 m/day (Corresponding to year 2050), would still provide an appropriate characterization of the failure mechanism and model the expected groundwater table. The critical strength reduction factor (SRF) under this condition was equal to 0.95, indicating a 5% decrease in the landslide stability (Figure 4.28a) compared to the baseline case.

For the extreme drawdown rates, the model encountered convergence problems, possibly due to the complete instability of the landslide. To address this, the convergence tolerance in the model was increased from 0.001 to 0.002 for these scenarios. After this adjustment, the slip surfaces also modelled adequately the expected slip surface. The SRFs were 0.92 and 0.89 for the

0.3 m/day and 0.4 m/day, respectively (Figure 4.28b, c), suggesting that the slope would be showing accelerated movements and may be transitioning towards collapse.

In the scenario aiming to model episodes with increased stability during a drawdown period (when compared to the base line – drawdown rate of 0.09 m/day), the resulting SRF is 1.01 (1% increase in stability) (Figure 4.28d). This was considered a marginal, non-significant change in the stability conditions of the landslide. The results of all scenarios are presented in Table 4.6 and Figure 4.27.

Table 4.6 Future drawdown rates: stability results summary

Scenario	Drawdown rate (m/day)	Fluctuation (Δ) (m)	Drawdown Time (Days)	SRF	Difference
Current Condition	0.19	8.2	43	1.0	-----
Year 2050	0.23	8.8	38	0.95	-5%
Further instability scenario	0.30	8.8	29	0.92	-8%
	0.40	8.8	22	0.89	-11%
Enhance stability scenario	0.09	4.8	53	1.01	+1%

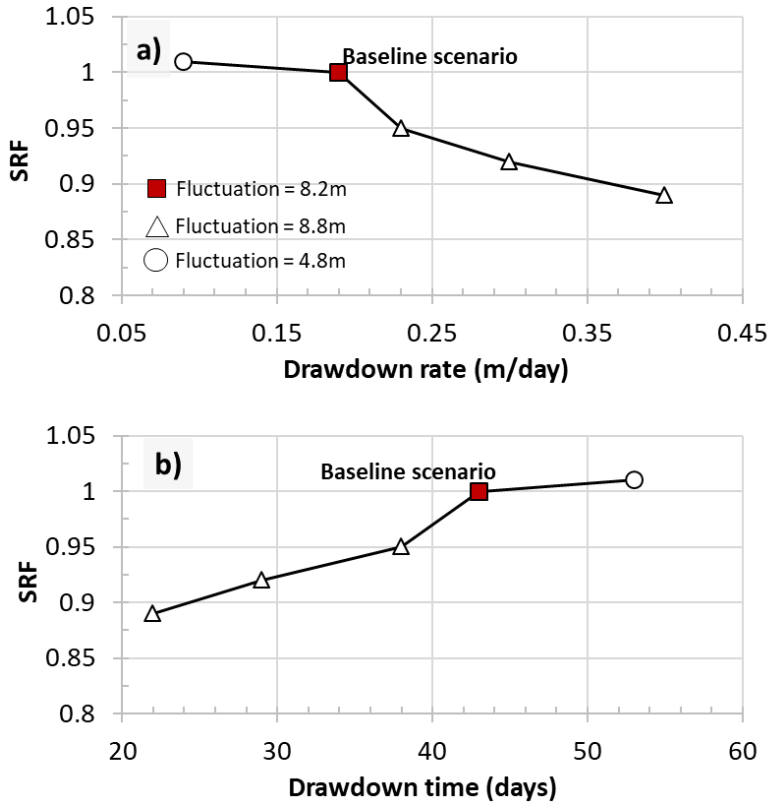

Figure 4.27 SRF vs drawdown rate and drawdown time

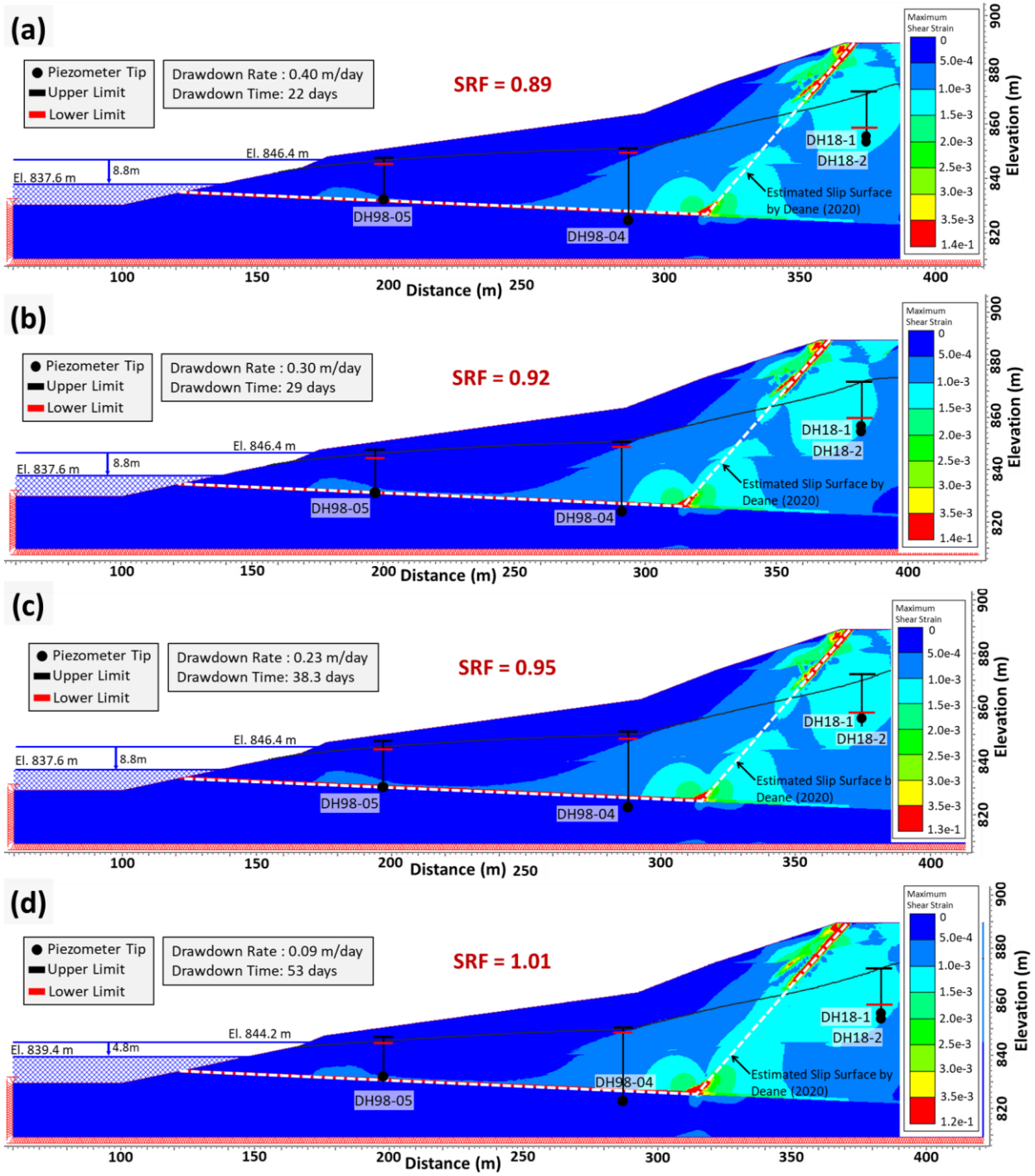

Figure 4.28 Stability results based on different drawdown rates(m/day): (a) 0.40, (b) 0.30, (c) 0.23 and (d) 0.09

4.5 Conclusions

This paper presents a methodology for analyzing the impacts of current and potential future drawdown scenarios on landslides resulting from climate change. It includes the estimation of reservoir water levels, drawdown rates, definition of hydraulic boundaries, shear strengths, and permeability properties. The effectiveness of the methodology was tested on the Chin Coulee landslide, known for increased displacements during summer when the reservoir water demands increase. The main conclusions of our work are as follows:

- The methodology provided landslide material properties consistent with previous studies in the area and similar materials in the region. The groundwater table within the landslide aligned perfectly with historical piezometer records for the current scenario and for the future scenarios, however, future groundwater levels were near the upper piezometer limits due to higher drawdown rates. Additionally, the slip surface obtained by the methodology matched previous studies, traversing the weak coal seam, indicating that the Mohr-Coulomb (M-C) model employed, featuring linearly degrading strength parameters with no cohesion at the residual state, adequately modelled the material behavior in the region.
- Estimating future drawdown rates is challenging, dependent on factors such as weather characteristics (evaporation, precipitation, and temperature), social factors, and physical constraints. The type of trend that drawdown rates may follow is uncertain. However, a practical approach suggested in this study is a linear trend, providing an average estimation and a glimpse of potential future scenarios. These extrapolations should be limited to a short period of years. In our case, approximately 29 years of data was then extrapolated approximately 25 years into the future. This constitutes a significant extrapolation and represents one of the challenges when forecasting the effects of climate change.
- Considering this linear trend, an estimation of the change in stability was conducted, observing a decrease in stability (5%) for a drawdown rate of 0.23 m/day, and this trend continued with

extreme drawdown rates, leading to a reduction in stability of up to 11% (for a drawdown rate of 0.40 m/day). These instabilities trends suggest that the Chin Coulee landslide could experience more displacement velocities or even transition towards collapse in the future if drawdown rates are not controlled, potentially affecting Highway 36 located near the headscarp.

- As the drawdown rates increase, the hydraulic boundary conditions at the landslide head scarp can change over time. This was not evaluated in the current study, and a simplification, considering a constant hydraulic boundary for all drawdown cases, was applied. However, with more information about the regional groundwater levels and infiltration rates, a detailed evaluation can be conducted as part of the workflow presented here. Additionally, the constitutive model considered in the present methodology accounts for small strains in the landslide material. However, as the drawdown increases, the formation of large strains also begins to occur, which needs to be considered depending on the failure mechanisms.

This manuscript has presented a practicable approach for estimating changes in landslide hazard because of potential drawdown scenarios due to climate change. The practicability of the approach has been demonstrated in a case study in Alberta, although it can be deployed in other jurisdictions. The authors are eager to see the implementation of this methodology in diverse jurisdictions, aiming to assess its resilience and suitability in varied settings and climatic conditions.

4.6 References

Alberta (2023a). About Dams. https:// www.alberta.ca/about-dams

Alberta (2023b). Dam Owernship. https://www.alberta.ca/dam-ownership

Alberta (2023c). Climate Change Impacts on Agriculture.
https://agriculture.canada.ca/en/environment/climate-change/climate-scenarios-agriculture

Alonso E, Pinyol N (2009). Slope Stability under Rapid Drawdown Conditions. In Proceedings of the First Italian Workshop on Landslides, Naples, Italy, pp. 11–27

Amec (2015). Instrumentation Monitoring Results – December 2015 Report, Geotechnical Risk Management Plan.

Ameratunga J, Sivakugan N, Das BM (2016). Correlation of Soil and Rock Properties in Geotechnical Engineering. Springer New Delhi Heidelberg New York Dordrecht London

Bayliss A (2022). Engineering geological considerations for dams constructed on the Paskapoo porcupine hills formations in western Alberta. GeoCalgary

Bayrock L, Jones F (1963). Surficial geology of the Vauxhall district, Alberta. Preliminary Report 63–2. Research Council of Alberta, Edmonton.

Berilgen M (2007). Investigation of stability of slopes under drawdown conditions, Computers and Geotechnics, Volume 34, Issue 2,2007, Pages 81-91

Berru I, Macciotta R, Rodriguez J, Gräpel C, Skirrow R, Tappenden K (In Press). Introduction and Testing of a Cost-Effective GNSS System for Landslide Monitoring. Natural Hazards.

Bjerrum L (1954). Theoretical and experimental investigations on the shear strength of soils. PhD thesis. ETH Zurich

Biagini L, Macciotta R, Gräpel C, Tappenden K, Skirrow R (2022). Characteristics, Kinematics and Contributing Factors of Compound and Translational Landslides in the Interior Plains of Canada. Geosciences 2022, 12, 289. https://doi.org/ 10.3390/geosciences12080289

Bo MW, Fabius M, Fabius K (2008). May. Impact of global warming on stability of natural slopes. In Proceedings of the 4th Canadian Conference on Geohazards: From Causes to Management, Presse de Univ. Laval, Quebec.

Bush E, Lemmen DS (2019). Canada's Changing Climate Report; Environment and Climate Change Canada, Government of Canada: Ottawa, ON, Canada, 2019

Carlà T., Macciotta R, Hendry M, Martin CD, Edwards T, Evans T, Intrieri E, Farina P, Casagli N (2017). Displacement of a landslide retaining wall and application of an enhanced failure forecasting approach. Landslides. Published online September 5, 2017 doi: 10.1007/s10346-017-0887-7

Cartier G, Pouget P (1988). Etude du comportement d'un remblai construit sur un versant instable, le remblai de Salledes. (Puy-de-Dome). Rapport de recherche LPC No. 153, Laboratoire Central des Ponts et Chaussées, Paris.

Chan DH, Morgenstern NR (1987). Analysis of progressive deformation of the Edmonton Convention Centre excavation. Canadian Geotechnical Journal. 24(3): 430-440.

Clark R, AndreichukI, Sauchyn D, McMartin DW (2017). Incorporating climate change scenarios and water-balance approach to cumulative assessment models of solution potash Mining in the Canadian Prairies. Clim. Chang. 145, 321–334.

Conte E, Silvestri F, Troncone A (2010). Stability analysis of slopes in soils with strain softening behaviour. Computers and Geotechnics 2010;37(5):710e22.

Cornish LJ, Moore DP (1985). Dam foundation investigations for a project on soft shale. In: Proceedings of the 38th Canadian geotechnical conference. Edmonton, p. 171e8.

Cruden DM and Varnes DJ (1996). Landslide Types and Processes; in Landslides: Investigation and Mitigation, (ed.) A.K. Turner and R.L. Schuster; U.S. Transportation Research Board, Special Report, no. 247, p. 36-75.

Davachi M, Sinclair B, Hartmaier H, Baggot B, Peters J (1991). Determination of the Oldman River Dam foundation shear strength. Canadian Geotechnical Journal. 28(5): 698-707.

Deane E, Macciotta R, Hendry M, Gräpel C, Skirrow R (2019). The use and limitations of modern technologies for slow, vegetated landslide monitoring – Chin Coulee landslide. In: 72nd Canadian Geotechnical Conference, Geo St. John's 2019. St. John's, NL, Canada

Deane E (2020). The Application of Emerging Monitoring Technologies on Very Slow Vegetated Landslides. Master's Thesis, University of Alberta, Edmonton, Canada. https://era.library.ualberta.ca/items/a669ecdc-4535-4145-8684-c071729875e3

Deane E, Macciotta R, Hendry M, Gräpel C, Skirrow R (2020). Leveraging historical aerial photographs and digital photogrammetry techniques for landslide investigation—a practical perspective. Landslides. Landslides. Published online May 23, 2020

DeJong J, Harris MC (1971). Settlements of two multistory buildings in Edmonton. Canadian Geotechnical Journal, 8: 217 – 235

Eigenbrod KD, Morgenstern NR (1972). A slide in Cretaceous bedrock, Devon, Alberta. In: C.O. Brawner and V. Milligan (Editors), Geotechnical Practice for Stability in Open Pit Mining. America n Institution for Mining and Metallurgy, New York, N.Y. pp.223—238.

Eisenstein Z, Morrison NA (1973). Prediction of foundation deformations in Edmonton using an in-situ pressure probe, Canadian Geotechnical Journal, 10: 193-210.

Elwood D, Martin DC (2010). Estimating Soil Properties Using Deformations Associated with Deep Excavations. Proceedings of GeoCalgary 2010: the 63. Canadian geotechnical conference and 6. Canadian permafrost conference. Canada.

Elwood D (2015). Yield Criterion for Sequentially Excavated Tunnels in Heavily Overconsolidated Fissured Soils. Doctoral's Thesis, University of Alberta, Edmonton, Canada, 2021. https://era.library.ualberta.ca/items/c45483fb-2098-4f47-8f20-1a5ee48e16a9

Glass DJ (1990). Lexicon of Canadian Stratigraphy, Volume 4, Western Canada, including Eastern British Columbia, Alberta, Saskatchewan and Southern Manitoba. Canadian Society of Petroleum Geologists, Calgary, Alberta, 772 p.

Golder (1998). Geotechnical Investigation –Report, Geotechnical Risk Management Plan.

Guthrie R (2013). Socio-economic Significance – Canadian Technical Guidelines and Best Practices related to Landslides: a national initiative for loss reduction; Geological Survey of Canada, Open File 7311.

Hayley DW (1968). Progressive Failure of a Clay Shale Slope in Northern Alberta. Unpublished M.Sc. Thesis Dep. of Civil Engineering, Univ. of Alberta, Edmonton, Alta., 61pp.

Hendry MJ (1980). Seepage investigation of lateral A (18, 19-13-16-4). Irrig. Div. Report, Alberta Agric., Lethbridge, Alberta. Hendry. M. 1982. Hydraulic conductivity of a Glacial till in Alberta.

Hendry MJ (1982). Hydraulic conductivity of a glacial till in Alberta. Ground Water. v. 20, no. 2, pp. 162– 169.

Hendry M, Macciotta R, Martin CD, Benjamin R (2014). Effect of Thompson River elevation on velocity and instability of Ripley Slide. Can. Geotech. J. 52: 257–267 (2015) dx.doi.org/10.1139/cgj-2013-0364

Hendry M, Macciotta R, Martin CD, Reich B (2015). Effect of Thompson River elevation on velocity and instability of Ripley Slide. Canadian Geotechnical Journal 52(3): 257-267 doi:10.1139/cgj-2013-0364

Hettler A, Vardoulakis I (1984). Behavior of dry sand tested in a large triaxial apparatus. Geotechnique 1984;34(2):183e97.

Hughes AT, Smerdon BD, Alessi DS (2017). Summary of hydraulic conductivity values for the Paskapoo Formation in west-central Alberta; Alberta Energy Regulator, AER/AGS Open File Report 2016-03, 25 p.

Joyce CB, Simpson M, Casanova M (2016). Future wet grasslands: Ecological implications of climate change. Ecosyst. Health Sustain. 2, e01240.

Journault J, Macciotta R, Hendry M, Charbonneau F, Huntley D, Bobrowsky P (2018). Measuring displacements of the Thompson River valley landslides, south of Ashcroft, BC, Canada, using satellite InSAR. Landslides 15(4):621-636

Klohn Crippen Berger (2018). S005 Hwy 36:02 Chin Coulee Slide Geotechnical Drilling and Instrument Installation Southern Region GRMP

Klohn Crippen Berger (2022). CON0022161 Southern Region GRMP Instrumentation Monitoring Site S005; H36:02, km 37.1 Chin Coulee Slide Section C – 2022 Spring Readings.

Kovari K (1977). The elasto-plastic analysis in the design practice of underground openings. In: Finite elements in geomechanics. Wiley; p. 377e412.

Kraemer B, Seimon A, et al (2020). Worldwide lake level trends and responses to background climate variation. Hydrol. Earth Syst. Sci., 24, 2593–2608, 2020

Lalonde K, Corbett B, Bradley C (2015). Southern Alberta's Watersheds: An Overview. Parire Conservation Forum

Lawrence A (2011). Effects of Groundwater Flow on the Distribution of Biogenic Gas in Parts of the Northern Great Plains of Canada and United States. Geological Survey Scientific Investigations Report 2010–5251, 24 p.

Lewis A, Breef-Pilz A, et al (2023). Reservoir drawdown highlights the emergent effects of water level change on reservoir physics, chemistry, and biology. ESS Open Archive . September 28, 2023.

Locker JG (1969). Petrographic and Engineering Properties of Fine-Grained Sedimentary Rocks of Central Alberta. Unpublished Ph. D Thesis, Dep. of Civil Engineering, University of Alberta, Edmonton, Alta. 285pp.

Macciotta R, Martin CD, Edwards T, Cruden DM, Keegan T (2015). Quantifying Weather Conditions for Rock Fall Hazard Management. Georisk: Assessment and Management of Risk for Engineered Systems and Geohazards 9(3):171-186 doi:10.1080/17499518.2015.1061673

Macciotta R, Martin CD, Morgenstern NR, Cruden D (2016a). Development and application of a quantitative risk assessment to a very slow moving rock slope and potential sudden acceleration. Landslides 13: 765-785 doi:10.1007/s10346-015-0609-y

Macciotta R, Hendry M, Martin CD (2016b). Developing an Early Warning System for a Very Slow Landslide Based on Displacement Monitoring. Natural Hazards 81(2): 887-907 doi:10.1007/s11069-015-2110-2

Macciotta R, Hendry M, Cruden D, Blais-Stevens A, Edwards T (2017). Quantifying Rock Fall Probabilities and Their Temporal Distribution Associated with Weather Seasonality. Landslides. 14:2025-2039

Macciotta R, Gräpel C, Keegan T, Duxbury J, Skirrow R (2019). Quantitative Risk Assessment of Rock Slope Instabilities That Threaten a Highway Near Canmore, AB, Canada: Managing Risk Calculation Uncertainty in Practice. Canadian Geotechnical Journal 57(3) 337-353

Macciotta R (2019). Review and latest insights into rock fall temporal variability associated with weather. Proceedings of the Institution of Civil Engineers – Geotechnical Engineering. Published online March 8, 2019 https://doi.org/10.1680/jgeen.18.00207

Macciotta R, Hendry M (2021). Remote sensing applications for landslide monitoring and investigation in Western Canada. Remote Sensing 13(3): 36

Manzari M, Drevininkas A, Olshansky D, Abdullah G (2014). Modelling of Toronto Glacial Soils and Implementation in Numerical Modelling.

Mebrahtu T,·Heinze T, Wohnlich S, Alber M (2022). Slope stability analysis of deep-seated landslides using limit equilibrium and finite element methods in Debre Sina area, Ethiopia. Bulletin of Engineering Geology and the Environment (2022) 81:403

Medeiros LV (1979). Deep excavations in stiff soils, Unpublished Ph.D. thesis, University of Alberta.

Mirhadi N, Macciotta R (2023). Quantitative correlation between rock fall and weather seasonality to predict changes in rock fall hazard with climate change. Landslides. Published online June 21, 2023

Muhammad A, Evenson GR, et al (2020). Climate Change Impacts on Reservoir Inflow in the Prairie Pothole Region: A Watershed Model Analysis. Water 2020, 12, 271.

Pawley SM, Hartman GMD, Chao DK (2018). Modelling the spatial distribution of landslide susceptible terrain of the Alberta portions of the Interior Plains and Shield Regions, Canada. GeoEdmonton 2018.

Plaxis (2021). Material Models Manual. Bentley

Porter M, Hove J Van, Barlow P, et al (2019). The estimated economic impacts of prairie landslides in western Canada. In: Proceedings of the 72nd Canadian Geotechnical Conference. St. John's, Newfoundland and Labrador, p 8

Potts DM, Kovacevic N, Vaughan PR (1997). Delayed collapse of cut slopes in stiff clay. Geotechnique 1997; 47(5):953e82.

Pratt C, Macciotta R, Hendry M (2019). Quantitative relationship between weather seasonality and rock fall occurrences north of Hope, BC, Canada. Bulletin of Engineering Geology and the Environment. 78:3239-3251

Renani H, Martin CD (2018). Stability Analysis of a Bedded Weak Rock Slope. Paper presented at the 52nd U.S. Rock Mechanics/Geomechanics Symposium, Seattle, Washington, June 2018

Renani H, Martin CD (2019). Factor of safety of strain-softening slopes [J]. Journal of Rock Mechanics and Geotechnical Engineering, 2020, 12(3): 473–483. DOI

Renani H, Martin CD (2020). Slope stability analysis using equivalent Mohr-Coulomb and Hoek-Brown criteria. Rock Mechanics and Rock Engineering 2020;53(1):13e21.

Ringheim AS (1964). Experience with the Bearpaw shale at the South Saskatchewan River Dam. 8th Int. Congr. On Large Dams, Edinburgoh,1 :529—550

Rodriguez J, Hendry M, Macciotta R, Gräpel C, Skirrow R (2020). UAVs for monitoring, investigation and mitigation design of a rock slope with multiple failure mechanisms – a case study. Landslides

Rodriguez J (2021). Assessing The Benefits of Cost-Effective Monitoring Technology on Unstable Slopes Sensitive to Weather. Doctoral's Thesis, University of Alberta, Edmonton,

Canada, 2021. https://era.library.ualberta.ca/items/3b6c65a4-7842-419e-82b1-49ba578c9d04

Rodriguez J, Deane E, Hendry M, Macciotta R, et al (2021). Practical evaluation of single-frequency dGNSS for monitoring slow-moving landslides. Landslides 18, 3671–3684 (2021)

Skempton AW (1964). Long-term stability of clay slopes. Geotechnique, 14(2):77e102.

Soltanieh A, Macciotta R (2022). Updated Understanding of the Thompson River Valley Landslides Kinematics Using Satellite InSAR. Geosciences 12(10):359

St-Jacques JM, Andreichuk Y, et al (2018). Projecting Canadian Prairie Runo_ for 2041–2070 with North American Regional Climate Change Assessment Program (NARCCAP) Data. JAWRA J. Am. Water Resour. Assoc. 2018, 54, 660–675.

Thomson S, Morgenstern NR (1979). Landslides in Argillaceous Rock, Prairie Provinces, Canada. In Voight, Barry (Editor), Rocsklides and Avalances, 2; Elsevier Scientific, Amsterdam, pp.515-540.

Troncone A (2005). Numerical analysis of a landslide in soils with strain-softening behaviour. Geotechnique 2005;55(8):585e96.

Wada Y, Wisser D, Bierkens MFP (2014). Global modeling of withdrawal, allocation and consumptive use of surface water and groundwater resources Earth Syst. Dynam., 5 (2014), pp. 15-40, 10.5194/esd-5-15-2014

Wittebolle RJ (1983). Influence of microfabric on the engineering properties of glacial tills, Unpublished M.Sc. thesis, University of Alberta.

Woods A, Hendry M, Macciotta R, Stewart T, Marsh J (2020). GB-InSAR monitoring of vegetated and snow-covered slopes in remote mountainous environments. Landslides. Published online May 4, 2020

Woods A, Macciotta R, Hendry M, Stewart T, Marsh J (2021). Updated understanding of the deformation characteristics of the Checkerboard Creek rock slope through GB-InSAR monitoring. Engineering Geology 281:105974

Yin Y, Huang B, et al (2016). Reservoir-induced landslides and risk control in Three Gorges Project on Yangtze River, China. Journal of Rock Mechanics and Geotechnical Engineering 8 (2016) 577e595

Zhang K, Cao P, Bao R (2013). Progressive failure analysis of slope with strain-softening behaviour based on strength reduction method. Journal of Zhejiang University-SCIENCE A (Applied Physics & Engineering) ISSN 1673-565X (Print); ISSN 1862-1775

5 CONCLUSION AND FUTURE WORK

The thesis objectives are to develop tools to enhance the risk management of landslides in the Canadian Plains under climate change scenarios, considering enhanced cost-effective monitoring strategies and landslide analysis methods. These objectives were accomplished by developing a practical methodology to assess landslide stability under current and future drawdown scenarios caused by climate change and customizing a low-cost monitoring system and further tested and deployed to determine its viability and reliability for monitoring displacement in the severe Canadian climate. The method and monitoring tool were tested through their application to a real case in southern Alberta. The key findings and outcomes of this study are presented in the following sections.

5.1 Cost-effective GNSS system

The geological features in the Canadian plains contribute to its vulnerability to landslides, a risk that may be exacerbated by how climate change impacts precipitation, temperature, and vegetation patterns in the region. Traditional displacement monitoring technologies like inclinometers are expensive, which restricts the number of monitoring points or their application in projects with limited resources. Due to this constraint, a low-cost alternative technology, consisting of two SparkFun GNSS rovers installed at the landslide mass and one SparkFun base point (Figure 3.8), was evaluated as landslide displacement monitoring tools in aspects such as accuracy, precision, cost, and resilience to the Canadian environment. The main conclusions after their assembly, deployment, and testing for six months are detailed below:

- The SparkFun rovers recorded data every sixty seconds, demonstrating it high frequency recording necessary for a displacement's evaluation.
- Both SparkFun rovers maintained horizontal and vertical accuracies of 14 mm and 10 mm, respectively, for more than 95% of the testing time. Additionally, the SparkFun errors in the horizontal direction ranged from 2.5 mm to 6.2 mm, while those in the vertical direction ranged

from 9 mm to 12.5 mm (Figure 3.17). These accuracies and error fall within the manufacturer's specified range.

- The SparkFun system reported smaller displacements in the horizontal and vertical displacements than the Geocubes. This discrepancy may be related to the SparkFun's shorter monitoring period (6 months compared to the 14 months of the Geocubes), which ended at the end of May. However, the monitoring data did indicate a rise in displacements during May (Figure 3.18), aligning with the period when the landslide displayed higher displacements.
- The SparkFun system displacement direction aligned both horizontally and vertically throughout the monitoring months with the Geocubes (Table 3.4 and Figure 3.20). For example, downward displacement at the headscarp (Rover 949E) and upward displacement near the landslide toe (Rover 9532) were identified, consistent with the identified failure mechanism of the landslide (Figure 3.20).
- During winter, the SparkFun units had power supply troubles, which caused difficulties in getting corrections and data gaps. However, these issues can be addressed by incorporating insulated battery boxes, installing a larger solar panel (above 50 Watts), and sealing the connections between the USB plug and the USB cables with electrical tape. Additionally, regular maintenance should be considered to guarantee the system's reliability as a monitoring system.
- The system had the limitation of not having a longer monitoring time, however, enhanced robustness, high-frequency recording, alignment with past monitoring campaigns, and failure mechanisms, combined with a capital cost of roughly USD$2000 per SparkFun unit, led to the conclusion that the SparkFun system is a promising and cost-effective solution for slow-moving landslides (Cruden and Varnes 1996). It enables installation at multiple locations to improve kinematic characterization at each site without incurring expensive costs and addresses the potential for additional slides induced by climate change in the region.

5.2 Methodology to assess Drawdown scenarios induced by Climate Change

The Canadian Plains are experiencing the effects of climate change, which include rising temperatures, more evaporation, and less precipitation. As a result, water reservoirs are used more frequently to irrigate agricultural lands, resulting in larger fluctuations in reservoir water levels. Drawdown has a significant impact on slope stability, with the potential to create and affect larger landslides in the region. To help agencies manage this hazard more effectively, a practical methodology for analyzing the effects of current and future drawdowns on landslide stability is provided.

The practicability, flexibility, and effectiveness of this methodology were assessed through its application to the Chin Coulee landslide. This landslide experiences larger displacements during the summer months when there is a greater reliance on reservoir water for irrigating nearby farmlands (Deane 2020, Rodriguez et al. 2021). The primary conclusions are as follows:

- The proposed methodology outlines a clear workflow that can be readily applied to numerous sites in the region. Furthermore, its use of a 2D model for landslide stability analysis provides flexibility compared to a site-specific 3D model.
- The methodology proposes to conduct a back analysis that considers the historical maximum drawdown rate and its corresponding fluctuation to estimate the most appropriate landslide material parameters. It also suggests reviewing site investigation reports, monitoring instrument reports, and similar works in the literature to pre-select these parameters.
- The back analysis results provided groundwater levels consistent with piezometer records. The estimated permeability and shear strength property values were also aligned with those from previous studies conducted in the landslide area and the literature review (Table 4.5).
- The method adopts the Mohr-Coulomb (M-C) constitutive model with linearly degrading strength parameters and no cohesion at the residual state to model material behavior in the Canadian Plains. The constitutive model provided a slip surface to be consistent with the

findings in studies by Deane (2020) and Rodriguez (2021), both of whom observed that the slip surface traverses the weak coal seam and extends to the landslide scarp (Figure 4.26), which demonstrate the ability to capture the landslide behavior in a practicable manner.

- The approach uses water reservoir levels to estimate present and future drawdown rates, which can be easily obtained from government websites or institutions without incurring significant costs. Due to uncertainties in forecasting future drawdown rates since it depends on factors such as human activities, environmental changes, or reservoir geometry. A linear extrapolation up to 26 years into the future is suggested as a simplified tool to evaluate potential instability. Further projections into the future were considered erroneous because the reservoir's historical data spans just 29 years.
- Applying a drawdown rate for the year 2050, the landslide stability analysis revealed a 5% reduction in stability compared to the current condition (Figure 4.28a). Extreme drawdown scenarios higher than the 2050-year scenario showed landslide stability decreased up to 11% (Figure 4.28b, c), while a lower drawdown rate provided an increase in stability of 1% (Figure 4.28d). These results indicate the methodology's sensitivity to changes in stability relative to the current conditions, providing a tool for entities to establish reservoir threshold levels to prevent larger displacements.
- These stability changes and overall results provided an insight that methodology allows informed decisions based on possible landslide hazard change using a practicable soil constitutive model, information open to the public to estimate variations in reservoir levels and drawdown rates. However, it's worth noting that the approach was tested on a slow-moving landslide in the Canadian Plains. Applying the approach to additional landslide places in Canada would help to assess its applicability and practicability.

5.3 Future Work

Some potential improvements to the proposed methodology and GNSS monitoring technology are as follows:

- The SparkFun dGNSS network was tested in a slow-moving compound landslide. For future work, this monitoring technology could be deployed on landslides experiencing higher velocities, such as moderate or slow landslides (Cruden and Varnes 1996). Additionally, it can be applied to other failure mechanisms to further assess its applicability. For example, retrogressive translational landslides and non-circular slope surfaces (Biagini et al. 2022) which also exist in Alberta.
- The SparkFun dGNSS network was deployed in a location with clear satellite signal reception and line-of-sight between the base and rovers. For further testing of its potential to establish the dGNSS network, the SparkFun technology might be deployed in a different location, such as western Alberta and British Columbia, where the presence of mountains may limit the number of satellites received to determine its position.
- The SparkFun dGNSS network exhibited good agreement with the Geocube displacement directions. However, comparing overall displacement magnitudes was challenging because the SparkFun's monitoring period was nearly half that of the prior Geocubes monitoring programs. For future studies, the SparkFun system should be tested for a longer monitoring period, particularly during the summer months when landslides may be affected by drawdown, potentially resulting in higher movements.
- The batteries, insulation of the battery boxes, and the USB plug encountered various issues during the monitoring period. For future research, it is recommended to explore more robust components to withstand the Canadian climate.
- The methodology evaluates the drawdown scenario induced by climate change. However, the snow patterns have also experienced changes (Joyse et al. 2016, St-Jacques et al. 2018).

The impact of earlier snowmelt on present and future landslide stability should be investigated, and a practical methodology for evaluating this impact should be provided.

- The methodology established hydraulic boundary conditions for the landslides head only using piezometers data, without considering other aspects like precipitation, infiltration, and evaporation. Future research should explore whether these boundary conditions at the headscarp are affected by the factors above mentioned, as well as how they vary over time.
- The methodology proposed the use of Mohr-Coulomb constitutive modeling with linear degradation to characterize the glacial till and shales found in the Canadian Plains. While the model was in good agreement with the observed slip failure, it did not clearly show the creation of the shear zone that separated the landslide's driving and passive wedges. Future studies could incorporate complex constitutive models like strain-softening into the methodology. This would help in determining whether the shear zone is more clearly defined.

6 REFERENCES

Alberta (2012). Agriculture and Irrigation in Alberta. https://albertawater.com/what-is-water-used-for-in-alberta/agriculture-in-alberta/

Alberta (2023a). About Dams. https:// www.alberta.ca/about-dams

Alberta (2023b). Dam Ownership. https://www.alberta.ca/dam-ownership

Alberta (2023c). Climate Change Impacts on Agriculture. https://agriculture.canada.ca/en/environment/climate-change/climate-scenarios-agriculture

Alberta Climate Information Service (ACIS) (2023). Current and Historical Alberta Weather Station Data Viewer. https://acis.alberta.ca/acis/weather-data-viewer.jsp

Alonso E, Pinyol N (2009). Slope Stability under Rapid Drawdown Conditions. In Proceedings of the First Italian Workshop on Landslides, Naples, Italy, pp. 11–27

Alonso E, Pinyol N (2016). Numerical analysis of rapid drawdown: Applications in real cases. Water Science and Engineering, Volume 9, Issue 3, 2016, Pages 175-182, ISSN 1674-2370, https://doi.org/10.1016/j.wse.2016.11.003.

Amec (2015a). Instrumentation Monitoring Results – December 2015 Report, Geotechnical Risk Management Plan.

Amec (2015b). Southern region geohazard assessment 2015 annual inspection report site S5: Highway 36:02, Chin Coulee. Calgary, Alberta

Ameratunga J, Sivakugan N, Das BM (2016). Correlation of Soil and Rock Properties in Geotechnical Engineering. Springer New Delhi Heidelberg New York Dordrecht London

Ardusimple (2023). Introduction to centimeter level GPS/GNSS. https://www.ardusimple.com/rtk-explained

Bagheri F (2022). Effects of climate change on slope stability of variably saturated embankments using local factor of safety and in-situ stress finite element analysis. York University. Toronto, Ontario.

Bayliss A (2022). Engineering geological considerations for dams constructed on the Paskapoo porcupine hills formations in western Alberta. GeoCalgary

Bayrock L, Jones F (1963). Surficial geology of the Vauxhall district, Alberta. Preliminary Report 63–2. Research Council of Alberta, Edmonton.

Benoit L, Briole P, Martin O, Thom C, Malet JP, Ulrich P (2015a). Monitoring landslide displacements with the Geocube wireless network of low-cost GPS. Eng Geol 195:111–121

Benoit L, Dehecq A, Thai Pham H, Vernier F, Trouvé E, Moreau L, Martin O, Thom C, Pierrot-Deseilligny M, Briole P (2015b). Multi-method monitoring of Glacier d'Argentière dynamics. Ann Glaciol 56:118–128. https://doi. Org/ 10. 3189/ 2015A oG70A 985

Berilgen M (2007). Investigation of stability of slopes under drawdown conditions, Computers and Geotechnics, Volume 34, Issue 2,2007, Pages 81-91

Berru I, Macciotta R, Gräpel C, Rodriguez J, Skirrow R, Tappenden K (2023). Cost-effective dGNSS system for landslide monitoring: system description, deployment, and initial findings at the Chin Coulee Landslide. GeoSaskatoon 2023

Berru I, Macciotta R, Gräpel C, Rodriguez J, Skirrow R, Tappenden K (In Press). Introduction and Testing of a Cost-Effective GNSS System for Landslide Monitoring. Natural Hazards.

Bhatti AZ, Farooque AA, Krouglicof N, Li Q, Peters W, Abbas F, Acharya B (2021). An Overview of Climate Change Induced Hydrological Variations in Canada for Irrigation Strategies. Sustainability 2021, 13, 4833. https://doi.org/ 10.3390/su13094833

Bjerrum L (1954). Theoretical and experimental investigations on the shear strength of soils. PhD thesis. ETH Zurich

Biagini L, Macciotta R, Gräpel C, Tappenden K, Skirrow R (2022). Characteristics, Kinematics and Contributing Factors of Compound and Translational Landslides in the Interior Plains of Canada. Geosciences 2022, 12, 289. https://doi.org/ 10.3390/geosciences12080289

Bo MW, Fabius M, Fabius K (2008). May. Impact of global warming on stability of natural slopes. In Proceedings of the 4th Canadian Conference on Geohazards: From Causes to Management, Presse de Univ. Laval, Quebec.

Bobrowsky PT, Dominguez MK (2012). Landslide Susceptibility Map of Canada. Annual Meeting of the Geological Association of Canada-Mineralogical Association of Canada, Program with Abstracts, Volume 36, Ottawa, Ontario, Canada 25–27 May 2011

Brown N, Troyer L, Zelzer O, Van Cranenbroek J (2006). Advances in RTK and post processed monitoring with single frequency GPS. J Glob Position Syst 5(1–2) :145–151

Bush E, Lemmen DS (2019). Canada's Changing Climate Report; Environment and Climate Change Canada, Government of Canada: Ottawa, ON, Canada, 2019

Caldera S, Barindelli S, Sansò F, Pardi L (2022) Monitoring of Structures and Infrastructures by Low-Cost GNSS Receivers. Appl. Sci. 2022, 12, 12468. https://doi.org/10.3390/app122312468

Carlà T., Macciotta R, Hendry M, Martin CD, Edwards T, Evans T, Intrieri E, Farina P, Casagli N (2017). Displacement of a landslide retaining wall and application of an enhanced failure forecasting approach. Landslides. Published online September 5, 2017 doi: 10.1007/s10346-017-0887-7

Cartier G, Pouget P (1988). Etude du comportement d'un remblai construit sur un versant instable, le remblai de Salledes. (Puy-de-Dome). Rapport de recherche LPC No. 153, Laboratoire Central des Ponts et Chaussées, Paris.

Chae B, Park H, Catani F (2017). Landslide prediction, monitoring and early warning: a concise review of state-of-the-art. Geosci J 21, 1033–1070 (2017). https://doi.org/10.1007/s12303-017-0034-4

Chan DH, Morgenstern NR (1987). Analysis of progressive deformation of the Edmonton Convention Centre excavation. Canadian Geotechnical Journal. 24(3): 430-440.

Cina A, Piras M (2015). Performance of low-cost GNSS receiver for landslides monitoring test and results, Geomatics, Natural Hazards and Risk, 6:5-7, 497-514, DOI: 10.1080/19475705.2014.889046

Clark R, AndreichukI, Sauchyn D, McMartin DW (2017). Incorporating climate change scenarios and water-balance approach to cumulative assessment models of solution potash Mining in the Canadian Prairies. Clim. Chang. 145, 321–334.

Conte E, Silvestri F, Troncone A (2010). Stability analysis of slopes in soils with strain softening behaviour. Computers and Geotechnics 2010;37(5):710e22.

Cornish LJ, Moore DP (1985). Dam foundation investigations for a project on soft shale. In: Proceedings of the 38th Canadian geotechnical conference. Edmonton, p. 171e8.

Cruden DM, Varnes DJ (1996). Landslide Types and Processes; in Landslides: Investigation and Mitigation, (ed.) A.K. Turner and R.L. Schuster; U.S. Transportation Research Board, Special Report, no. 247, p. 36-75.

Davachi M, Sinclair B, Hartmaier H, Baggot B, Peters J (1991). Determination of the Oldman River Dam foundation shear strength. Canadian Geotechnical Journal. 28(5): 698-707.

Davies L, Gather U (1993). The identification of multiple outliers, J. Am. Stat. Assoc., 88, 782–792, 1993.

Deane E, Macciotta R, Hendry M, Gräpel C, Skirrow R (2019). The use and limitations of modern technologies for slow, vegetated landslide monitoring – Chin Coulee landslide. In: 72nd Canadian Geotechnical Conference, Geo St. John's 2019. St. John's, NL, Canada

Deane E (2020). The Application of Emerging Monitoring Technologies on Very Slow Vegetated Landslides. Master's Thesis, University of Alberta, Edmonton, Canada. https://era.library.ualberta.ca/items/a669ecdc-4535-4145-8684-c071729875e3

Deane E, Macciotta R, Hendry M, Gräpel C, Skirrow R (2020). Leveraging historical aerial photographs and digital photogrammetry techniques for landslide investigation—a practical perspective. Landslides. Landslides. Published online May 23, 2020

DeJong J, Harris MC (1971). Settlements of two multistory buildings in Edmonton. Canadian Geotechnical Journal, 8: 217 – 235

Doberstein D (2012) Fundamentals of GPS Receivers. Springer, Nipomo, CA, USA

Echuan Y, Xingqiao X, Xiangyi L, Xijie Y (2009). Analysis on the Deformation of Tangjiao Village Landslide under Reservoir Water Level Drawdown Condition. Geological Engineering: Proceedings of the 1st International Conference (ICGE 2007). Ed. Ma, B. ASME Press, 2009.

Eigenbrod KD, Morgenstern NR (1972). A slide in Cretaceous bedrock, Devon, Alberta. In: C.O. Brawner and V. Milligan (Editors), Geotechnical Practice for Stability in Open Pit Mining. America n Institution for Mining and Metallurgy, New York, N.Y. pp.223—238.

Eisenstein Z, Morrison NA (1973). Prediction of foundation deformations in Edmonton using an in-situ pressure probe, Canadian Geotechnical Journal, 10: 193-210.

Elwood D, Martin DC (2010). Estimating Soil Properties Using Deformations Associated with Deep Excavations. Proceedings of GeoCalgary 2010: the 63. Canadian geotechnical conference and 6. Canadian permafrost conference. Canada.

Elwood D (2015). Yield Criterion for Sequentially Excavated Tunnels in Heavily Overconsolidated Fissured Soils. Doctoral's Thesis, University of Alberta, Edmonton, Canada, 2021. https://era.library.ualberta.ca/items/c45483fb-2098-4f47-8f20-1a5ee48e16a9

Emlid (2020) Single-band vs Multi-band. https://docs.emlid.com/reach/tutorials/basics/single-multi/

Eyo E, Musa TA, Omar KM, Idris KM, Bayrak T, Onuigbo I, Opaluwa YD (2014) Application of Low-Cost GPS Tools and Techniques for Landslide Monitoring: A Review.

Fergus CE, Brooks JR, Kaufmann PR, Pollard AI, Mitchell R, Geldhof GJ, et al. (2022). Natural and anthropogenic controls on lake water-level decline and evaporation to-inflow ratio in the conterminous United States. Limnology and Oceanography, 67(7), 1484–1501. https://doi.org/10.1002/lno.12097

Gili J, Corominas J, Rius J (2000) Using Global Positioning System techniques in landslide monitoring, Engineering Geology, Volume 55, Issue 3, 2000, Pages 167-192, ISSN 0013-7952. https://doi.org/10.1016/S0013-7952(99)00127-1.

Glass DJ (1990). Lexicon of Canadian Stratigraphy, Volume 4, Western Canada, including Eastern British Columbia, Alberta, Saskatchewan and Southern Manitoba. Canadian Society of Petroleum Geologists, Calgary, Alberta, 772 p.

Golder (1998). Geotechnical Investigation –Report, Geotechnical Risk Management Plan.

Guthrie R (2013). Socio-economic Significance – Canadian Technical Guidelines and Best Practices related to Landslides: a national initiative for loss reduction; Geological Survey of Canada, Open File 7311.

Hamza V, Stopar B, Sterle O, Pavlovˇciˇc-Prešeren P (2023) A Cost-Effective GNSS Solution for Continuous Monitoring of Landslides. Remote Sens. 2023, 15, 2287. https://doi.org/10.3390/rs15092287

Harris S (2023) Global Navigation Satellite System (GNSS) and Satellite Navigation Explained. https://www.advancednavigation.com/tech-articles/global-navigation-satellite-system-gnss-and-satellite-navigation-explained/

Hayley DW (1968). Progressive Failure of a Clay Shale Slope in Northern Alberta. Unpublished M.Sc. Thesis Dep. of Civil Engineering, Univ. of Alberta, Edmonton, Alta., 61pp.

Hendry MJ (1980). Seepage investigation of lateral A (18, 19-13-16-4). Irrig. Div. Report, Alberta Agric., Lethbridge, Alberta. Hendry. M. 1982. Hydraulic conductivity of a Glacial till in Alberta.

Hendry MJ (1982). Hydraulic conductivity of a glacial till in Alberta. Ground Water. v. 20, no. 2, pp. 162– 169.

Hendry M, Macciotta R, Martin CD, Benjamin R (2014). Effect of Thompson River elevation on velocity and instability of Ripley Slide. Can. Geotech. J. 52: 257–267 (2015) dx.doi.org/10.1139/cgj-2013-0364

Hendry M, Macciotta R, Martin CD, Reich B (2015). Effect of Thompson River elevation on velocity and instability of Ripley Slide. Canadian Geotechnical Journal 52(3): 257-267 doi:10.1139/cgj-2013-0364

Hettler A, Vardoulakis I (1984). Behavior of dry sand tested in a large triaxial apparatus. Geotechnique 1984;34(2):183e97.

Hughes AT, Smerdon BD, Alessi DS (2017). Summary of hydraulic conductivity values for the Paskapoo Formation in west-central Alberta; Alberta Energy Regulator, AER/AGS Open File Report 2016-03, 25 p.

Jiang J, Ehret D, Xiang W, Rohn J, Huang L, Yan S, Bi R (2009). Numerical simulation of Qiaotou Landslide deformation caused by drawdown of the Three Gorges Reservoir, China. Environ Earth Sci (2011) 62:411–419. DOI 10.1007/s12665-010-0536-0

Jiang T, Wang D, Wei S, Yan J, Liang J, Chen X, et al. (2018). Influences of the alternation of wet-dry periods on the variability of chromophoric dissolved organic matter in the water level fluctuation zone of the Three Gorges Reservoir area, China. Science of The Total Environment, 636, 249–259. https://doi.org/10.1016/j.scitotenv.2018.04.262

Joyce CB, Simpson M, Casanova M (2016). Future wet grasslands: Ecological implications of climate change. Ecosyst. Health Sustain. 2, e01240.

Journault J, Macciotta R, Hendry M, Charbonneau F, Huntley D, Bobrowsky P (2018). Measuring displacements of the Thompson River valley landslides, south of Ashcroft, BC, Canada, using satellite InSAR. Landslides 15(4):621-636

Keller PS, Marcé R, Obrador B, Koschorreck M (2021). Global carbon budget of reservoirs is overturned by the quantification of drawdown areas. Nature Geoscience, 14(6), 402–408. https://doi.org/10.1038/s41561-021-00734-z

Kintner PM, Ledvina BM, De Paula ER (2007). GPS and ionospheric scintillations. Sp. Weather 5:1–23. https://doi. Org/ 10. 1029/ 2006S W0002 60

Klohn Crippen Berger (2018). S005 Hwy 36:02 Chin Coulee Slide Geotechnical Drilling and Instrument Installation Southern Region GRMP

Klohn Crippen Berger (2022). CON0022161 Southern Region GRMP Instrumentation Monitoring Site S005; H36:02, km 37.1 Chin Coulee Slide Section C – 2022 Spring Readings.

Kovari K (1977). The elasto-plastic analysis in the design practice of underground openings. In: Finite elements in geomechanics. Wiley; p. 377e412.

Kraemer B, Seimon A, et al (2020). Worldwide lake level trends and responses to background climate variation. Hydrol. Earth Syst. Sci., 24, 2593–2608, 2020

Labajo AL, Egido M, Martín Q, Labajo J, Labajo JL (2014). Definition and temporal evolution of the heat and cold waves over the Spanish Central Plateau from 1961 to 2010. Atmósfera, 27(3), 273-286

Lalonde K, Corbett B, Bradley C (2015). Southern Alberta's Watersheds: An Overview. Parire Conservation Forum

Lawrence A (2011). Effects of Groundwater Flow on the Distribution of Biogenic Gas in Parts of the Northern Great Plains of Canada and United States. Geological Survey Scientific Investigations Report 2010–5251, 24 p.

Lewis A, Breef-Pilz A, et al (2023). Reservoir drawdown highlights the emergent effects of water level change on reservoir physics, chemistry, and biology. ESS Open Archive. September 28, 2023.

Locker JG (1969). Petrographic and Engineering Properties of Fine-Grained Sedimentary Rocks of Central Alberta. Unpublished Ph. D Thesis, Dep. of Civil Engineering, University of Alberta, Edmonton, Alta. 285pp.

Liu H, Shah S, Jiang W (2004). On-line outlier detection and data cleaning, Comput. Chem. Eng., 28, 1635–1647, 2004.

Macciotta R, Martin CD, Edwards T, Cruden DM, Keegan T (2015). Quantifying Weather Conditions for Rock Fall Hazard Management. Georisk: Assessment and Management of Risk for Engineered Systems and Geohazards 9(3):171-186 doi:10.1080/17499518.2015.1061673

Macciotta R, Martin CD, Morgenstern NR, Cruden D (2016a). Development and application of a quantitative risk assessment to a very slow moving rock slope and potential sudden acceleration. Landslides 13: 765-785 doi:10.1007/s10346-015-0609-y

Macciotta R, Hendry M, Martin CD (2016b). Developing an Early Warning System for a Very Slow Landslide Based on Displacement Monitoring. Natural Hazards 81(2): 887-907 doi:10.1007/s11069-015-2110-2

Macciotta R, Hendry M, Cruden D, Blais-Stevens A, Edwards T (2017). Quantifying Rock Fall Probabilities and Their Temporal Distribution Associated with Weather Seasonality. Landslides. 14:2025-2039

Macciotta R, Gräpel C, Keegan T, Duxbury J, Skirrow R (2019). Quantitative Risk Assessment of Rock Slope Instabilities That Threaten a Highway Near Canmore, AB, Canada: Managing Risk Calculation Uncertainty in Practice. Canadian Geotechnical Journal 57(3) 337-353

Macciotta R (2019). Review and latest insights into rock fall temporal variability associated with weather. Proceedings of the Institution of Civil Engineers – Geotechnical Engineering. Published online March 8, 2019 https://doi.org/10.1680/jgeen.18.00207

Macciotta R, Hendry M (2021). Remote sensing applications for landslide monitoring and investigation in Western Canada. Remote Sensing 13(3): 36

Malet J, Maquaire O, Calais E (2002). The use of global positioning system techniques for the continuous monitoring of landslides: Application to the Super-Sauze earthflow (Alpes-de-Haute-Provence, France). Geomorphology 43: 33 – 54.

Manzari M, Drevininkas A, Olshansky D, Abdullah G (2014). Modelling of Toronto Glacial Soils and Implementation in Numerical Modelling.

Mebrahtu T,·Heinze T, Wohnlich S, Alber M (2022). Slope stability analysis of deep-seated landslides using limit equilibrium and finite element methods in Debre Sina area, Ethiopia. Bulletin of Engineering Geology and the Environment (2022) 81:403

Medeiros LV (1979). Deep excavations in stiff soils, Unpublished Ph.D. thesis, University of Alberta.

Miller S, Zhang X, Spanias A (2015). Multipath effects in GPS receivers: a primer. Morgan & Claypool. https:// doi. org/ 10. 2200/ S0068 2ED1V 01Y20 1511C OM011

Mirhadi N, Macciotta R (2023). Quantitative correlation between rock fall and weather seasonality to predict changes in rock fall hazard with climate change. Landslides. Published online June 21, 2023

Muhammad A, Evenson GR, et al (2020). Climate Change Impacts on Reservoir Inflow in the Prairie Pothole Region: A Watershed Model Analysis. Water 2020, 12, 271.

Notti D, Cina A, Manzino A, Colombo A, Bendea IH, Mollo P, Giordan D (2020). Low-cost GNSS solution for continuous monitoring of slope instabilities applied to Madonna Del Sasso Sanctuary (NW Italy). Sensors 20:289

NRC (2008). Canada's Most Damaging Landslides. Geofacts. www.publications.gc.ca/collections/collection_2008/nrcan/M4-59-2-2008E.pdf [April 19, 2019].

Ophelia-Sensors (2019). https://ophelia-sensors.com/geocube

Pawley SM, Hartman GMD, Chao DK (2018). Modelling the spatial distribution of landslide susceptible terrain of the Alberta portions of the Interior Plains and Shield Regions, Canada. GeoEdmonton 2018.

Pearson RK (2002). Outliers in process modeling and identification, IEEE Trans. Contr. Syst. T., 10, 55–63, 2002.

Pinyol N, Alonso W, Corominas J, Moya J (2011). Canelles landslide: modelling rapid drawdown and fast potential sliding. Landslides (2012) 9:33–51. DOI 10.1007/s10346-011-0264-x

Plaxis (2021). Material Models Manual. Bentley

Porter M, Hove J Van, Barlow P, et al (2019). The estimated economic impacts of prairie landslides in western Canada. In: Proceedings of the 72nd Canadian Geotechnical Conference. St. John's, Newfoundland and Labrador, p 8

Potts DM, Kovacevic N, Vaughan PR (1997). Delayed collapse of cut slopes in stiff clay. Geotechnique 1997; 47(5):953e82.

Pratt C, Macciotta R, Hendry M (2019). Quantitative relationship between weather seasonality and rock fall occurrences north of Hope, BC, Canada. Bulletin of Engineering Geology and the Environment. 78:3239-3251

Renani H, Martin CD (2018). Stability Analysis of a Bedded Weak Rock Slope. Paper presented at the 52nd U.S. Rock Mechanics/Geomechanics Symposium, Seattle, Washington, June 2018

Renani H, Martin CD (2019). Factor of safety of strain-softening slopes [J]. Journal of Rock Mechanics and Geotechnical Engineering, 2020, 12(3): 473–483. DOI

Renani H, Martin CD (2020). Slope stability analysis using equivalent Mohr-Coulomb and Hoek-Brown criteria. Rock Mechanics and Rock Engineering 2020;53(1):13e21.

Ringheim AS (1964). Experience with the Bearpaw shale at the South Saskatchewan River Dam. 8th Int. Congr. On Large Dams, Edinburgoh,1 :529—550

Rocsience (2004). A New Era in Slope Stability Analysis: Shear Strength Reduction Finite Element Technique. https://static.rocscience.cloud/assets/verification-and-theory/RocNews-pdfs/StrengthReduction.pdf

Rodriguez J, Hendry M, Macciotta R, Evans T (2018). Cost-effective Landslide Monitoring GPS System: Characteristics, Implementation and Results. Geohazards 7, Proceedings Paper, 8 p

Rodriguez J, Hendry M, Macciotta R, Gräpel C, Skirrow R (2020). UAVs for monitoring, investigation, and mitigation design of a rock slope with multiple failure mechanisms – a case study. Landslides

Rodriguez J (2021). Assessing The Benefits of Cost-Effective Monitoring Technology on Unstable Slopes Sensitive to Weather. Doctoral's Thesis, University of Alberta, Edmonton, Canada, 2021. https://era.library.ualberta.ca/items/3b6c65a4-7842-419e-82b1-49ba578c9d04

Rodriguez J, Deane E, Hendry M, Macciotta R, et al (2021). Practical evaluation of single-frequency dGNSS for monitoring slow-moving landslides. Landslides 18, 3671–3684 (2021)

Septentrio (2023). Why multi-frequency and multi-constellation matters for GPS/GNSS receivers?. https://www.septentrio.com/en/learn-more/about-GNSS/why-multi-frequency-and-multi-constellation-matters

Sharifi S, Hendry M, Macciotta R, Evans T (2022). Evaluation of filtering methods for use on high-frequency measurements of landslide displacements, Nat. Hazards Earth Syst. Sci., 22, 411–430, https://doi.org/10.5194/nhess-22-411-2022, 2022.

Shen N Chen L, Liu J.;Wang L, Tao T, Wu D, Chen R (2019). A Review of Global Navigation Satellite System (GNSS)-Based Dynamic Monitoring Technologies for Structural Health Monitoring. Remote Sensing. 2019; 11(9):1001. https://doi.org/10.3390/rs11091001

Skempton AW (1964). Long-term stability of clay slopes. Geotechnique, 14(2):77e102.

Smethurst J, Smith A, Uhlemann S, Wooff C, Chambers J, Hughes P, Lenart S et al. (2017). Current and future role of instrumentation and monitoring in the performance of transport infrastructure slopes. Q J Eng Geol Hydrogeol 50:271–286. https:// doi. Org/ 10. 1144/ qjegh 2016- 080

Soltanieh A, Macciotta R (2022). Updated Understanding of the Thompson River Valley Landslides Kinematics Using Satellite InSAR. Geosciences 12(10):359

SparkFun. 2023a. https://www.SparkFun.com/about_SparkFun

SparkFun. 2023b. https://www.sparkfun.com/products/17370

SparkFun. 2023c. https://www.sparkfun.com/products/18589

SparkFun. 2023d. SparkFun Schematic. https://cdn.sparkfun.com/assets/c/1/b/d/8/SparkFun_RTK_Surveyorv13.pdf?_gl=1*1pwu48q*_ga*MTk4NjE3MzQyOS4xNjc4MTE4OTA2*_ga_T369JS7J9N*MTY5NDY1MTc5OS4zMi4xLjE2OTQ2NTEMDQuNTUuMC4w

SparkFun. 2023e. https://learn.SparkFun.com/tutorials/terminal-basics/tera-term-windows

SparkFun RTK Surveyor. (n.d.). GPS-18443 – SparkFun Electronics. https://www.SparkFun.com/products/18443

St-Jacques JM, Andreichuk Y, et al (2018). Projecting Canadian Prairie Runo_ for 2041–2070 with North American Regional Climate Change Assessment Program (NARCCAP) Data. JAWRA J. Am. Water Resour. Assoc. 2018, 54, 660–675.

Schuster RL (1979). Reservoir-induced landslides. Bulletin of the International Association of Engineering Geology 1979;20(1):8e15.

Tagliavini F, Mantovani M, Marcato G, Pasuto A, Silvano S (2007). Validation of landslide hazard assessment by means of GPS monitoring technique – A case study in the Dolomites (Eastern Alps, Italy). Natural Hazards and Earth System Science (European Geosciences Union) 7 (1): 185-193.

Takasu T, Yasuda A (2009). Development of the low-cost RTK GPS receiver with the open-source program package RTKLIB. International Symposium on GPS/GNSS. International Convention Centre Jeju, Korea, 2009

Tao H, Gemmer M, Jiang J, Lai X, Zhang Z (2012). Assessment of CMIP3 climate models and projected changes of precipitation and temperature in the Yangtze River Basin, China. Climatic change, 111(3), 737-751.

Tappenden KM, Skirrow RK (2020). Vision for Geotechnical Asset Management at Alberta Transportation. In: GeoVirtual 2020. Edmonton, Alberta

Thomson S, Morgenstern NR (1979). Landslides in Argillaceous Rock, Prairie Provinces, Canada. In Voight, Barry (Editor), Rocsklides and Avalances, 2; Elsevier Scientific, Amsterdam, pp.515-540.

Troncone A (2005). Numerical analysis of a landslide in soils with strain-softening behaviour. Geotechnique 2005;55(8):585e96.

Ublox (2022). ZED-F9P: u-blox F9 high precision GNSS module. https://content.u-blox.com/sites/default/files/ZED-F9P_IntegrationManual_UBX-18010802.pdf

Ublox (2023a). https://www.u-blox.com/en/product/zed-f9p-module#tab-documentation-resources

Ublox (2023b). https://www.u-blox.com/en/product/zed-f9r-module

Ublox (2023c). https://content.u-blox.com/sites/default/files/u-center_Userguide_UBX-13005250.pdf

Ublox (2023d). https://content.u-blox.com/sites/default/files/ZED-F9R_Integrationmanual_UBX-20039643.pdf

Vincent LA, Zhang X, Mekis É, Wan H, Bush EJ (2018). Changes in Canada's Climate: Trends in Indices Based on Daily Temperature and Precipitation Data, AtmosphereOcean, 56:5, 332-349, DOI: 10.1080/07055900.2018.1514579

Wada Y, Wisser D, Bierkens MFP (2014). Global modeling of withdrawal, allocation and consumptive use of surface water and groundwater resources Earth Syst. Dynam., 5 (2014), pp. 15-40, 10.5194/esd-5-15-2014

Wittebolle RJ (1983). Influence of microfabric on the engineering properties of glacial tills, Unpublished M.Sc. thesis, University of Alberta.

Woods A, Hendry M, Macciotta R, Stewart T, Marsh J (2020). GB-InSAR monitoring of vegetated and snow-covered slopes in remote mountainous environments. Landslides. Published online May 4, 2020

Woods A, Macciotta R, Hendry M, Stewart T, Marsh J (2021). Updated understanding of the deformation characteristics of the Checkerboard Creek rock slope through GB-InSAR monitoring. Engineering Geology 281:105974

Xue C, Psimoulis P, Meng X (2022). Feasibility analysis of the performance of low-cost GNSS receivers in monitoring dynamic motion. Measurement. https://doi.org/10.1016/j.measurement.2022.111819

Yao Z, Xie J, Tian Y, Huang Q (2019). Using Hampel identifier to eliminate profile-isolated outliers in laser vision measurement, J. Sensors, 2019, 3823691, https://doi.org/10.1155/2019/3823691, 2019.

Yin Y, Huang B, et al (2016). Reservoir-induced landslides and risk control in Three Gorges Project on Yangtze River, China. Journal of Rock Mechanics and Geotechnical Engineering 8 (2016) 577e595

Zangerl C, Eberhardt E, Perzlmaier S (2010). Kinematic behaviour and velocity characteristics of a complex deep-seated crystalline rockslide system in relation to its interaction with a dam reservoir. Engineering Geology. Volume 112, Issues 1–4, 26 March 2010, Pages 53-67. https://doi.org/10.1016/j.enggeo.2010.01.001

Zhang K, Cao P, Bao R (2013). Progressive failure analysis of slope with strain-softening behaviour based on strength reduction method. Journal of Zhejiang University-SCIENCE A (Applied Physics & Engineering) ISSN 1673-565X (Print); ISSN 1862-1775

Zimek A, Filzmoser P (2010). There and back again: Outlier detection between statistical reasoning and data mining algorithms, WIREs Data Min. Knowl., 8, 1280, https://doi.org/10.1002/widm.1280, 2018.